Influence of basicity in Fischer-Tropsch synthesis over supported iron-based catalysts

Thesis submitted in the partial fulfilment for the Masters degree in Applied Science in Chemical Engineering

By

Annalie Blignaut

B.Sc. (Hon.)

Department of Chemical Engineering

University of Cape Town

Rondebosch

7701

South Africa

2007

DECLARATIONS:

(i) I hereby grant the University of Cape Town free licence to reproduce for the purpose of research either the whole or any portion of the contents in any manner whatsoever of the above dissertation. I am presenting this dissertation in **FULL/PARTIAL** fulfilment of the requirements for my degree.

(ii) I know the meaning of plagiarism and declare that all of the work in the document, save for that which is properly acknowledged, is my own.

Signed by candidate

Signature

25/10/2007

Date

ACKNOWLEDGEMENTS

I would like to extend my gratitude to numerous sources for technical and moral assistance:

- Prof. Eric van Steen for his encouragement, advice and support throughout this work.
- Dr. Michael Clayes for his advice and suggestions.
- Catalysis Research Unit student and staff who help to contribute to this work, with you guys it would not have been possible.
- My friends and family for their love and support.

Synopsis

The Fischer-Tropsch synthesis catalyzed by iron is a well-established process for the production of synthetic fuels, waxes and high-value chemicals, such as α-olefins. A draw-back of the currently used iron-based catalysts is their short life-time, caused by sintering and particle break-up. These disadvantages might be overcome by utilizing a supported iron-based catalyst. However, supported iron Fischer-Tropsch synthesis, which has been tested up to now, show a high methane selectivity. This might be caused by a lack of alkali near the catalytic site, which can be alleviated by using a basic support. Classical basic supports such as CaO and MgO will react with CO_2 (a major by-product in iron-catalyzed Fischer-Tropsch synthesis) yielding carbonates and can therefore not be used, since the formation of carbonates will result in a large particle expansion. An alternative would be to generate a silica-based basic support by attaching basic groups to the silica.

In this study iron Fischer-Tropsch catalysts supported on silica were tested for conversion of synthesis gas to hydrocarbon products. Silica was modified with aminopropyltriethoxysilane (APTeS) by impregnation followed by calcination to provide basic surface groups onto the silica surface. The CHN analysis and IR-analysis indicate the presence of amine groups in the APTeS-modified silica. The pore radius distribution of silica is slightly shifted towards higher pore radii in comparison to APTeS-modified silica. It might thus be stated that aminopropyltriethoxysilane covers the pore walls and does not seem to result in pore blockage. Thermal gravimetric analysis indicates that the thermal stability of APTeS-modified silica is low. A major difference between silica and APTeS-modified silica was their zeta-potential. Whereas the surface of silica is mainly negatively charged in the pH-range of interest during impregnation, the surface of APTeS-modified silica is mainly positively charged. This is attributed to the presence of amine groups on the surface.

Iron was brought onto the support by impregnation. The surface modification of silica with APTeS seems to be destroyed upon calcination of the impregnated catalysts. The iron phase in the calcined iron catalyst supported on silica catalysts is mainly hematite (Fe_2O_3), whereas the iron phase in the calcined iron catalyst supported on APTeS-modified silica catalysts is mainly iron oxide hydroxide FeOOH. The presence of basic amine groups may favour the formation of FeOOH crystallites during the impregnation/calcination on the APTeS-modified silica. The FeOOH-crystallites on the APTeS-modified silica support are typically smaller than the Fe_2O_3 crystallites on silica.

The maximum catalytic activity is obtained at 0.01 mol K / mol Fe for the iron catalyst supported on silica and at 0.02 mol K / mol Fe for the APTeS-modified catalyst, indicating the optimum potassium loading. The difference in the optimum potassium loading might be linked to the smaller crystallite sizes obtained with the APTeS-modified catalyst. All the potassium promoted catalysts show a lower methane selectivity compared to the 0 K iron catalyst supported on silica and the 0 K iron catalyst supported on APTeS-modified silica. The 1-olefin and n-olefin content in the fraction of linear hydrocarbons increase with increasing potassium loading over all the iron catalyst supported on silica promoted with potassium except for the catalysts 0.005 K and 0.01 K.

Increasing potassium content on the catalyst resulted in higher 1-olefin content in the fraction of linear olefins. The trend suggests that potassium promotion suppresses secondary double bond isomerisation of 1-olefin into internal olefins. The high degree of branching obtained with the 0.005 K catalyst and the 0.01 K catalyst, is characteristic of weak alkali promotion. The iron catalysts supported on APTeS-modified silica indicate an increase in the degree of branching with increasing potassium content.

Table of Contents

List of Tables

1. INTRODUCTION

1.1 Fischer-Tropsch Synthesis

Schulz (1985) characterized the Fischer-Tropsch synthesis as the hydrogenation of carbon monoxide in a heterogeneously catalyzed reaction over a metal catalyst, which can adsorb CO dissociatively and catalyses C-C coupling. The Fischer-Tropsch synthesis product spectrum consists of a complex mixture of linear and branched hydrocarbons and oxygen containing product compounds. The main products are linear olefins, mainly α-olefins, and n-paraffins (van der Laan and Beenackers, 1999). Some of the overall reactions, which can take place under conditions of the Fischer-Tropsch synthesis (FTS), are summarized in Table 1.1.

A number of other reactions may take place during the Fischer-Tropsch synthesis, besides the formation of organic product compounds, (olefins, paraffins and oxygenated compounds, such as alcohols), such as the water gas shift reaction yielding CO_2, oxidation/reduction/carburization of the catalyst and carbon deposition through the Boudouard reaction (see Table 1.1).

Table 1.1: Reactions taking place during the Fischer-Tropsch synthesis.

Main reactions	
1. Olefin formation	$2nH_2 + nCO \rightarrow C_nH_{2n} + nH_2O$
2. Paraffin formation	$(2n + 1)H_2 + nCO \rightarrow C_nH_{2n+2} + nH_2O$
3. Alcohols	$2nH_2 + nCO \rightarrow C_nH_{2n+2}O + (n - 1)H_2O$
4. Water-gas-shift reaction	$CO + H_2O \leftrightarrows CO_2 + H_2$
5. Catalyst oxidation/reduction	(a) $M_xO_y + yH_2 \leftrightarrows yH_2O + xM$
	(b) $M_xO_y + yCO \leftrightarrows yCO_2 + xM$
6. Bulk carbide formation	$2yCO + xM \leftrightarrows M_xC_y + y\ CO_2$
7. Boudouard reaction	$2CO \rightarrow C + CO_2$

1.1.1 Reactor and Process Development

The basic Fischer-Tropsch reaction can be viewed as:

$CO + 2H_2 \rightarrow (CH_2) + H_2O$ (ΔH_R (250 °C) = -140 to -160 kJ/mol be consumed)

with the CH_2 units subsequently forming a range of hydrocarbons. The heat released per mole of CO consumed averages at about 150 kJ (Anderson, 1956; Dry, 1996). Rapid removal of this heat is a major consideration in the design of suitable reactors for the Fischer-Tropsch synthesis. The objective is to minimize the temperature rise within the catalyst bed. This requires rapid heat removal in the direction perpendicular to the flow of the reactants.

One approach is to pack the catalyst particles into narrow tubes (see Figure 1.1), which are surrounded on the outside by boiling water. Synthesis gas is passed through the tubes at a high flow rate to decrease mass transfer limitations. This type of reactor is known as a Tubular Fixed Bed Reactor. The use of the narrow tubes ensures that the distance between the hot catalyst particles and the heat exchanger surface is short. Furthermore, the ratio of the heat exchanger surface area to the catalyst mass is then high ensuring effective heat transfer out of the reaction zone. This type of reactor was first introduced in Germany in 1936. Thereafter Ruhrchemie and Lurgi jointly developed the ARGE reactors. The first commercial ARGE reactors were commissioned at Sasol One site in 1955 and are still in operation (Dry, 1996).

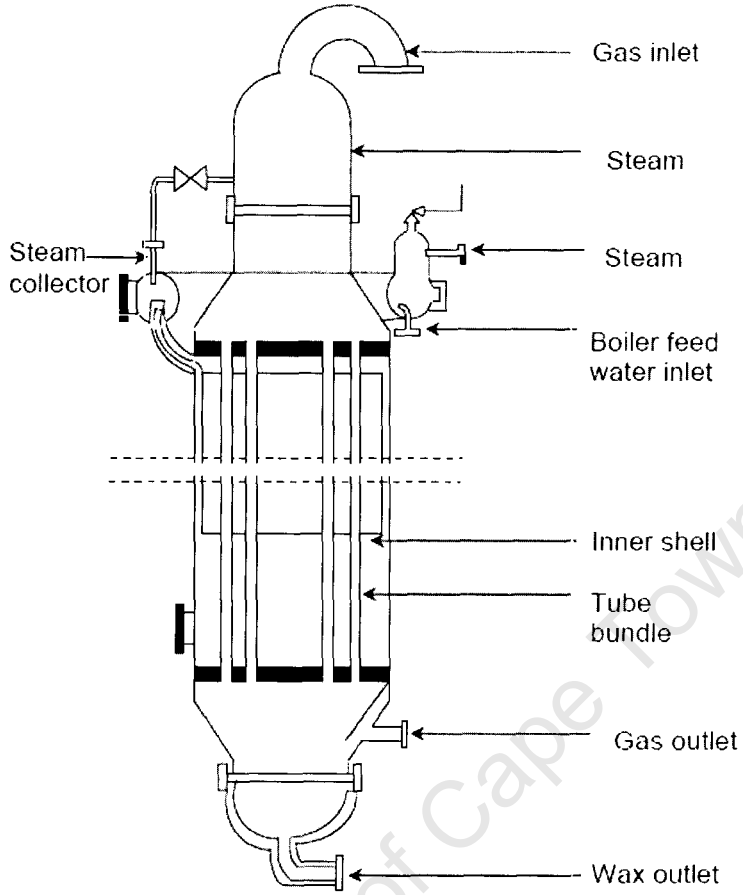

Figure 1.1 : Schematic drawing of the ARGE multi tubular fixed bed reactor for the Fischer-Tropsch synthesis (Steynberg et al., 2004).

The multi tubular fixed bed reactors are simple to operate (Dry, 1996). Furthermore, they can be used over wide temperature ranges irrespective of whether the FT products are gaseous or liquids, or both, under reaction conditions. Furthermore, separating liquid products from the catalyst is not problematic with this type of reactor. There are however many economic disadvantages in using multi-tubular reactors. They are expensive to construct. Furthermore, the high gas flow rate through the packed bed results in a high differential pressure over the reactor leading to high compression costs, if unconverted synthesis gas is to be recycled (which is usually the case). Larger catalyst particle sizes need to be implemented to minimize pressure drop at the

cost of increasing mass transfer limitations. The catalyst, which looses its activity with time on stream, has to be replaced periodically.

The slurry phase reactor (see Figure 1.2) was developed by Sasol. It is much simpler than the tubular fixed bed reactor and 40% less expensive to fabricate (Espinoza et al., 1999). It consists of a shell fitted with cooling coils in which steam is generated. Synthesis gas is distributed at the bottom and it rises through the slurry. The slurry consists of liquid reaction products, predominantly wax, with catalyst particles suspended in it.

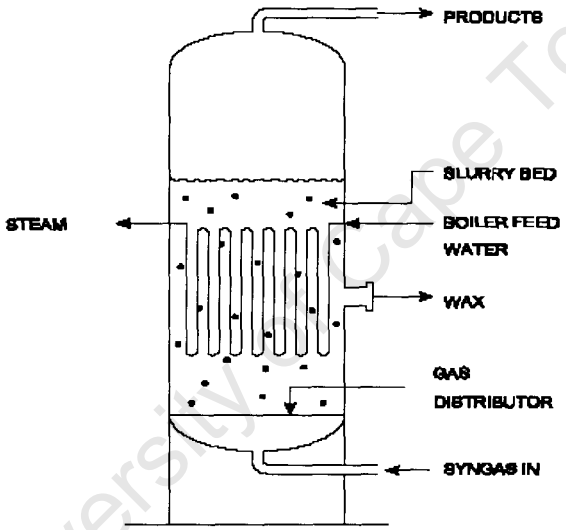

Figure 1.2: Schematic drawing of the slurry bed reactor for the Fischer-Tropsch synthesis (Steynberg et al., 2004).

Kölbel and co-workers did a considerable amount of work on the concepts of slurry bed reactors from the 1950's to the late 1970's (Kölbel and Ralek, 1980). Isothermal conditions are maintained much better in the slurry bed than in a multi-tubular fixed bed reactor, because the heat of reaction is removed by circulating the slurry through external heat exchangers or by heat exchangers immersed directly into the slurry bed. The pressure drop over the slurry bed is significantly lower, which translates to lower compression costs. The reactor can

stay on-line for longer times than the tubular fixed reactors, if the catalyst can be replaced on-line.

The Synthol or Circulating Fluidised Bed reactors (see Figure 1.3) are still being used commercially in South Africa and have a long history of continuous development and improvement (Dry, 1981). With this set-up the catalyst powder flows down a standpipe as a dense phase aerated powder. Pressure builds up on going down the standpipe to give the highest pressure in the system at the bottom. The catalyst flows through a slide valve and is picked up by the high velocity synthesis gas stream and is carried into the vertical reactor section. The heat of reaction is removed from the reactor section by cooling coils. On leaving the reactor section, the catalyst passes through the upper transfer bend into a hopper and flows down the standpipe. Although the Circulating Fluidised Bed reactors have performed successfully, they are complex to operate (Dry, 1996).

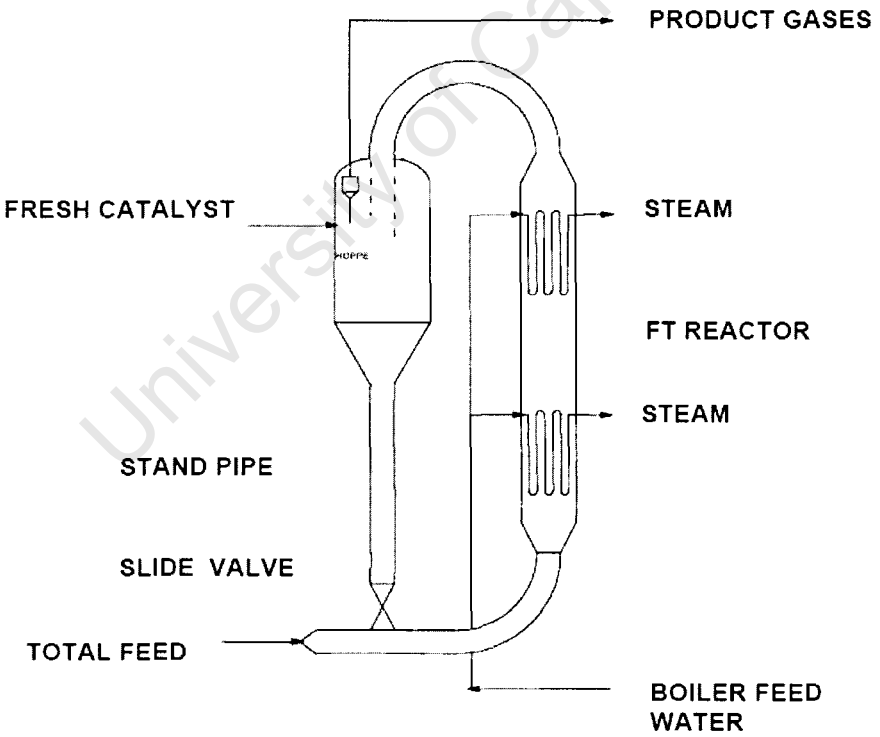

Figure 1.3: Schematic drawing of the circulating fluidized bed reactor for the Fischer-Tropsch synthesis (Steynberg, et al., 2004).

The Sasol Advanced Synthol (SAS) reactor (see Figure 1.4) is a conventional fluidized bed that may be designed to operate at pressures ranging from 20 to 40 bar and temperatures of around 340 °C using an iron catalyst similar to that used in the Circulating Fluidised Bed reactors (Steynberg, et al., 2004).

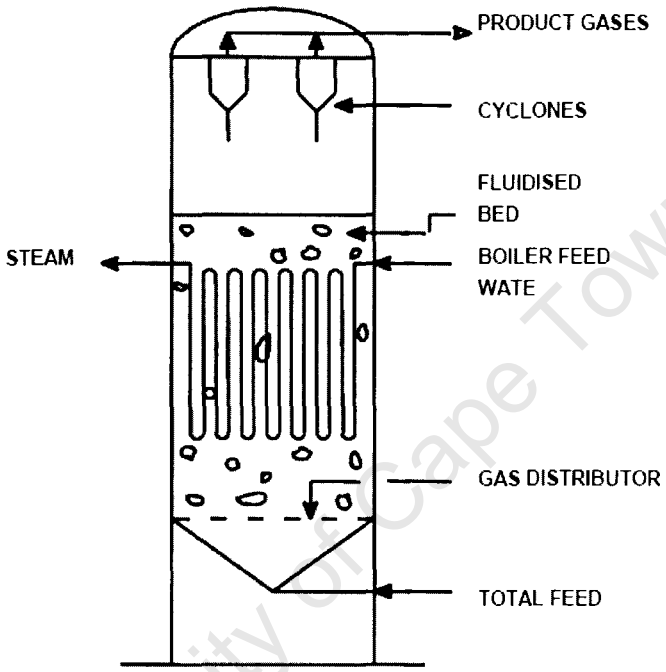

Figure 1.4: Schematic drawing of the fluidized bed reactor for the Fischer-Tropsch synthesis (Steynberg et al., 2004).

The fluidized bed reactor consists of a vessel with a gas distributor, a fluidized bed containing the catalyst, cooling coils in the bed and cyclones to separate entrained catalyst from the gaseous product stream. Sasol has recently replaced the 16 Synthol reactors at Secunda with eight SAS reactors.

The advantages of the fluidized bed reactor compared to the Synthol circulating fluidized bed reactor are numerous. The fluidized bed reactor is much cheaper to construct. Erosion problems are eliminated and therefore the need for regular

inspection/maintenance. The total amount of catalyst is in the reaction zone; therefore higher conversions are achieved (Dry, 1996).

1.1.2 Mechanisms describing Fischer-Tropsch Synthesis

The Fischer Tropsch synthesis is a polymerization reaction (Anderson, 1956; Schulz et al., 1988) which will have three different types of reactions viz., generation of a chain initiator, chain growth or propagation and chain growth termination or desorption. Various mechanisms have been put forward to explain the conversion of synthesis gas into higher hydrocarbons.

1.1.2.1 The 'Alkyl' (or Carbide) Mechanism

The alkyl mechanism is currently the most widely accepted mechanism for chain growth in the FT synthesis. Fischer and Tropsch (1926) first suggested the carbide theory, which was later elaborated by Craxford (1939).

According to this mechanism, the first step in the process is the dissociation of carbon monoxide on the catalyst surface, corroborated by Araki et al. (1976) and Sachtler et al. (1979). CO adsorbs chemically onto an active site, and can dissociate and subsequently be hydrogenated. Blyholder (1964) postulated that CO is bonded to the metal surface in a carbon-down position with its molecular axis perpendicular to the surface. C-O bond cleavage is obtained by electron donation into the 2 π^* antibonding orbital of the CO molecule.

Surface oxygen is removed from the surface by reaction with adsorbed hydrogen yielding water or with adsorbed carbon monoxide yielding CO_2 (Claeys and van Steen, 2004). Surface carbon is subsequently hydrogenated yielding in a consecutive reaction CH, CH_2 and CH_3 surface species.

The existence of CH, CH_2 and CH_3 has proven by employing mass spectroscopy during the hydrogenation of carbon monoxide over a nickel catalyst (Kaminsky et al., 1986).

Chain growth can take place by the combination of a surface alkyl group with a reactive surface carbon, CH-species or CH_2-species, which results in the formation of the species **1, 2 and 3** in Figure 1.5.

Brady and Petitt (1980, 1981) showed the involvement of surface CH_2-species in the chain growth process. Diazomethane was converted in the presence and absence of hydrogen over transition metal catalysts. Ethene was the only product formed in the absence of hydrogen implying a CH_2-coupling and subsequent desorption. A product spectrum similar to the one obtained in the Fischer-Tropsch synthesis was observed when hydrogen is present. This shows that CH_2 surface species can act as the monomer or are involved in the formation of monomer species for the formation of long chain hydrocarbons.

Branched compounds may occur if species **2** combines with an adsorbed methyl species, which will result in the formation of species **4**.

During the termination steps adsorbed alkyl species can either desorb as olefins by β-elimination or it can be hydrogenated yielding a paraffin, (see Figure 1.5).

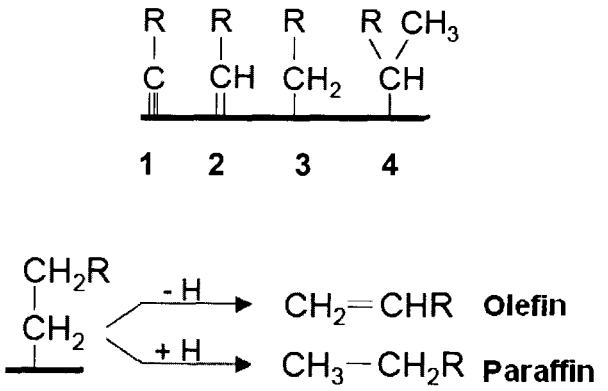

Figure 1.5: 'Alkyl' mechanism (Claeys and van Steen, 2004).

1.1.2.2 Enol Condensation Mechanism

Storch et al. (1951) suggested that the C-C bonds are formed through a condensation reaction between hydroxyl-methylene groups on the catalyst surface, see Figure 1.6. Chain growth is assumed to occur by hydrolysis of one of the carbon-metal bonds, thus allowing chain growth. Termination of the chain growth process or desorption yield oxygenates (aldehydes and alcohols) and α-olefins. According to this mechanism n-paraffins are formed secondarily by hydrogenation of primarily formed olefins. An alternative reaction pathway is required for the primary formation of n-paraffins.

Initiation:

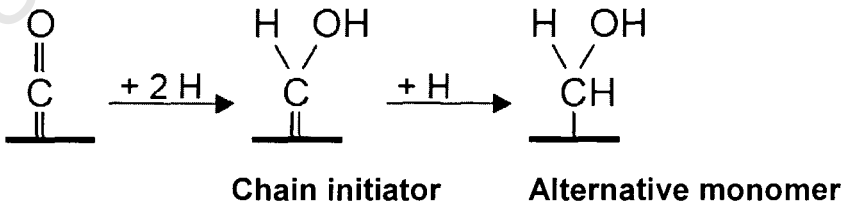

Propagation:

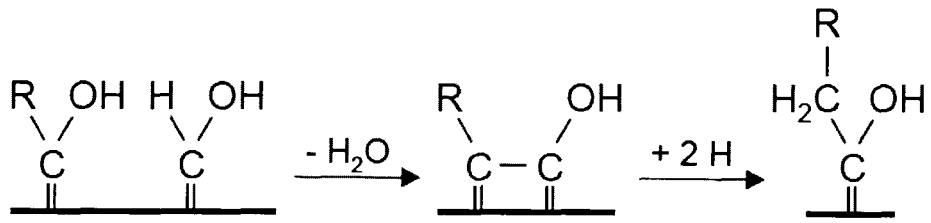

Termination/desorption:

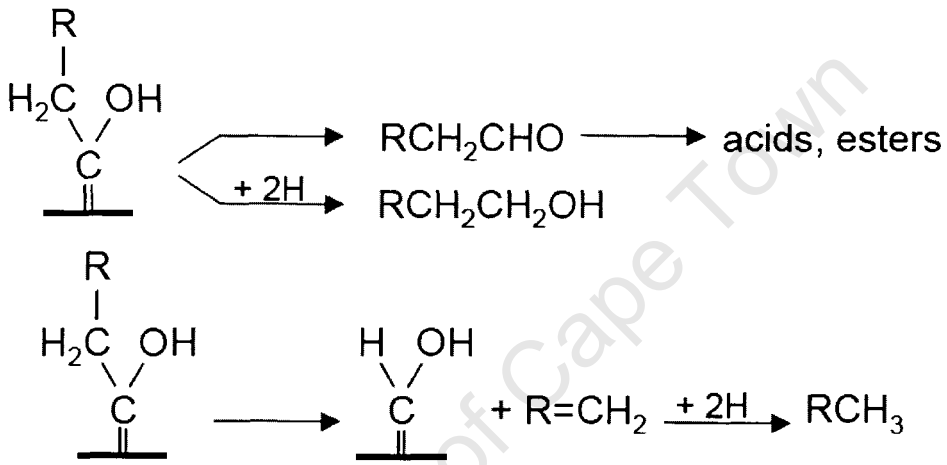

Figure 1.6: Enol condensation mechanism (according to Storch et al., 1951).

1.1.2.3 CO Insertion Mechanism

Pichler and Schulz (1970) suggested that chain growth takes place by CO-insertion in a metal-alkyl bond analogous to the well-known insertion of CO in homogeneous systems. Various reaction pathways are proposed for product desorption, (see Figure 1.7).

Initiation:

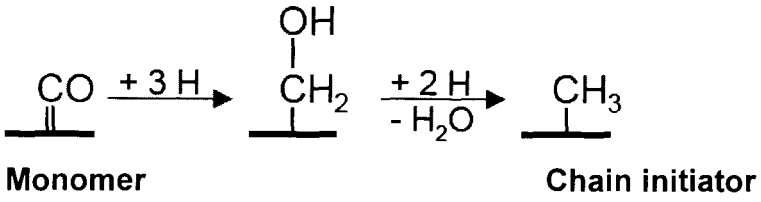

Propagation:

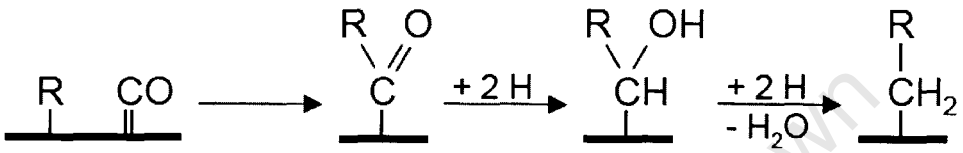

Termination/desorption:

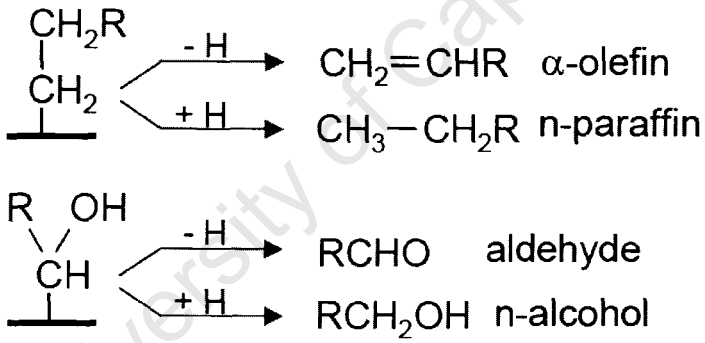

Figure 1.7: CO Insertion Mechanism (proposed by Pichler and Schulz, 1970).

1.1.3 Product distribution

The Fischer-Tropsch synthesis can be viewed as a non-trivial surface polymerization (Schulz et al., 1988a, 1988b, 1988c, 1994). The molar amount of products in individual carbon number fractions declines exponentially with carbon number (Schulz et al., 1988a). This is characteristic for a polymerization

reaction, proceeding via stepwise addition of a C_1 monomer. Figure 1.8 gives the polymerization growth scheme, which occurs on the surface of the catalyst.

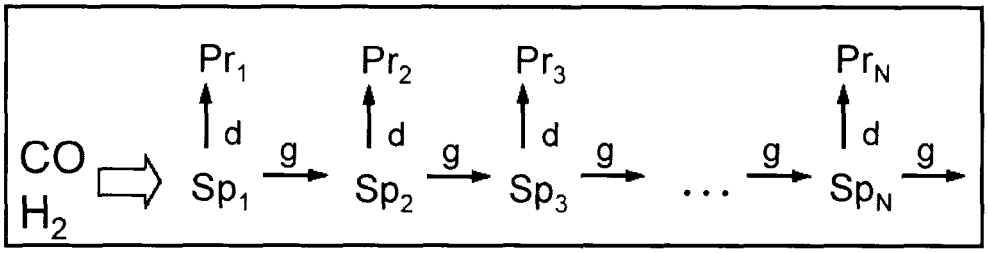

Figure 1.8: Ideal chain growth and formation of one sort of products (Schulz et al., 1988a).

Carbon monoxide and hydrogen are adsorbed on the catalyst surface. After dissociation monomers and chain starters (C_1 surface species, Sp_1) are formed. The surface species Sp_1 can desorb to form a C_1 products molecule (Pr_1) or grow via insertion of a C_1 monomer. The ideal case, the chain growth probability of a surface species (i.e. the rate of chain growth relative to the rate of chain growth plus the rate of desorption, p_g) can be viewed to be independent of carbon number. The chain growth probability p_g, is often referred to as α. The molar product distribution may then be presented as:

$$x_N = (1-p_g) \cdot p_g^{N-1}$$

When plotted straight lines are observed as in figure 1.9 and the chain growth probabilities can be determined from their slope it is presented as:

$$\lg x_n = \lg \frac{(1-p_g)}{p_g} + n \cdot \lg p_g$$

Figure 1.9 shows in a semi-logarithmic plot the molar product distributions as a function of carbon number with different chain growth probabilities. These plots are called Anderson-Schulz-Flory (ASF) distributions, which are typically used to characterize FT synthesis product spectrum.

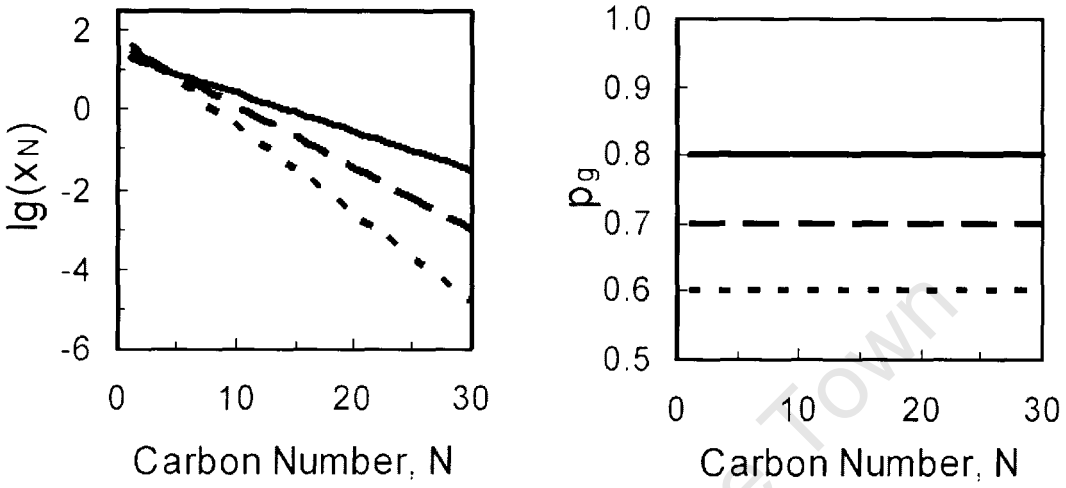

Figure 1.9: Ideal product distribution (Claeys and van Steen, 2004)
Left: logarithmic molar product content versus carbon number (ASF)
Righ: corresponding chain growth probabilities

The Anderson-Schulz-Flory distribution of the product formation put constraints on the selectivity, which can be obtained for a certain class of products on a weight basis (see Figure 1.10). Methane can be produced with selectivity of 100 wt.%, at a chain growth probability of 0 (methanation). The maximum middle distillate yield ($C_{10} - C_{20}$) is ca. 40 wt.% and can be obtained at $p_g \approx 0.85$. Thus, maximizing the selectivity of a certain class of products will be limited by the chain growth probability.

According to the model of the non-trivial surface polymerization (Schulz et al., 1988b), each species Sp_n can desorb as an olefin, paraffin or oxygenate. In the ideal case, the desorption for a given product class is independent of carbon number. The primary probability for desorption as an olefin is believed to be

independent of carbon number and between 0.7-0.9 (Claeys and van Steen, 2004). Deviations from the ideal distribution are obtained, when secondary reactions convert primarily formed product compounds, such as olefins. It could be argued that the longer the residence times the greater the likelihood that primary alkenes will undergo secondary reactions. This concurs with the observed decrease of the alkene/alkane ratio of the products with increasing carbon number (Dry, 2004b).

Secondary reactions of an alkene requires the re-adsorption of the alkenes onto the catalyst. Chain growth probability for the 'CH_2' surface species is lower, and that of the 'C_2H_4' species is higher, than for the higher carbon number surface species. It is possible that an isolated methylene unit (CH_2) on the catalyst surface is more likely to be hydrogenated to methane than re-adsorbed alkenes to the corresponding alkanes (Dry, 2004b). .

The Anderson-Schulz-Flory equation presents a straight line when plotting the molar product fractions (W_N/N) logarithmically over the carbon number; the slope reflects the chain growth probability. Real Fischer-Tropsch products often deviate from this behaviour (Claeys and van Steen, 2004).

The lower than expected C_2 production, i.e. the higher probability of chain growth, may be due to the likelihood that an adsorbed methylene group can attach itself to a re-adsorbed ethene specie. For C_3 and higher re-adsorbed alkene species, the methylene group, can attach itself to the alkene species more readily form one side than from the other due to steric hindrance.

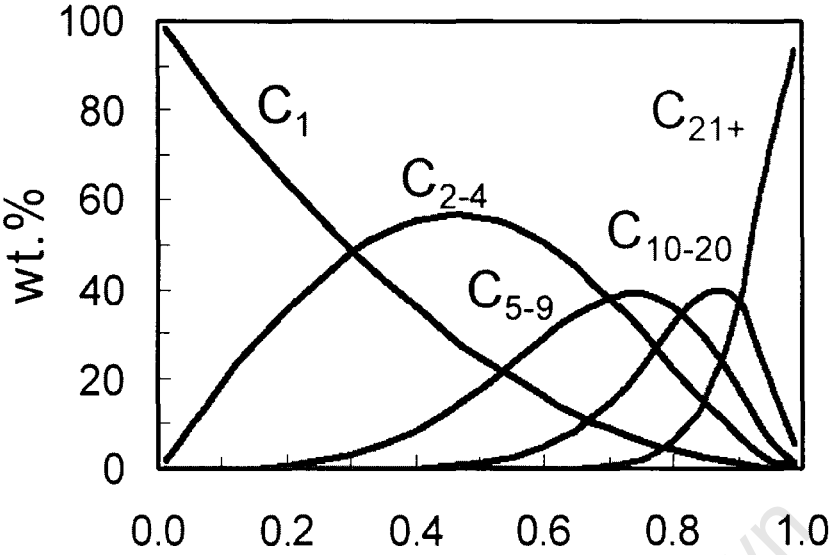

Figure 1.10: Product composition as function of chain growth probability (ASF kinetics) (Claeys and van Steen, 2004).

1.1.4 Water-Gas Shift Activity

The generation of organic product compounds in the Fischer-Tropsch synthesis is generally associated with water as a co-product (see Table 1.1; van der Laan and Beenackers, 1999). With some catalysts, especially iron-based catalysts, CO_2 is formed as well. The formation of carbon dioxide can be viewed as a separate reaction, the water-gas shift reaction.

$$CO + H_2O \rightarrow CO_2 + H_2 \qquad (\Delta H_R(250\ ^{\circ}C) = -40\ kJ/mol)$$

The water-gas shift (WGS) reaction allows usage of syngas with H_2/CO-ratio of less than 2. The Fischer-Tropsch product selectivity over different catalyst is not always simply related to a single factor such as the H_2/CO ratio within the catalyst bed, but that the actual partial pressures of CO, H_2, CO_2 and H_2O or some more complex ratio of these partial pressures may be involved (Dry, 1981). It may reach equilibrium at high temperatures on catalysts with a high water-gas shift activity (Hindermann et al., 1993). The formation of carbon dioxide is especially pronounced with iron-based catalysts. The water-gas shift reaction

might be taken place on a different site e.g. magnetite (Fe_3O_4) is the most active phase for the WGS reaction on iron catalysts (Hindermann et al., 1993), whereas iron carbide is thought to be the active phase for the formation of hydrocarbons (Dry, 1981).

Iron is an active catalyst for water gas shift (WGS) reaction, whereas cobalt is not (Dry, 2004b). At low temperatures the WGS is far from equilibrium, and there is much more water present than CO_2 (Dry, 2004b). This observation supports the concept that water is the primary product of Fe Fischer-Tropsch synthesis and carbon dioxide is the result of the subsequent water gas shift reaction and not the result of CO reacting with free O atoms on the catalyst surface.

1.2 Effect of reaction conditions on product selectivity

1.2.1 Effect of catalyst pretreatment

The pre-treatment of the catalyst defines the initial stage of the catalyst, from where the steady-state catalyst will be developed. A high temperature pre-treatment is expected to reduce the surface area of the catalyst and thus reduce the activity of the catalyst (with all associated consequences for the selectivity).

Pretreatment conditions of promoted iron catalysts on the hydrocarbon selectivity and activity were studied by Bukur and co-workers (1995). Figure 1.11 shows the effect of pretreatment conditions on the hydrocarbon selectivity. Reduction at 280 °C causes a shift to products with higher carbon number relative to reduction at 250 °C. Reduction with CO or carbon monoxide was reported to enhance the olefin selectivity.

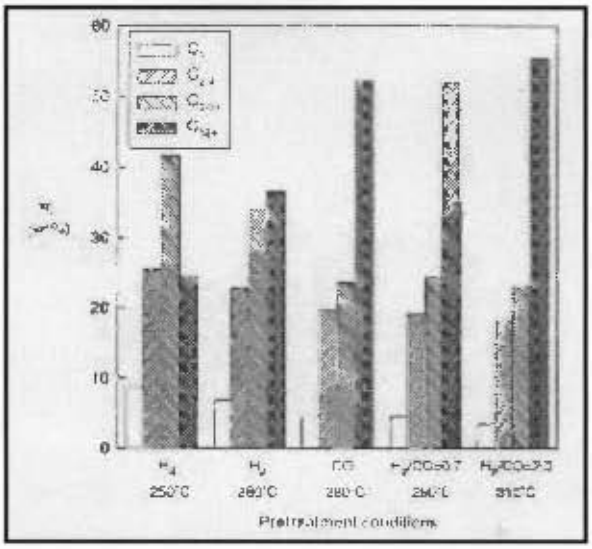

Figure 1.11: Effect of pretreatment conditions on the hydrocarbon selectivity on a promoted iron catalyst (van der Laan and Beenackers, 1999).

1.2.2 Effect of time on stream

Catalysts can deactivate during the Fischer-Tropsch synthesis. This will affect the selectivity to hydrocarbon products. According to Donnelly and Satterfield (1989) the selectivity to oxygenates increases after a period of 1300 h time-on-stream with a precipitated promoted iron catalyst. An increase of the methane selectivity and low-molecular-weight products is observed on iron catalysts (Bukur et al., 1990). The change in selectivity with time-on-stream might be caused by the formation of carbonaceous deposits on sites with potassium promoters (Dry, 2004a).

1.2.3 Effect of space velocity

The extent of secondary reactions is minimized with increasing space velocity. Thus, the selectivity for primary products, such as olefins, will increase with increasing space velocity. Bukur et al. (1990) observed the increase of the olefin-to-paraffin ratio with increasing space velocity on a commercial supported iron catalyst ($Fe/Cu/K/SiO_2$). With cobalt-based catalysts the average molecular

weight of the products decreases with increasing space velocity, whereas the selectivity toward paraffins remains unchanged (Iglesia et al., 1993). Thus, for e.g. optimal C_6-C_{12} olefin selectivity, the space velocity needs to be optimized, if the change in the chain growth probability observed by Iglesia et al. (1993) for cobalt-based catalysts can also be observed for iron-based catalysts.

It should be kept in mind that with increasing space velocity the overall conversion will decrease. Thus, the optimum productivity for C_6-C_{12} olefins will be a function of the decrease in secondary olefin reactions and of the decrease in the overall conversion with increasing space velocity.

1.2.4 Effect of partial pressure of H_2 and CO

The reaction kinetics is primarily governed by the partial pressures of the kinetically relevant compounds, such as hydrogen and carbon monoxide.

Most studies show, that product selectivity shifts to heavier products and to more oxygenates with increasing total pressure (Dry, 2004a). The increase in H_2/CO ratios in the reactor, result in lighter hydrocarbons and a lower olefin content. According to Donnelly and Satterfield (1989) the olefin-to-paraffin ratio decreases form 6 to 1 by increasing H_2/CO ratio from 0.3 to 4. Thus, to maximize the olefin selectivity a high pressure and a low H_2/CO-ratio should be applied.

1.2.5 Effect of reaction temperature

An increase of temperature results in a shift toward products with a lower carbon number on iron catalyst (Dictor and Bell, 1986). Higher temperatures should increase the rate of desorption which would then result in a shift to lower molecular mass products (Dry, 2004). They observed an increase of the olefin-to-paraffin ratio on potassium-promoted precipitated iron catalysts with increasing temperature. However, they reported a decrease of the olefin selectivity with increasing temperature for un-alkalized iron oxide powders. The latter might be

attributed to a larger extent of secondary olefin hydrogenation. Thus, maximizing the olefin selectivity in the range of C_6-C_{12} requires an optimization with respect to temperatures.

1.3 Catalyst for the Fischer-Tropsch synthesis

Vannice (1975) tested the activity of group VIII metals for their activity and selectivity in the Fischer-Tropsch synthesis. The most active and selective metals were Co, Ru and Fe.

1.3.1 Cobalt catalyst

Cobalt is an active FT-catalyst with high chain growth probability and a low branching probability (Schulz et al., 1994). Because of the high cost of cobalt it is important to minimize the cobalt content and at the same time have a high cobalt metal surface area. This can be achieved by putting cobalt on stable oxide support materials having the required surface area and pore size distribution (Dry, 2004a).

Cobalt based catalysts are in general not very sensitive to the chemical nature of promoters of supports (Dry, 2004a). Alkali promotion on a supported cobalt catalyst operated at atmospheric pressure increased the selectivity of the wax. The early German studies with cobalt supported on kieselguhr, when operating at atmospheric pressure the alkali increased the selectivity of the wax. At pressures above 1.5 MPa (pressure preferred for industrial Fischer Tropsch plants), the effect of alkali promoter was minimal.

1.3.2 Iron catalyst

Iron catalysts have been used industrially, because of their low cost (Dry, 2004a). Industrially applied iron-based catalysts are either (co-)precipitated or fused iron-based catalysts.

The iron catalyst is typically promoted with a structural promoter to enhance the mechanical strength and reduce sintering of the catalyst. Furthermore, potassium is added to the catalyst to enhance the activity and selectivity of iron-based catalysts.

The yield of olefins is usually larger with iron-based catalysts than with cobalt-based catalysts (Schulz et al., 1994).

1.3.2.1 Active phase in iron-based Fischer-Tropsch catalysts

A number of phases can be present in iron-based Fischer-Tropsch catalysts (Dry, 2004a). These include metallic iron (α-Fe), iron oxides (hematite, α-Fe_2O_3; magnetite Fe_3O_4, and Fe_xO), and different forms of iron carbides, O-carbides (ε-Fe_2C, ε'- $Fe_{2.2}C$, and Fe_xC), and TP-carbides, χ-$Fe_{2.5}C$ and Fe_3C. The formation of these iron phases as a function of time on stream depends on the process conditions, catalyst deactivation, and catalyst composition.

Dictor and Bell (1986) concluded that a mixture of χ- and ε'-carbides is the active phase in iron catalysts. Zhang and Schrader (1985) concluded that two active sites operated simultaneously on the surface of iron catalysts: Fe^0/Fe-carbides and Fe-oxide (Fe_3O_4). The carbide phase is active toward dissociation of CO and formation of hydrocarbons, whereas the oxide phase adsorbs CO associatively and produces predominantly oxygenated products.

1.3.2.2 Chemical promoters for iron-based catalysts

Chemical promoters affect electronic properties of catalytically active material, (e.g. alkali added to Fe catalysts or Cu as a reduction promoter). Iron based catalysts contain potassium as promoter to improve activity and selectivity (Yang et al., 2004).

Potassium donates electrons to iron and facilitates CO chemisorption, since CO tends to accept electrons from iron (Yang et al., 2004). Thus, the promotion of iron-based catalysts with potassium enhances surface coverage with C and decreases the coverage with H. Potassium increases the selectivity of olefins, suppresses the formation of methane, shifts the product distribution to higher molecular products, increases the activity of WGS and influences the FTS activity (Yang et al., 2004).

According to the heats of adsorption of CO, CO_2 and H_2, as the alkali lowers the heat of hydrogen adsorption the coverage of the surface by hydrogen would be expected to be lowered. The alkali should therefore depress the hydrogenation on the surface and chain termination results from the hydrogenation of the iron-carbon bond, which should therefore enhance the statistical probability of continued chain growth (Dry et al. 1969). Bonzel and Krebs (1982) claimed that potassium lowered the methane formation rate and increased the carbon deposition rate. It was found that the deposited carbon was covered by potassium compounds rather than sitting on top of the promoter, implying that potassium in the catalyst is mobile.

Dry (2004b) reported the effect of K_2O on iron-based catalysts (see Figure 1.12). The activity of the unsupported iron-based catalyst increases with increasing amount of alkali up to a relative level of 2. Increasing the alkali content further, leads to a decrease in the catalyst activity.

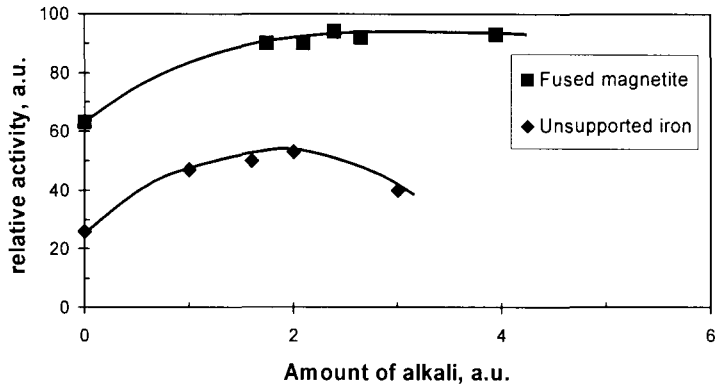

Figure 1.12: Effect of potassium on activity of iron-based catalysts (230 °C; $H_2/CO = 2$; 1.8 MPa) (drawn with data from Dry, 2004b).

Figure 1.13 shows the effect of potassium promotion on the methane selectivity (top) and the olefin selectivity (bottom). With increasing potassium content in the catalyst, the methane selectivity decreases and the olefin content increases.

The observed changes in the selectivity are consistent with the above stated effect of potassium promotion, i.e. facilitating CO adsorption and dissociation of the C-O bond, thereby lowering the strength of the metal-hydrogen and the metal-oxygen bond and leading to an enhanced surface coverage with carbon and reduced coverage with surface hydrogen. The reduced coverage with hydrogen lead to a smaller probability for desorption as a paraffin, and thus also of methane.

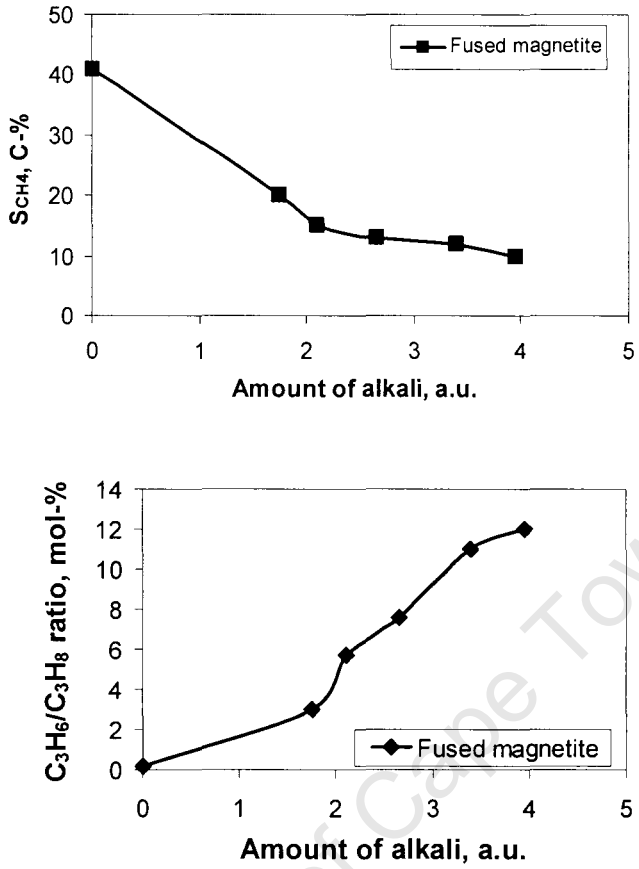

Figure 1.13: Effect of potassium on selectivity of iron-based catalysts (drawn with data from Dry, 2004b) (Fluidized bed operation at 330 °C)
Top: Methane selectivity
Bottom: Olefin to paraffin ratio

Luo et al. (2003a) investigated the effect of potassium loading on a precipitated iron catalyst (100 Fe/4.6 Si/2.0 Cu – atomic ratios) in a slurry reactor. Similarly to Dry (2004b), they observed an strong increase in the catalytic activity up to a potassium loading of 5 K/100 Fe, after which the activity remained constant. Furthermore, the chain growth probability increased up to a loading of 5 K/100 Fe. Beyond a loading of 5 K/100 Fe, Luo et al. (2003a) did not observe a change in methane and CO_2 selectivity, possible reason could be that they reached their potassium optimum (already at plato) (see Figure 1.14).

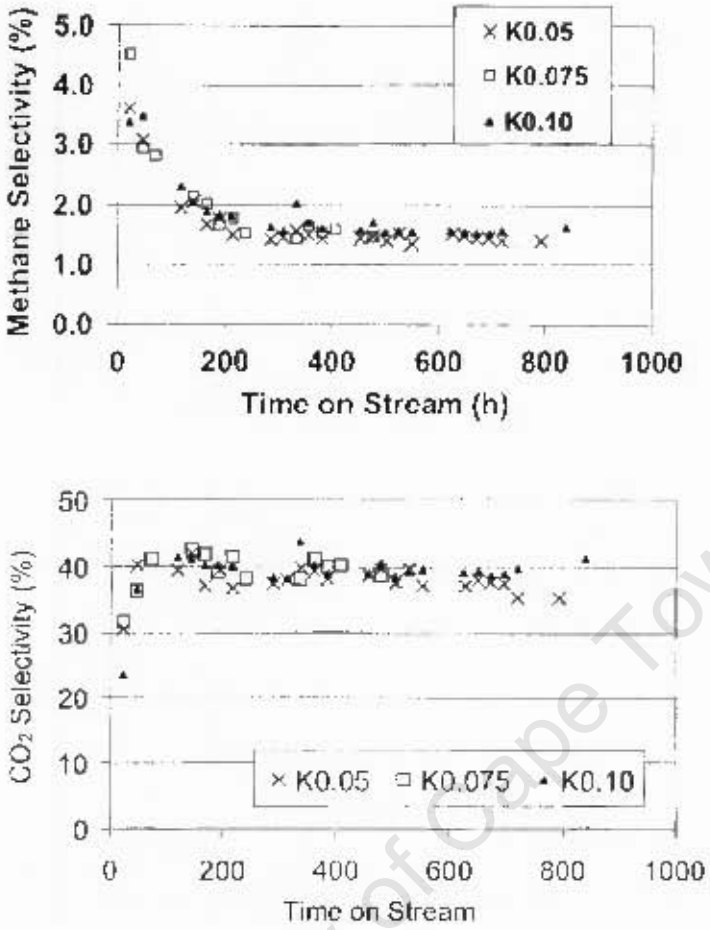

Figure 1.14: Effect of potassium loading on a precipitated iron catalyst (100 Fe/4.6 Si/2.0 Cu) on methane selectivity (top) and CO_2-selectivity (bottom)(T = 230 °C, P =1.20 MPa, H_2/CO = 0.67 (extracted from Luo et al., 2003a).

Dry (2004b) reported that potassium as a promoter shows a greater effect than sodium. which might be due to the solubility of sodium in the magnetite phase and/or due to the higher basicity of potassium.

Luo and Davis (2003b) investigated the behaviour of Group II earth-alkali metals as promoters for an iron-based Fischer-Tropsch catalyst (100 Fe/4.6 Si/2.0 Cu – atomic ratios). Figure 1.15 shows the effect of the type of promoter on an iron-based catalyst for its activity in the Fischer-Tropsch synthesis. Potassium

promotes the CO-conversion, whereas e.g. Mg promoted catalyst yielded CO conversions similar to the un-promoted catalyst. None of the earth-alkali metals enhanced the activity in the Fischer-Tropsch synthesis significantly and calcium even seems to have a negative effect on the activity.

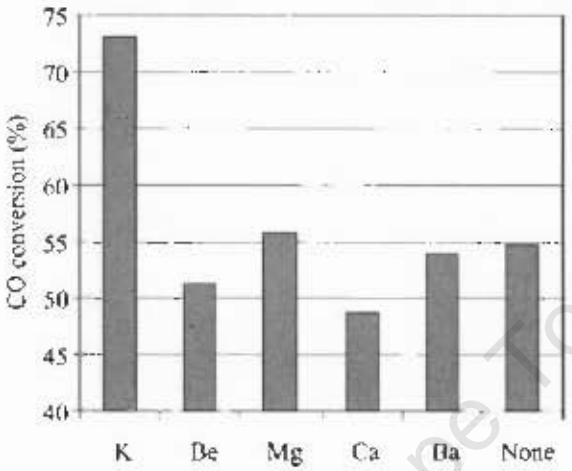

Figure 1.15: Effect of earth-alkali metal promoter on iron catalyst activity for CO conversion (T = 270 °C, P= 1.3 MPa, H_2/CO = 0.7, 10 SL/h g-Fe, Promoter : Fe = 1.44 : 100) (Luo and Davis, 2003b).

1.3.2.3 Structural promoters and supports for iron-based catalysts

The bulk iron based catalyst (precipitated or fused) has low mechanical strength, thus structural promoters need to be added (Dry, 2004a). Furthermore, structural promoters and support materials will reduce sintering of the catalyst. Upon activation of iron-based catalyst a large extent of shrinkage takes place, which makes operation in fixed bed reactors problematic. This can be avoided by supporting the catalytic active material

A supported iron catalyst has a carrier which functions as a support for the metal. The carrier has to have a high surface area for high dispersion of the metal as well as the right pore size to allow easy diffusion of the feed molecules into the

catalyst (Dry, 2004a). The support will increase the mechanical strength and reduce sintering.

Structural promoters enhance the surface area of the active metal compound by dispersing the metal. Typical structural promoters added to the catalyst formulation are SiO_2, Al_2O_3. The addition of these compounds to the catalyst may lead to the formation of support-metal compounds, which cannot be reduced easily. Furthermore, these materials will react with the promoter added to the Fischer-Tropsch catalyst (Dry, 2004b).

In the presence of silica the alkali can react with it to form alkali-silicates which will be less basic (alkaline) than the 'free' alkali and hence the basicity of the working iron surface would be lowered (Dry, 2004b). The amount of alkali that has to be added in order to attain the required basicity of the iron surface needs to be adjusted to take into account the chemical nature and the surface areas of the other components present.

Herranz et al. 2006, prepared a series of silica-supported iron samples by the micro-emulsion technology method and some catalyst was promoted with potassium. Fe content was set to a final value of 5 wt-% in all samples. For FeSi-2, the micro-emulsion containing the oxide precursor was added to the ammonia micro-emulsion. After stirring, the silica suspension was added and the mixture was stirred. The same method used to prepare FeSi-2 was used to prepare 95FeSi-CuK and potassium was added to this sample by wet impregnation. Table 1.2 shows the catalytic performance in the CO hydrogenation reaction.

Table 1.2: Catalytic performance in the CO hydrogenation reaction (T = 573 K, P= 1.01 MPa, H_2/CO = 2, GHSV = 0.0021 L/g/s). (Herranz et al., 2006).

					Product selectivity (%) CO_2 free				
Catalyst	CO conversion (%)	Olefin/Paraffin ratio	α	CO_2 (%)	Oxygenates	CH_4	C_2-C_4	C_5-C_{12}	C_{13+}
MF Fe-Si[a]	5.2	0.9	0.55	7.2	1	24.9	49.4	24.7	0
FeSi-2	13.5	0.6	0.62	6.4	1.4	21.5	55.6	19.8	1.7
95FeSi-CuK	18.1	0.9	0.62	8.8	1.4	18.4	44.9	35.3	0

[a] Pure iron sample diluted with silica and activated in the same conditions.

It has been reported that supported iron catalysts, especially when supported over silica, exhibit a lower catalytic activity than the unsupported ones. On this study, it is remarkable that the FeSi-2 and pure iron (MF Fe-Si) catalysts exhibited a higher hydrocarbon production per gram of iron. The selectivity values were somewhat different, when taking into account the differences in carbon monoxide conversion. Thus, the olefin-to-paraffin ratio was lower in the supported catalysts (FeSi-2), while the short-chain products selectivity was higher.

The chain growth probability was similar for catalysts FeSi-2, MF Fe-Si and 95FeSi-CuK (0.55 – 0.62). The selectivity to carbon dioxide over the supported samples (FeSi-2) was low when compared with that of the pure iron catalyst (M Fe-Si). The double promoted sample 95FeSi-CuK exhibited a better catalytic performance than the un-promoted sample (FeSi-2). The hydrocarbon productivity for 95FeSi-CuK was also higher than that of the un-promoted pure iron sample (MF Fe-Si). The methane selectivity for 95FeSi-CuK catalyst was slightly lower than that of FeSi-2 catalyst and its selectivity to long-chain products was higher, especially within the gasoline fraction (C_5-C_{12}) hydrocarbons.

The FeSi-2 catalyst exhibited a higher catalytic activity per gram of iron than a pure iron catalyst (MF Fe-Si). Promotion of supported samples with copper did not have any effect on the reducibility of iron because silicon ions inhibited the

Cu promotion effect. Alkaline promotion increased the catalytic performance and the selectivity to long-chain products.

Compounds such as MgO and CaO could be used as a structural promoter/support material as well. The basic properties of these materials seem to be too weak to act as an effective promoter (Luo and Davis, 2003b), but the use of a basic material might limit the mobility of potassium as a promoter. However in the Fischer-Tropsch synthesis over iron-based catalysts carbon dioxide is formed as a co-product (van der Laan and Beenackers, 1999), which may react with these materials yielding the corresponding carbonates (see Figure 1.16).

Carbonate formation is exothermic and the likelihood for the reaction decreases with increasing temperature. At a typical Fischer-Tropsch reaction temperature of 550K, the equilibrium partial pressure of CO_2 for the formation of $CaCO_3$ equals 1.5×10^{-9} bar and for the formation of $MgCO_3$ 0.37 bar. If the partial pressure of CO_2 is larger than the equilibrium pressure, CaO or MgO can be converted into the corresponding carbonates.

The transformation of the oxide to the carbonate is accompanied by a large expansion. For example, the transformation of CaO into $CaCO_3$ is accompanied by an increase in the volume of 100%, whereas the transformation of MgO into $MgCO_3$ is accompanied by an increase in the volume of 150%. This large increase in the volume may result in particle break-up, and will lead to unstable support materials. Thus, CaO is unsuitable as a support material, whereas if MgO is used as a support material, the partial pressure of CO_2 needs to be controlled (at 550K the partial pressure of CO_2 should be kept below 0.37 bar).

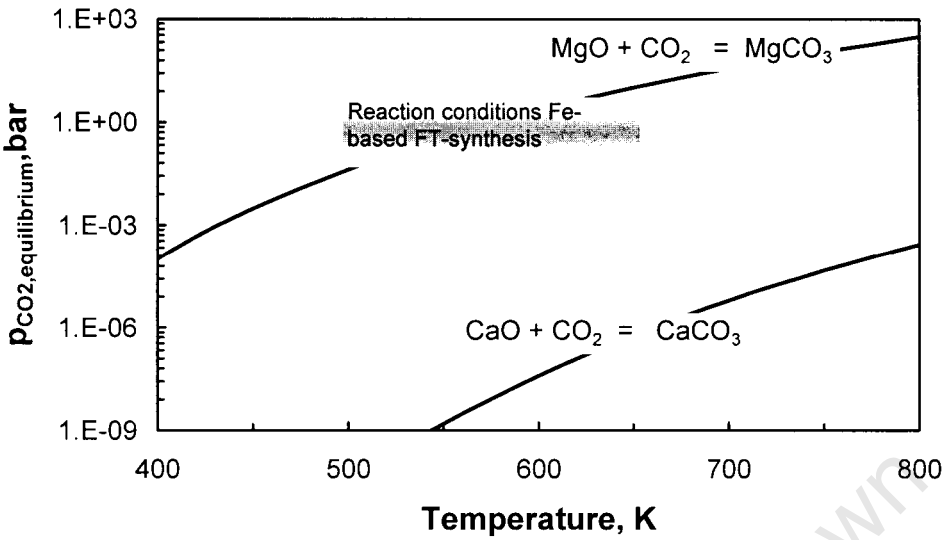

Figure 1.16: Equilibrium partial pressures of CO_2 as a function of temperature for the transformation of CaO and MgO into their respective carbonates (calculated using the data from Knacke et al., 1990).

1.3.2.4 Modified silica as a support material for iron-based Fischer-Tropsch catalysts

Sintering in a catalyst can be reduced by putting the active material on a support. However, as outlined above supporting iron-based Fischer-Tropsch catalyst on a classical support is accompanied by catalyst deactivation, due to the reactivity of the alkali promoter with SiO_2 and Al_2O_3. Classical basic supports, such as MgO and CaO cannot be used either, since they will be converted to the corresponding carbonates under realistic Fischer-Tropsch conditions.

An alternative is to create an alternative basic support. This can be achieved by attaching basic amine groups to a classical support material such as silica. The matrix of the primary silica gel particle consists of a core of silicon atoms joined together with oxygen atoms by siloxane bonds (silicon-oxygen-silicon bonds). The uncondensed hydroxyl groups confer upon silica gel its polar properties and with these hydroxyl groups the silane reagents react to form the bonded phases. The silica surface contains more than one type of hydroxyl group, strongly bound

or 'chemically' adsorbed water and loosely bound or 'physically adsorbed' water (Scott et al., 1993a).

Surface hydroxyl group can be one of three types. Firstly, a single hydroxyl group that is attached to a silicon atom which has three siloxane bonds joining it to the silica matrix. Secondly, two hydroxyl groups attached to the same silicon atom which, in turn is joined to the matrix by only two siloxane bonds (germinal hydroxyl groups). Thirdly, three hydroxyl groups attached to a silicon atom which is now only joined to the silica matrix by a single siloxane bond.

The preparative route to silylated silicon dioxide surfaces has a remarkable effect on the quality of the aminopropylalkoxysilane support (Iiskola et al., 2003). According to Iiskola et al. (2003), the densest molecular layers were achieved with γ-aminopropyldiethoxymethyksilane (APDMS) and aminopropyl-triehoxysilane (APTeS) as coupling agents, aminopropyltriethoxysilane was chosen as an example for this project because the availability of these compounds is limited. It affects the coating morphology which includes layer thickness, surface density, orientation of the surface molecules, and the type of interaction between the surface groups and the precursor molecules. The presence of water has a significant influence on the mechanism of molecular layer formation and therefore on the structure of the deposited layer.

Halasz and Sebastian (1979), made the first attempt to bond an organic group by attaching aliphatic hydrocarbon chains to the surface by means of the silicon-oxygen-carbon linkage to silica gel for chromatographic purposes. The silicon-oxygen-carbon linkage is very weak and the bonded phases may hydrolyze rapidly from the surface.

The most efficient bonded phase is one that has the minimum number of hydroxyl groups unreacted and the maximum surface coverage. Due to steric hindrance from the bonded moiety itself only a proportion of the silanol groups

can be bonded and there is little that can be done to avoid this problem. Incomplete silanization can occur as a result of the reagent molecule being excluded from the smaller pores of the silica (Scott et al., 1993b). It is therefore, important to choose a silica gel that has a relatively large pore size. This will ensure that the vast majority of the pores will be accessible to the silianizing reagent.

Silylated surfaces can be prepared in the gas or liquid phase. The ALCVD (atomic layer chemical vapour deposition) technique has found convenient for modification of the silica, since total saturation of the surface with APDMES (aminopropyldimethylethoxysilane) molecules takes place, impregnation of APDMES on the silica from the liquid phase rarely results in total saturation of the surface (Pakkanen et al., 1999). The thickness of the deposited layer is unpredictable because of uncontrolled condensation reactions. The interaction of hydrolyzed alkoxy groups and surface silanol groups through hydrogen bonds results in the formation of siloxane bonds and leads to a three-dimensional polymeric network.

The solvents normally used in liquid deposition of silanes are aromatic hydrocarbons e.g. toluene. Stringent precautions must be taken to eliminate all traces of water which may cause linear polymerization during the modification of the silica with aminopropyltriethoxysilane.

1.4 Project motivation and objectives

Motivation

Industrially applied iron-based catalysts are either (co-)precipitated or fused iron-based catalysts. The iron catalyst is typically promoted with a structural promoter to enhance the mechanical strength and reduce sintering of the catalyst. Furthermore, potassium is added to the catalyst to enhance the activity and

selectivity of iron-based catalysts. The yield of olefins is usually larger with iron-based catalysts than with cobalt-based catalysts.

A supported iron catalyst has a carrier which functions as a support for the metal. The carrier has to have a high surface area for high dispersion of the metal as well as the right pore size to allow easy diffusion of the feed molecules into the catalyst. Aminopropyltriethoxysilane has been used to increase the basicity of the silica surface. Potassium increase the selectivity of olefins, suppresses the formation of methane, increase the formation of higher molecular products, increases the activity of WGS and influence the FTS activity, the same results would be expected with the APTeS modified silica.

In the presence of silica the alkali can react with it to form alkali-silicates which will be less basic (alkaline) than the 'free' alkali and hence the basicity of the working iron surface would be lowered. The amount of alkali that has to be added in order to attain the required basicity of the iron surface needs to be adjusted to take into account the chemical nature and the surface areas of the other components present.

Objectives

During this project the focus was to synthesize the APTeS modified silica support with impregnation of APTeS with silica. Iron nitrate was impregnated into the support to synthesize a supported iron catalyst. Standard silica supported iron catalysts were prepared to compare the influences of the basicity of the APTeS modified silica supported iron catalyst and the potassium promotion the Fischer-Tropsch synthesis during conversion of synthesis gas.

2. EXPERIMENTAL

The fundamental objective of this study was to study the influence of the support basicity on a supported Fe/SiO_2-catalyst for the Fischer-Tropsch synthesis.

2.1 Support and Catalyst Preparation

2.1.1 Silica support

The silica (Sigma-Aldrich, particle size 60-100 mesh, surface area 300 m^2/g, pore diameter 150 Å) was pre-treated under synthetic air at a flow rate of 50 ml (NTP)/min from room temperature, heating rate of 10 °C/min to 300 °C, it was kept for 6 hrs at 300 °C and cooled down to room temperature in order to dehydroxylate silica surfaces. The sample was transferred to a dessicator; a silica gel drying agent was present in the dessicator.

2.1.2 Modified silica support

Silica was pretreated by calcinations. Silica was heated from room temperature to 300°C, heating rate of 10 °C/min where it was kept for 6hrs (flow rate: 50ml(NTP)/min). It was subsequently cooled down to room temperature in air. Six grams of silica gel was added to a mixture of 4.56 ml aminoproyltriethoxysilane (APTeS) in 100 ml dry toluene. The degree of chemical bonding is controlled by the number of surface hydroxyls if a relative excess of silane over surface silanols is used. The slurry was refluxed for 20 h under continuous stirring. The APTeS modified silica obtained was filtered, washed with 10 ml toluene, 10 ml acetone and 10 ml methanol and then dried at 120 °C for 4 hrs. Modified samples were stored in a desiccator to avoid hydrolysis of free alkoxy groups.

2.1.3 Impregnation of support material with iron

The catalyst precursor was prepared by using an incipient wetness impregnation method. For the preparation of this catalysts 7.23 g $Fe(NO_3)_3.9H_2O$ were dissolved in 20 cm^3 of deionised water. This mixture was added drop-wise to 10 g of silica support. The resulting slurry dried in a rotavaporator at 90 °C for 20min.

After drying the catalysts in the rotavaporator they were calcined in argon at a flow rate of 50 ml (NTP)/min. They were heated from room temperature to 250 °C for 6hrs (heating rate: 10 °C/min).

2.1.4 Potassium promoted catalyst precursor promoted with potassium

The catalyst made by incipient wetness impregnation method was impregnated further with an aqueous K_2CO_3 solution to yield the desired K-content in the final catalyst. The catalyst was dried at 130 °C overnight in an oven and calcined in argon at 250 °C for 6hrs (heating rate = 10 °C/min; flow rate: 50 ml(NTP)/min). Thus, catalysts with different potassium loading of K/Fe = 0.005, 0.01, 0.02, 0.04, 0.06 and 0.08 (atomic ratio) were prepared. All the catalysts were transferred to a dessicator; a drying agent was present in the dessicator.

2.2 Support characterization

2.2.1 Infrared Spectroscopy (IR)

Infra red spectra were recorded of the support and modified support using a Perkin Elmer Spectrum One within spectral range 450 – 4000 cm^{-1} and peak resolution of 5.0 cm^{-1}. Supports (silica and modified silica) were studied as a powder dispersed in a KBr pellet. The support and KBr (support:KBr was 2:1 (mass ratio)) were grind together and 3 tons of pressure was applied for 1 minute to form the pellet .

2.2.2 CHN-analysis

The carbon and nitrogen contents of aminosilane-modified silica samples were analyzed in Thermo Flash 1112 CHNS – 0 elemental analyzer. Samples were weighed to about 2 mg, wrapped in a tin capsule, then combusted in a stream of helium with a spurt of oxygen. The evolved combustion gas CO_2 is monitored by infrared detector. NO_x reduced to N_2 which was quantitatively measured by thermal conductivity. H_2O reduced to H_2 was measured by the thermal conductivity detector.

2.2.3 Thermo gravimetric analyses (TGA)

Thermo gravimetric analysis (TGA) was used to investigate the stability of aminopropyltriethoxysilane bonded to silica as a function of temperature. Thermogravimetric analysis were performed using a SDT 2960 DSC-TGA TA instrument in the temperature range 22 – 330 °C in argon (flow rate: 50 ml(NTP)/min) at a heating rate of 10 °C/min. It was kept at 100 °C for 10 min and ramped further to 330 °C.

2.2.4 Zeta Potential determination

Zeta potentials of functionalized silica particles were measured with a Malvern Zeta-sizer Nano-ZS. 0.1 g of the support (silica or modified silica) was finely ground in a pestle and mortar and suspended in 50 ml of 0.05 M KCl solution. The pH (stabilized for 15 min) of the suspension was adjusted with hydrochloric acid or potassium hydroxide and stabilized for 15 minutes. For each pH adjustment the sample cell was filled and analysed in the zeta-sizer, which was set to give 3 measurements form which an average zeta potential was determined. The zeta-sizer was operated at 25 °C, the pH was determined independently on a pH 210 Microprocessor pH meter.

2.3 Catalyst characterization

Catalyst characterization plays an important role in catalysis. The catalytic properties of a surface are determined by its composition and structure on the atomic scale. To obtain insight about the chemical and physical properties of the synthesised catalysts, the following methods were used: AAS, BET, TEM, SEM, XRD and TPR.

2.3.1 Atomic Adsorption Spectroscopy (AAS)

The catalyst was analysed using a Varian AA.30 atomic spectrometer. The catalyst was finely milled. 0.1 g of catalyst was weighed into a 250 ml Erlenmeyer flask and digested in 10 ml HCl/HF mixture (volume ratio of 4:1) and heated to boil. 10 ml of HNO_3 was added to flask and the mixture was boiled to evaporate until about 2 ml liquid remained in the flask. 5 ml of $HClO_4$ was added to the mixture and also allowed to evaporate until 2 ml of liquid was left. The sample was transfer to 100 ml volumetric flask and made up to 100 ml distilled water. The AAS data atomic spectrometer gave the concentration of iron and potassium per catalyst sample.

2.3.2 Brunauer-Emmett Teller method (BET)

The specific surface area and pore size distributions of the support and catalyst were determined via a N_2 adsorption/desorption according to BET method using a Micrometrics ASAP 2000 analyzer. 0.5 g of sample was loaded. A pre-treatment procedure was applied to remove water. The sample was kept at 90 ^{o}C for 1 hr. A constant heating rate of 10 ^{o}C/min was attained from 90 to 350 ^{o}C and kept for 4 hrs at 350 ^{o}C. The BET surface area and pore volume measurements were obtained by nitrogen physisorption at 77 K.

2.3.3 Temperature programmed reduction (TPR)

Temperature hydrogen reduction was used to investigate the reduction behaviour of the supported samples. Temperature programmed reduction was carried out in a U-type quartz reactor on a Micrometrics AutoChem 2910. The sample (≈ 50 mg) were treated under 5 %H_2/Ar gas flow at a flow rate of 50 ml (NTP)/min from 30 to 800 °C with a constant heating rate of 10 °C/min, measured by a thermocouple placed 2 mm above the sample. The consumption of H_2 was measured using a thermal conductivity detector which was calibrated using samples with known reduction behaviour of Ag_2O.

2.3.3 Transmission Electron Microscopy (TEM)

Transmission electron microscope pictures were taken using a LEO 912 EM system, which operate at 120 kV. The catalyst was finely ground and ultrasonically suspended in methanol. A drop of each sample was placed on a carbon coated copper grid. The copper grid is then covered with formvar (polyvinyl formal). The copper grid loaded with sample was taken out of the water and placed on a filter paper to dry. The samples were then viewed under Transmission Electron Microscopy under different magnifications. Transmission Electron Microscopy was applied to determine the iron particle distribution on the silica support.

2.3.4 Scanning Electron Microscopy (SEM)

Scanning electron microscope pictures were taken using a LEO S444 SEM. Scanning electron microscopy is carried out by rastering a narrow electron beam over the surface and detecting the yield of either secondary or back-scattered electrons as a function of the position of the primary beam. Back-scattered electrons come from deeper and carry information on the composition of the

sample, because heavy elements are more efficient scatters and appear brighter in the image.

Sample preparation involved sprinkling dry powder of the sample on an aluminium stub coated with glue containing graphite. Here, graphite is used to conduct electrons thereby preventing charge build up. The samples were then coated with carbon which does not interfere with the elemental analysis. The main difference between SEM and TEM is that SEM sees contrast due to the topology of a surface, whereas TEM projects all information in a two-dimensional image, is of sub nanometer resolution.

2.3.5 X-ray Diffraction (XRD)

XRD is used to identify bulk phases and to estimate particle sizes. XRD method is based on the orderliness of the repeating planes that form a particle. When X-rays are directed on the crystal, they are reflected by these ordered planes yielding a diffraction pattern unique to a specific plane. Diffraction patterns can be used to identify the various phases in a catalyst. The width of diffraction peaks carries information on the dimensions of the reflecting planes.

A Phillips X-ray diffractometer was used to obtain X-ray diffraction spectra for the different catalyst. The operational settings on the diffractometer were:

- Voltage 40 kV
- Current 20 mA
- 2θ range 20 – 80 °
- Step Width 0.02 seconds

The phases present in the catalyst were identified by comparing it with known reference XRD patterns for elements/compounds. The Derbye-Scherrer formula was used to estimate the iron crystallite diameter.

The Scherrer formula:

$$L_{hkl} = \frac{\kappa \lambda}{\beta \cos \theta}$$

in which λ is the wavelength of X-ray radiation employed in the analysis, β is the full width at half the maximum peak intensity, is and θ is the angular position of the peak maximum. κ was taken to be 0.9 and β was estimated at half the peak width.

2.4 Fischer Tropsch synthesis

2.4.1 Experimental set-up

Experimental set-up used to test the Fischer-Tropsch catalyst performance is shown in Figure 2.1. Appropriate CO and H_2 flow rates for Fischer-Tropsch synthesis are set using Brooks Series 3850 mass-flow controllers. The CO and H_2 flowrates are set to obtain (H_2/CO) mole ratio of 2. The hydrogen and the carbon monoxide streams are premixed before the 4-way valve. Argon is introduced for the purpose of pressurising the system to 20 bar. The needle valve is positioned immediately after the wax trap for the purpose of pressure regulation. A fixed bed reactor (1-mm diameter; 40-mm length) was used. The inlet and exit line of the reactor were insulated with glasswool to prevent heat loss.

Heavy products of the Fischer-Tropsch reaction were removed form the product mixture by a wax trap situated immediately after the reactor. The wax trap temperature was controlled by temperature controller and was set at 180 °C. to facilitate the removal of high molecular weight hydrocarbons form the product stream. The wax trap is surrounded by an aluminium block equipped with external electrical heating, which is connected to a temperature controller. The whole downstream line was kept at 180 °C to the ampoule sampling station to

prevent product condensation in the lines. During certain time intervals online GC TCD sampling in conjunction with ampoule sampling technique for compound analysis for hydrocarbon product analysis were taken of the Fischer-Tropsch reaction.

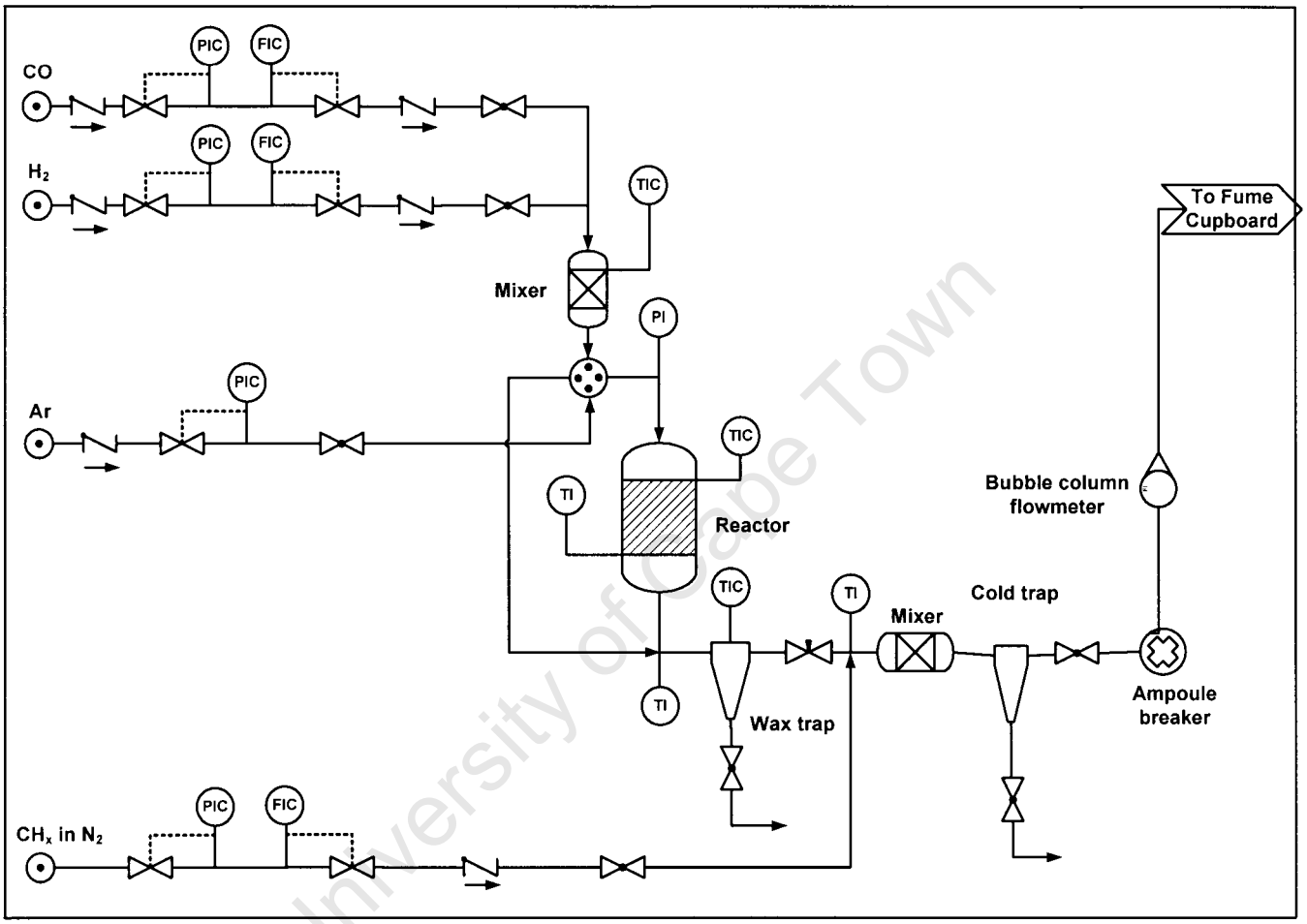

Figure 2.1: Experimental set-up fro testing catalyst performance in Fischer-Tropsch synthesis reaction.

2.4.2 Catalyst Loading

1 g of the calcined catalyst (size range 50 - 150μm) was initially mixed with 2.5 g of ~250 -μm silicon carbide (SiC). n-Hexane was used to make a paste. The purpose of mixing the catalyst with SiC in n-hexane was to ensure an even distribution of the catalyst in the reaction zone. Mixing the catalyst with SiC

lowered the pressure drop and also aid over the catalyst bed in eliminating temperature gradients. The thermowell was placed in and a little bit of glass wool plugged all-round the thermowell, when loading the catalyst care was taken to ensure that the catalyst was filled the same height around the thermowell. After loading, the reactor was plugged with glass wool and filled with SiC to the top of the reactor. This step was necessary to prevent catalyst from moving away from the isothermal zone or being blown out of the reactor. The loaded reactor was then connected and a pressure test was performed using argon to check for any gas leaks.

2.4.3 Catalyst Activation

To obtain the active catalyst for the Fischer-Tropsch reaction, in-situ reduction carried out in hydrogen (45 ml/(NTP) min) and at atmospheric pressure. The reduction step involved ramping up the temperature from room temperature at 10 °C/min to 350 °C. The reduction was done at this temperature for 16 hours. The temperature was subsequently allowed to drop to reaction temperature of 270 °C. The reaction temperature was maintained for 70 hours to perform the synthesis reaction.

2.4.4 Reaction Start-up

The Fischer-Tropsch reaction was carried out upon completion of the reduction procedure. Initially the 4-way valve was set to bypass so that the reactants did not pass through the reactor before proper synthesis gas setting were composition and flow rates obtained. Flow settings were adjusted using the flow controllers untill a hydrogen to carbon ratio (H_2/CO) of 2 was achieved. The reaction zone was pressurised with argon to 20 bar using the pressure regulator.

The total flowrate of the synthesis gas (H_2 + CO), reference gas and argon was set to be 100 ml/min (NTP) using the bubble meter. The reference gas was

made up of a mixture of 0.15 mol-% cyclo hexane in nitrogen. Table 2.1 summarises the reaction conditions.

The exit gas was analysed in a Hewlett Packard 589 gas chromatography with a thermal conductivity detector (TCD). The amounts of the reactants relative to the reference gas where obtained from which conversion and selectivity calculations were based. After satisfactory TCD analysis (H_2/CO ratio of 1.96 – 2.01) the 4-way valve was switched to reactor to start the reaction.

Table 2.1: Reduction and Fischer Tropsch reaction conditions.

Reduction	
Reduction Temperature (° C)	350
Reduction Time (hours)	16
Hydrogen flow (ml/(NTP) min)	45
Reaction conditions	
Mass catalyst (g)	1
Mass SiC (g)	2.5
Reaction pressure (bar)	20
Reaction temperature (° C)	270
Wax-trap and exit line temperature (° C)	180
Flowrates (ml/(NTP)min)	
H_2	40
CO	20
Reference gas (0.15 mol-% cyclo hexane in N_2)	20

2.4.5 Product Analysis

Gas conversion measurements were obtained online on a Hewlett Packard 5890 with thermal conductivity detector (TCD). Nitrogen was used as an internal standard for the on-line analysis where H_2, N_2, CO, CH_4 and CO_2 were analysed. Cyclohexane was used as an internal standard for offline-analyses of organic products using a Agilent Technologies 6890 N equipped with a flame ionization

detector (FID). Conditions of the two gas chromatographic analyses are given in Table 2.2.

Table 2.2: Conditions for gas chromatographic analyses.

Gas chromatograph	**Hewlett Packard 5890 (on line)**
Detector	Thermal conductivity detector (TCD)
Column type	Packed, stainless steel, 3 m x 2.1 mm
Stationary phase	10 FT x 1/8 S.S. Support 100/120 Carbosive SII
Carrier gas	Argon
Flow rate	30 ml (NTP)/min
Analysis temperature	140 °C
	at 4 °C/min to 190 °C (isothermal)
Gas chromatograph	**Agilent Technologies 6890N (off line) (adapted to ampoule technique)**
Detector	Flame ionisation detector (FID), T = 250 °C
Column type	Capillary column, Chrompac CP7692, 25 m x 150 mm
Carrier gas	Hydrogen
Column head pressure	109.4 kPa
Injector	Split injector T = 250 °C Split ratio 100:1
Temperature program	at -60 °C, 5 min (isothermal)
	at -30 °C, 50 min (isothermal)
	at 249 ° C, 5 min (isothermal)
Temperature (Ampoule breaker device)	250 °C

2.4.5.1 Fischer-Tropsch synthesis data analysis

CO and H_2 conversion was calculated from calibrated TCD gas chromatograms. TCD calibration was done by injecting a mixture of H_2, CO, CH_4, N_2 and CO_2 of known composition.

The response factor ($R_{F,i}$) for each compound was calculated based on N_2, and determined from the peak areas and the content of each gas as follows:

$$R_{F,i} = \left(\frac{\% \cdot i}{\% \cdot N_2}\right) \times \left(\frac{A_{N2}}{A_i}\right)$$

The CO and N_2 peak areas, A_{CO} and A_{N2} are obtained from the TCD trace. Typical response factors were: $R_{fTCD,H2}$ = 0.083; $R_{fTCD,CO}$ = 1.0901; $R_{fTCD,CO2}$ = 0.9789; $f_{TCD,CH4}$ = 0.3024.

CO conversion (X_{CO}) is defined as the amount of CO converted into CO_2 and the organic product and was determined from the relative areas:

$$X_{CO} = \left(\frac{\left(A_{CO}/A_{N2}\right)_{Bypass} - \left(A_{CO}/A_{N2}\right)_{Reactor}}{\left(A_{CO}/A_{N2}\right)_{Bypass}}\right) \cdot 100\%$$

CO_2 yield (Y_{CO2}) is defined as the fraction of the CO converted to CO_2.

$$Y_{CO2} = \left(\frac{\left(A_{CO2}/A_{N2}\right)_{out} \cdot R_{F,CO2}}{\left(A_{CO}/A_{N2}\right)_{feed} \cdot R_{F,CO}}\right) \cdot 100\%$$

CO_2 selectivity (S_{CO2}) is the fraction of product that goes to CO_2 per total CO converted.

$$S_{CO2} = \frac{Y_{CO2}}{X_{CO}}$$

Methane yield (Y_{CH4}) is defined as the fraction of the CO converted to methane.

$$Y_{CH4} = \left(\frac{\left(A_{CH4} / A_{N2} \right)_{out} \cdot R_{F,CH4}}{\left(A_{CO} / A_{N2} \right)_{feed} \cdot R_{F,CO}} \right) \cdot 100\%$$

Methane selectivity (S_{CH4}) is the fraction of product that goes to methane per total CO converted.

$$S_{CH4} = \frac{Y_{CH4}}{X_{CO}}$$

Methane content (S'_{CH4}) is the fraction of product that goes to methane per total hydrocarbon product.

$$S'_{CH4} = \frac{Y_{CH4}}{X_{CO+CO2}}$$

X_{CO+CO2} is the CO conversion and the CO_2 selectivity added together to determine the organic product and CO_2 formed, $X_{CO}(1-S_{CO2})$

The yield of total organic product and the selectivity of the products were determined using FID gas chromatograph. The fraction of each organic product based on the known molar fraction of cyclohexane in the reference gas (0.15 mol-% cyclohexane in nitrogen).

The response of a FID detector is strictly carbon specific; oxygen containing compounds give a weaker response. In order to account for this, theoretical mass specific response factors have been used following an incremental approach suggested by Kaiser (1969). Here the response of all carbon atoms which are not bonded to an oxygen atom is 1, the response of carbon atoms with a single bond to an oxygen atom is 0.55 and those carbon atoms with C=O double bonds are considered to give no response. The resulting factor for a component is then calculated using this equation:

$$f_i = \frac{N_c}{N_{C(noO)} + 0.55N_{C(O)}}$$

where N_C is the total number of carbon atoms in a molecule, N_C(no O) is the number of carbon atoms not connected to oxygen and N_C(O) is the number of carbon atoms connected to one oxygen atom with a single bond.

2.4.5.1.1 n-Olefin content

The olefin content in a given carbon number fraction was expressed as a percentage of the total sum n-olefins with carbon number N per total sum of linear hydrocarbons with carbon number N:

$$S_{n\text{-Olef.,\ N}} = \left(\frac{\sum A_{n-Olef.,N}}{\sum A_{LHC,N}} \right) \cdot 100\%$$

$S_{n\text{-Olef.,\ N}}$ is the olefin content in linear product with carbon number N, $\Sigma A_{n\text{-Olef.,\ N}}$ is the total FID area of all linear olefins with carbon number N and $\Sigma A_{LHC.,\ N}$ is the total FID area of all linear hydrocarbons with carbon number N.

2.4.5.1.2 1-Olefin content

1-olefin content in a given carbon number fraction was expressed as a percentage of the total linear olefin product with carbon number N:

$$S_{1\text{-Olef., N}} = \left(\frac{\sum A_{1-Olef.,N}}{\sum A_{n-Olef.,N}} \right) \cdot 100\%$$

$S_{1\text{-Olef., N}}$ is the 1-olefin content in linear olefin product with carbon number N, $\Sigma A_{1\text{-Olef., N}}$ is the FID area of the linear 1-olefin with carbon number N and $\Sigma A_{n\text{-Olef., N}}$ is the total FID area of n-olefins with carbon number N.

2.4.5.1.3 Oxygenate content

Oxygenate content per carbon number fraction was expressed as a percentage of the total linear hydrocarbons plus oxygenate product of a corresponding carbon number.

$$S_{Ox., N} = \left(\frac{\sum A_{Ox.,N}}{\sum A_{LHCO.,N}} \right) \cdot 100\%$$

$S_{Ox, N}$ is the oxygenate content in linear product with carbon number N, $\Sigma A_{Ox,N}$ is the total FID area of all oxygenates with carbon number N and $\Sigma A_{LHCO, N}$ is the sum of all linear hydrocarbons and oxygenates with carbon number N.

2.4.5.1.4 Branching

The content of branching products was expressed as a fraction of the hydrocarbons of a given carbon number fraction.

$$S_{Brch., N} = \left(\frac{\sum A_{Brch.,N}}{\sum A_{HC.,N}} \right) \cdot 100\%$$

$S_{Brch,\ N}$ is the content of branched carbon number N, $\Sigma A_{Brch,N}$ is the total FID area of all branched products with carbon number N and $\Sigma A_{HC,N}$ is the sum of all hydrocarbons with carbon number N.

3. RESULTS

Different support materials were used to prepare supported iron catalysts, viz. silica and silica modified with aminopropyltriethoxysilane (APTeS). Each time, the same amount of iron per unit weight support was impregnated. Incipient wetness impregnation method was used to load different amounts of K_2CO_3.

3.1 Support Characterization

3.1.1 BET Area, pore volume and pore diameter

Modified silica was characterised using BET-analysis after impregnation with aminopropyltriethoxysilance and drying at 90°C for 1 hr (see Table 3.1). The surface area, total pore volume and pore diameter of the silica decrease upon introduction of amonipropyltriethoxysilane in the silica. The coverage of the silane on the silica decreased the diameter which will lead to the decrease in surface area and pore volume.

Table 3.1 : BET surface area, total pore volume and average pore diameter for silica and APTeS-modifed silica after drying.

Support	Specific surface BET area (m^2/g)	Total pores volume (cm^3/g)	Average pore diameter (Å)
Silica	315	1.24	157
APTeS modified silica[a]	288	1.01	141

[a] Stored for 14 days in a desiccator with drying agent before the analysis was done

The pore radius distribution of silica is slightly shifted towards higher pore radii in comparison to APTeS-modified silica (see Figure 3.1). It might thus be stated that aminopropyltriethoxysilane covers the pore walls and does not seem to result in pore blockage. The coverage of the walls with aminopropyltriethoxysilane would result in a decrease in the average pore

diameter and pore volume, and thus resulting in a decrease in the BET-surface area.

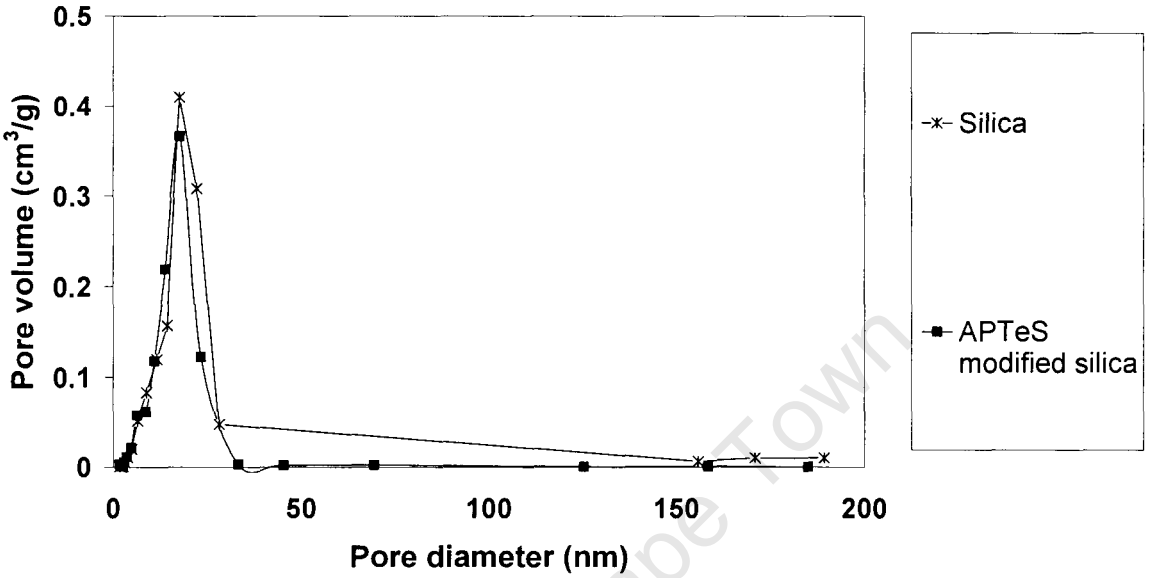

Figure 3.1: Pore size distribution of silica and APTeS modified silica.

3.1.2 Zeta potential determination

The zeta potential of pure SiO_2 (dried at 250 °C in argon and stored in a desiccator with drying agent) and the APTeS-modified SiO_2 was impregnated after the 6 hr 250 °C drying in argon, were determined as a function of pH. At some intermediate pH, known as the point of zero charge (PZC) or iso-electric point (IEP) the net charge of the particles is zero.

Figure 3.2 shows the experimentally observed trends in the zeta potential as function of pH for the supports under study. The zeta potential of bare silica gel at pH range 3.5 - 6 (pH-range of typical iron nitrate impregnation solutions) was determined to be -12.6 mV, which indicates that silica exhibits a negative charge. The negative zeta potential for silica in this pH-range is due to the dissociation of protons form the weakly acidic silanol groups. The iso-electric point (IEP) of silica

was at about pH=1.8 in agreement with measurements by Xu et al. (2003). The zeta-potential as a function of pH is quite different for the APTeS-modified silica. The zeta potential of bare silica gel at pH range 3.5 - 6 (pH-range of typical iron nitrate impregnation solutions) was determined to be +20-25 mV, which indicates that APTeS-modifed silica exhibits a positive surface charge. The iso-electric point of the APTeS modified silica was at about pH=8.5. Chen et al. (2006) prepared the APTeS modified silica in a similar manner and observed their iso-electric point for APTeS modified silica to be at pH=7.6.

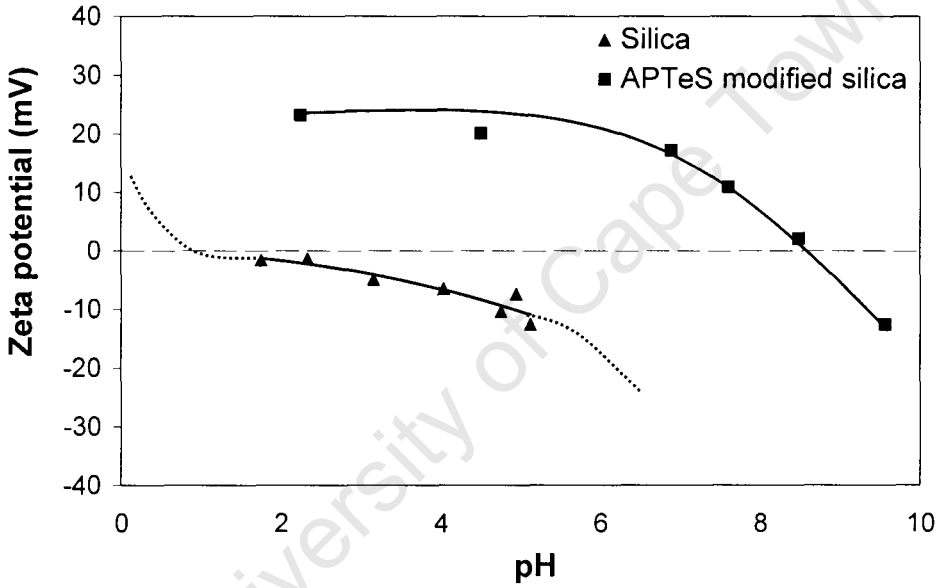

Figure 3.2: Zeta potential as function of pH of silica and APTeS modified silica (APTeS-modified silica was stored for 5 days before the analysis was done).

The surface charge of silica comes from the dissociation of the silanol groups, so in this case the pH controls the zeta potential of the silica powder through the following process: $SiOH_2^+ \overset{H^+}{\longleftrightarrow} SiOH \overset{H^+}{\longleftrightarrow} SiO^-$ (Xu et al., 2003). After modification of the silica support with the aminopropyltriethoxysilane, the amino groups can accept protons and become positively charged NH_3^+ species:

$RNH_3^+ \overset{H^+}{\longleftrightarrow} RNH_2 \overset{H^+}{\longleftrightarrow} RNH^-$. Under alkaline conditions (pH 9.56) the zeta potentials of the APTeS-modified silica exhibit negative zeta potentials probably due to the dissociation of protons from the amino groups and the residual silanol (Si-OH) groups to form ($-NH^-$) and ($Si-O^-$) species.

The silanol group is more acidic (smaller pK_a value) and the RNH_2 group is a weaker acid (higher pK_a value). The variation in the zeta-potential as a function of pH can thus be explained in terms of the acid-base properties of the silanol groups versus those of the amino-group. The amino-group is a weaker acid, and thus the release of a proton will only occur at a much higher pH, or otherwise stated the amino-group is a much stronger base than the silanol-group, and thus the uptake of a proton is much more favoured. The release of a proton results in a negative surface charge, whereas the uptake of a proton results in a positive surface charge.

3.1.3 Infra red Spectroscopy (IR)

The presence of various functional groups on silica and the APTeS-modified silica were observed with infrared transmission spectroscopy.

The active silica surface with large specific surface area is of great importance in adsorption and ion exchange. At the surface the structure terminates in either siloxane group with the oxygen atom on the surface, or one of several forms of silanol groups. The silanol groups could be isolated (free silanol groups), where the surface silicon atom has three bonds into the bulk structure and the fourth attached to a OH group and the vicinal or bridged silanols, where two isolated silanol groups attached to two different silicon atoms are bridged by H-bond. A third type silanols called germinal silanols consists of two hydroxyl groups attached to one silicon atom (Jal et al., 2004).

Interpreted by DRIFTS at low calcination temperature (<450 °C), there are more H-bonded silanols (germinal hydroxyl groups) on silica than isolated silanols (single bonded hydroxyl groups) (Iiskola et al., 2003). The infra red analysis done on the silica which was calcined at 250 °C for 6 hrs in argon to detect the OH stretch vibration was negligible because the noise ratio was higher than the peaks detected, which is opposite the results obtained by previous researchers (Iiskola et al., 2003).

The spectra of the APTeS modified silica is given in Figure 3.3. The N-H stretching vibrations occur at 3427 cm^{-1}, but the peak could also be attributed to OH stretching vibration which adsorb at the same frequency. Absorption due to C-N stretching occurs at 1113 cm^{-1} as medium band intensity for amines. A weak N-H out-of-plane band is observed at 874 cm^{-1} and seen most easily in aliphatic amines. Bending of the N-H bond in amines results in adsorption near 1604 cm^{-1}.

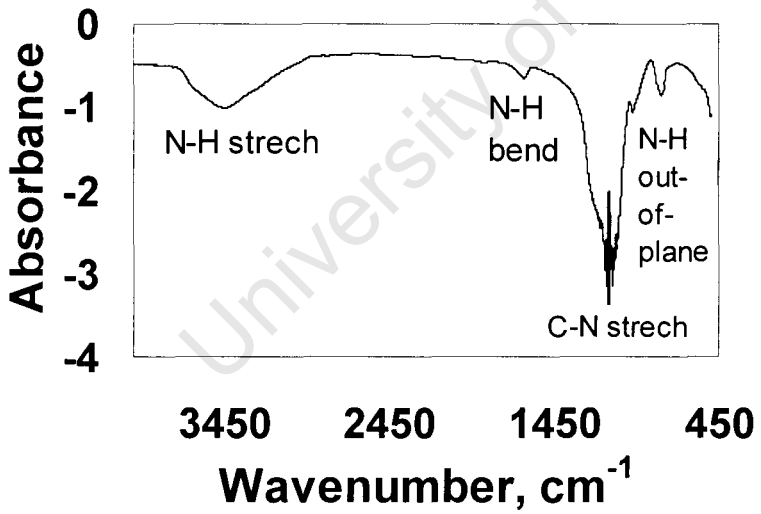

Figure 3.3: Absorbance as a function of wavenumber for APTeS-modified silica. (APTeS-modified silica was stored for 5 days before the analysis was done).

Table 3.2 shows the absorbance maxima of the APTeS modified silica compared to n-propylamine (http://webbook.nist.gov/cgi/cbook.cgi). The absorbance maxima observed for the APTeS-modified silica are in general in agreement with those observed for n-propylamine. The absorbance maxima for the APTeS modified silica are shifted towards higher frequencies as compared to those for n-propylamine. The higher frequency obtained for the APTeS modified silica is attributed to the higher reduced mass in APTeS. It can thus be concluded that amine groups are present in the APTeS-modified silica.

Table 3.2: Infra red absorbance maxima and vibration peaks of the APTeS modified silica and the n-propylamine.

Vibration peaks	APTeS modified silica absorbance maxima (cm^{-1})	n-propylamine absorbance maxima (cm^{-1})
N-H strech [a]	3427	2900
C-N strech	1113	1100
N-H out-of-plane	784	770
N-H bend	1604	1600

[a] N-H stretch vibration peak may overlap with the O-H stretch peak.

3.1.4 CHN –analysis

Table 3.3 shows the APTeS-modified silica which was dried for 4 hrs at 120 °C in an oven. The carbon loading is 4.49 wt.-%, hydrogen loading is 1.14 wt.-% and the nitrogen loading is 1.08 wt.-% for the APTeS-modified silica. The amount of APTeS impregnated on silica should correspond to 48.79 wt-% carbon, 10.39 wt-% hydrogen and 6.32 wt-% nitrogen. The carbon and hydrogen content are ca. 10% of the initially amount loaded on silica, whereas it is ca. 17% for the nitrogen content. This indicates a transformation of the APTeS molecule upon impregnation on silica followed by a 4h drying process at 130 °C, and storage. This indicates that only 17% of APTeS is loaded, which corresponds to a loading

of 0.13 g APTeS/g silica, if it can be assumed that decomposition of propylamine group does not occur under the applied conditions.

The C/N ratio and the C/H ratio in APTeS are 7.7 g/g and 4.69 g/g, respectively. The C/N ratio in APTeS modified silica was less than APTeS, which indicates that ethoxy groups disappear upon impregnation, followed by drying and storage. The C/N-ratio of the APTeS-modified silica corresponds to the presence of one ethoxygroup and one propylamine group indicating the removal of two ethoxy-groups from APTeS upon interaction with silica (see Appendix).

The removal of ethoxy-groups leads to the formation of additional silanol-groups. The removal of ethoxy-groups results in the formation of hydroxyl groups. The C/H-ratio indicates that more silanol-groups are formed than can be attached to the original APTeS-molecule. The decomposition products may induce the formation of additional silanol-groups, but it should be taken into consideration that silanol groups may also be formed on silica upon air exposure with low water content.

Table 3.3: Carbon, hydrogen and nitrogen contents of APTeS and APTeS-modified silica (APTeS modified silica was stored for 6 days before the analysis).

Support	C (wt-%)	H (wt-%)	N (wt-%)	C/N ratio (g/g)	C/H ratio (g/g)
APTeS [a]	48.79	10.39	6.32	7.71	4.70
APTeS modified silica[b]	4.49	1.14	1.08	4.16	3.94

[a] CHN contents determined theoretically, if all APTeS impregnated on silica is still present.

[b] CHN contents detected experimentally for APTeS modified silica.

3.1.5 Thermogravimetric analysis (TGA)

Thermogravimetric analysis is carried out by suspending the sample form continuously recording micro balance in a temperature controlled furnace. The sample is heated from a defined starting temperature to a specified final temperature at a given heating rate.

The derivative weight loss (DTA) of the prepared modified support is illustrated in Figure 3.4. The APTeS modified support was prepared by reflux for 20 h at 125 °C, washed with toluene, acetone and methanol and then dried in 120 °C for 4 hrs.

The dark black line indicates the temperature profile which was used. The DTG-curve is characterized by three ranges of weight loss, viz.

1. Weight loss in the low temperature range with peak maximum at ca. 80°C
2. Weight loss in the isothermal phase at 100°C after ca, 10 minutes at this temperature
3. Weight loss in the high temperature range with a peak maximum at ca. 350°C

The weight loss obtained for various temperature ranges are given in Table 3.4. The increase in the rate of weight loss during the isothermal phase at 100 °C after ca. 15 min is rather unexpected and might be caused by an auto-catalytic effect, i.e. a product interacts with the APTeS on silica, e.g. water.

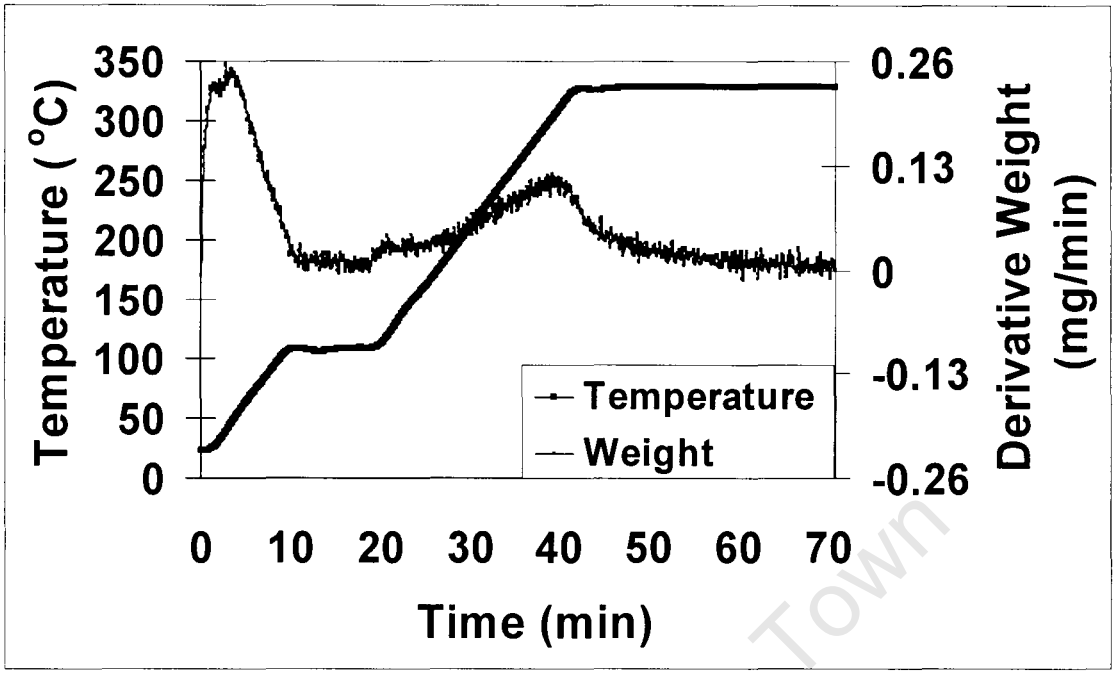

Figure 3.4: TGA profiles of silica impregnated with APTeS in an argon atmosphere. (APTeS-modified silica was stored in a dessicator with drying agent for 70 days before analysis was done).

Table 3.4: Sample weight loss for different compounds.

Temperature range (°C)	Weight loss (mg/16.2028mg sample) original weight	Weight loss (%)
25 - 110	0.267	1.65
120 - 330	0.323	1.99

The weight loss at low temperature could be due to the decomposition/polymerisation of adsorbed APTeS yielding the relative volatile compounds ethanol and diethylether. The high temperature weight loss might be due to the amine groups. Further investigation are required utilising a Mass Spectrometer to elucidate the exact decomposition of APTeS on a silica surface.

3.2 Catalyst Precursor Characterization

3.2.1 Atomic Adsorption Spectroscopy (AAS)

Atomic adsorption was used to ascertain the elemental composition of the modified catalyst and the base silica supported catalysts. All the catalysts were analyzed for iron (Fe).

Table 3.6 showed that the iron loading was between 7.6 – 8.2 wt.-%. Table 3.7 iron loading for the APTeS-modified support catalyst was between 8.5 – 9.2 wt.-%. The higher loadings obtained with the APTeS-modified supports can be ascribed to the weight-loss of the support during catalyst preparation as shown in Table 3.5. The iron loading of the catalyst supported on the APTeS-modified support is higher than that of the silica supported catalysts; calcination of the catalyst of the catalyst eliminated the amino-groups initially present on the APTeS-modified support.

Table 3.5: CHN-analysis for the iron catalyst supported on APTeS modified silica.

Catalysts	C (wt-%)	H (wt-%)	N (wt-%)	C/N ratio (g/g)	C/H ratio (g/g)
APTeS MS 0 K	1.88	0.55	0.15	12.53	3.42
APTeS MS 0.005 K	1.49	0.34			4.38
APTeS MS 0.01 K	1.04	0.44			2.36
APTeS MS 0.02 K	0.79	0.26			3.04

Titration is a laboratory technique by which we can determine the concentration of iron using a standard concentration of potassium dichromate. It is shown in appendix that the AAS results and the titration results are in agreement with each other.

Table 3.6: Iron (Fe) content determined experimentally for catalyst prepared with incipient wetness method and promoted with potassium.

Catalyst Precursor	Fe (wt.-%)
0 K	7.8
0.005 K	7.8
0.01 K	8.2
0.02 K	7.6
0.04 K	8.1
0.06 K	8.1
0.08 K	7.9

Table 3.7: Iron (Fe) content determined experimentally for catalyst prepared with incipient wetness method, supported on APTeS modified support and promoted with potassium.

Catalyst Precursor	Fe (wt.-%)
APTeS MS 0 K	8.6
APTeS MS 0.005 K	8.5
APTeS MS 0.01 K	8.9
APTeS MS 0.02 K	9.2

3.2.2 BET Area and Pore Volume

The BET surface area, pore volume, average pore diameter of the silica-supported catalysts with different potassium levels are illustrated in Table 3.8. The BET-surface area fluctuates strongly and no definite trend can be observed as a function of the potassium loading. A similar fluctuation can be seen in the pore volume, resulting in an approximate constant average pore diameter of ca. 15-16nm. The BET-surface areas of the calcined Fe-catalysts supported on silica are significantly lower than the surface area of silica (315 m^2/g).

Table 3.8: BET surface area, total pore volume and average pore diameter for the catalysts supported on silica and promoted with different amounts of potassium.

Catalyst precursors	Specific surface BET area (m^2/g)	Total pores volume (cm^3/g)	Average pore diameter (Å)
0 K	262	0.99	151
0.005 K	266	0.99	149
0.01 K	305	1.12	148
0.02 K	239	0.97	155
0.04 K	257	0.97	151
0.06 K	244	0.97	159
0.08 K	225	0.95	169

Figure 3.5 shows the pore size distribution of the iron catalyst supported on silica. The pore radii distributions seem unaltered as a function of the potassium loading. The change in surface area is thus not due to potassium pore blockage. Yang et al. (2004) concluded over Fe/K precipitated catalyst that the pore diameter of the catalyst increases with the increase of the potassium content and the loss of surface area is due to crystallite growth. Milburen et al. (1996) obtained over silica promoted iron catalyst a decrease in surface area with an increase in potassium loading.

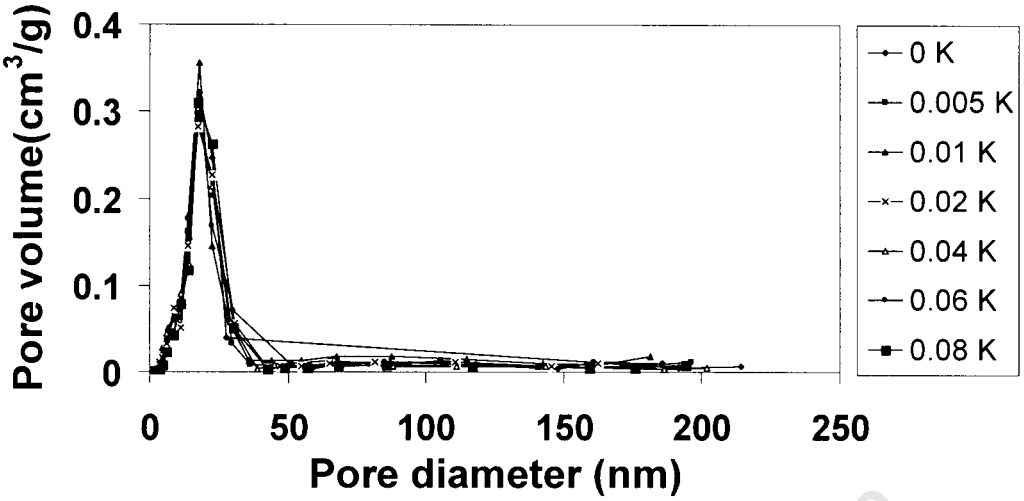

Figure 3.5: Pore size distribution of the iron catalysts supported on silica with different potassium loadings.

Table 3.9 shows that potassium addition showed no influence on the surface area, pore volume and pore diameter on the APTES modified silica catalysts, although a slightly lower surface area was obtained for the catalyst APTeS MS 0.01K.

Table 3.9: BET surface area, total pore volume and average pore diameter for the modified catalyst promoted with different amounts of potassium.

Catalyst precursors	Specific surface BET area (m^2/g)	Total pores volume (cm^3/g)	Average pore diameter (Å)
APTeS MS 0 K	272	0.85	125
APTeS MS 0.005 K	272	0.85	125
APTeS MS 0.01 K	262	0.85	130
APTeS MS 0.02 K	272	0.87	128

Figure 3.6 shows that potassium does not influence the pore size distribution for the iron catalyst supported on APTeS-modified silica.

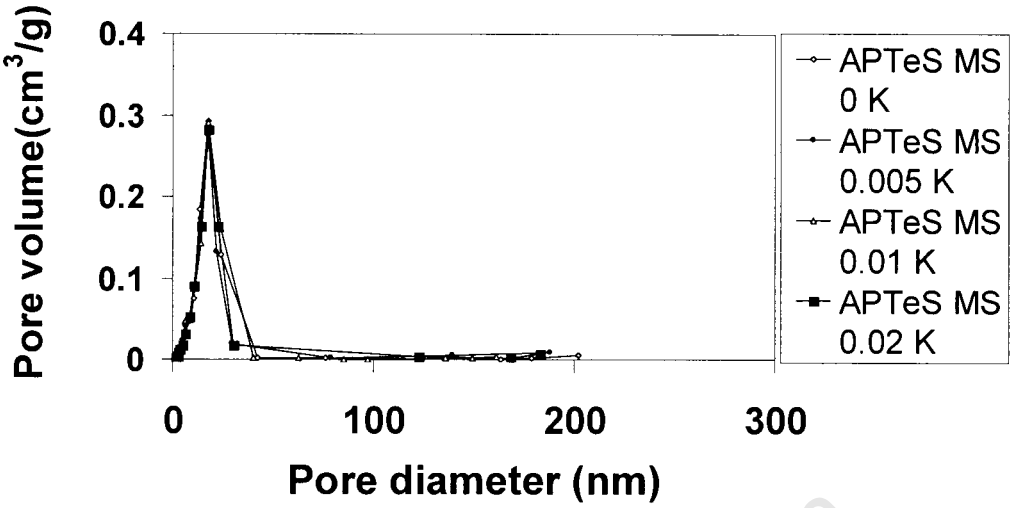

Figure 3.6: Pore size distribution as prepared with iron catalysts supported on APTeS modified silica with different potassium loadings.

3.2.3 X-ray diffraction (XRD)

The XRD pattern of the calcined catalysts is shown in Figure 3.7 – 3.8. Notable differences can be seen in the XRD-spectra of the iron catalyst supported on silica compared to those supported on APTeS-modified silica. The iron phase in the iron catalyst supported on silica catalysts is mainly hematite (Fe_2O_3), whereas the iron phase in the iron catalyst supported on APTeS-modified silica catalysts is mainly iron oxide hydroxide FeOOH. The presence of basic amine groups may favour the precipitation of FeOOH crystallites during the impregnation on the APTeS-modified silica.

Table 3.10 shows the diffraction angles of hematite and the iron phase in the iron catalyst supported on silica catalysts and of FeOOH and the iron phase in the iron catalyst supported on APTeS-modified silica. The diffraction angels obtained for hematite and iron oxide hydroxide for the catalysts prepared were in agreement with the diffraction peaks obtained in literature.

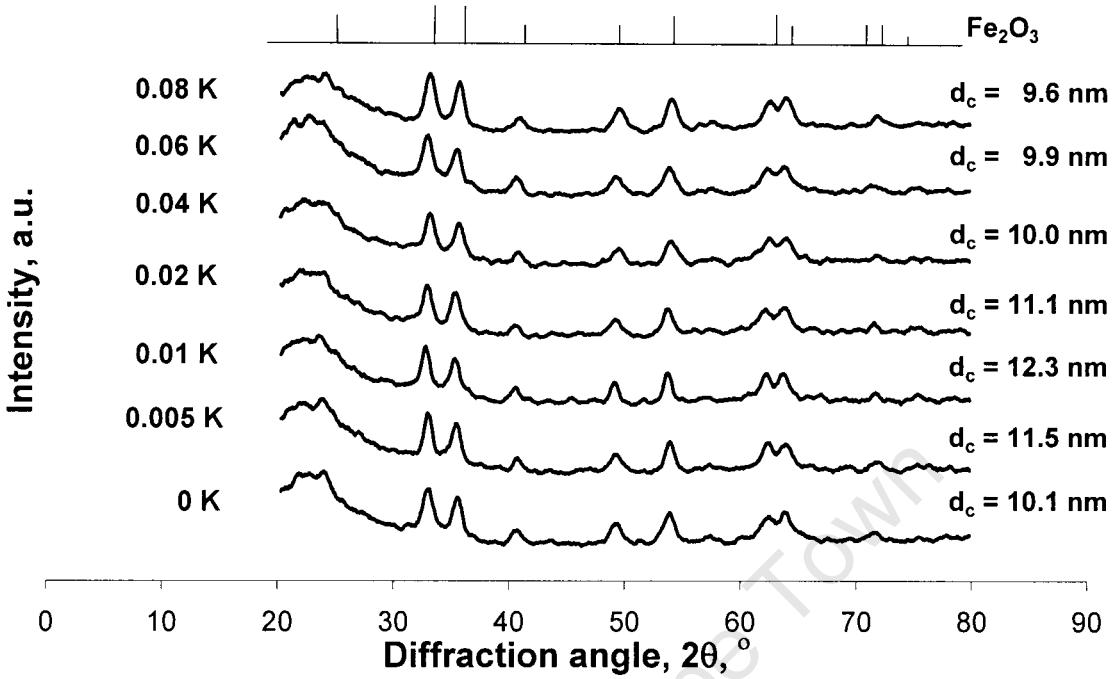

Figure 3.7: XRD pattern of the iron supported on silica promoted with potassium.

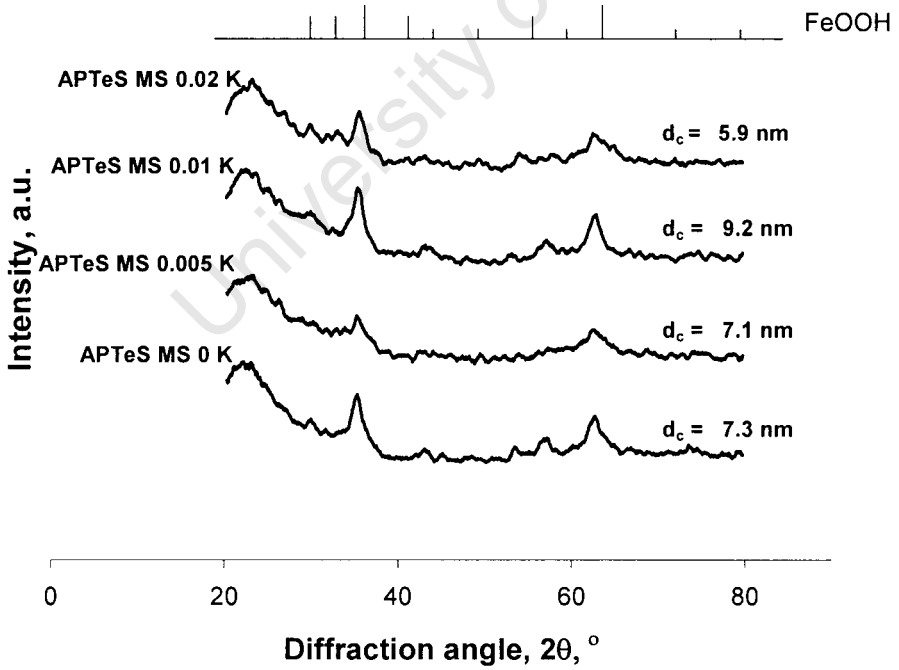

Figure 3.8: XRD pattern of the iron supported on APTeS-modified silica promoted with potassium.

Table 3.10: Diffraction angles for the iron phase in the iron catalyst supported on silica and the Iron phase in the iron catalyst supported on APTeS modified-silica in comparison to the diffraction angles for hematite and FeOOH.

Hematite diffraction angles (2 θ, °)[a]	Hematite diffraction angles (2 θ, °)[b]	Iron oxide hydroxide diffraction angles (2 θ, °)[c]	Iron oxide hydroxide diffraction angles (2 θ, °)[d]
24.2	24.2	26.8	26.8
33.2	33.2	28.2	28.2
35.8	35.8	33.2	33.2
	39.2	35.9	35.9
41.8	41.8		39.5
	43.5	41.2	41.2
49.5	49.5		46.8
54.2	54.2	49.0	49.0
	56.2	56.2	56.2
	57.5	62.8	62.8
	57.8		64.2
62.5	62.5		
64.0	64.0		
	66.0		
	69.8		
72.0	72.0		
72.3	72.3		
	75.5		
	77.8		
	78.9		

[a] Diffraction angles observed for the iron phase in the iron catalyst supported on silica.

[b] Diffraction angles for hematite (Fe_2O_3) as given by JCPDS [e].

[c] Diffraction angles obtained for the iron phase in the iron catalyst supported on APTeS-modified silica.

[d] Diffraction angles for iron oxide hydroxide (FeOOH) as given by JCPDS [e].

[e] Joint Committee for Powder Diffraction Standards.

The average crystallite size of Fe_2O_3 and FeOOH crystallite size was estimated by line broadening analysis, using the Debye-Scherrer equation. There are no observed trends pointing towards an effect of potassium loading on the crystallite size of the iron phase present in the catalysts. The iron catalyst supported on

APTeS modified silica crystallite size was smaller than the iron catalyst supported on silica. The Fe_2O_3–crystallite size in the iron catalyst supported on silica was between 9.6 – 12.3 nm. The FeOOH-crystallite size in the iron catalyst supported on APTeS-modified silica catalysts were between 5.9 – 9.2 nm.

3.2.4 Temperature programmed reduction (TPR)

Temperature programmed reduction (TPR) experiments were carried out to study the reduction behaviour of the catalysts under study. The recorded rate of hydrogen consumption obtained during the reduction of the samples is shown in Figure 3.9 and 3.10. The total amount of hydrogen consumed for the iron catalysts supported on silica and APTeS-modified silica, respectively, is given in Tables 3.11 and 3.12.

Figure 3.9 shows the TPR-profile of supported iron catalysts on silica with 2 intense reduction peaks at ca. 350 °C and ca. 500 °C. These reduction peaks were attributed to the sequential reduction of Fe_2O_3 to Fe_3O_4 and from Fe_3O_4 to Fe^0 in the following manner:

$$3Fe_2O_3 + H_2 \rightarrow 2Fe_3O_4 + H_2O \quad (1)$$
$$Fe_3O_4 + 4H_2 \rightarrow 3Fe + 4\,H_2O \quad (2)$$

The peak at ca. 350 °C corresponds to the reduction of Fe_2O_3 to Fe_3O_4. The peak at ca. 500 °C is associated with the reduction of Fe_3O_4 to metallic Fe (Bukur et al., 2002).

The low temperature peak at ca. 350 °C is preceded by two additional peaks in the range of 200 – 300 °C for the iron catalyst supported on silica with 0.01 K.

A third peak can be seen in the TPR profiles at ca. 620 °C, except for the 0.005 K catalyst which shows only two peaks. This peak might be attributed to the

reduction of iron hydro-silicate phase. It might be speculated; that the small extra peak at 600 °C observed during TPR for the catalyst is because the support is not in intimate contact with the metal oxide. Previous work implied that iron supported on silica is harder to reduce (Jin et al., 2000). Zhang et al. (2006) concluded that metal-silica interaction exists in silica-supported catalyst, i.e. intimate contact between iron and the silica matrix leads to the formation of the difficult reduced iron (II) silicate phases. The TPR profiles of silica-free catalyst shows three reduction peaks (Zhang, et al., 2006). This is a representative TPR profile of hematite reduction to α-Fe, the reduction at high temperatures does not direct to α-Fe which process via two steps.

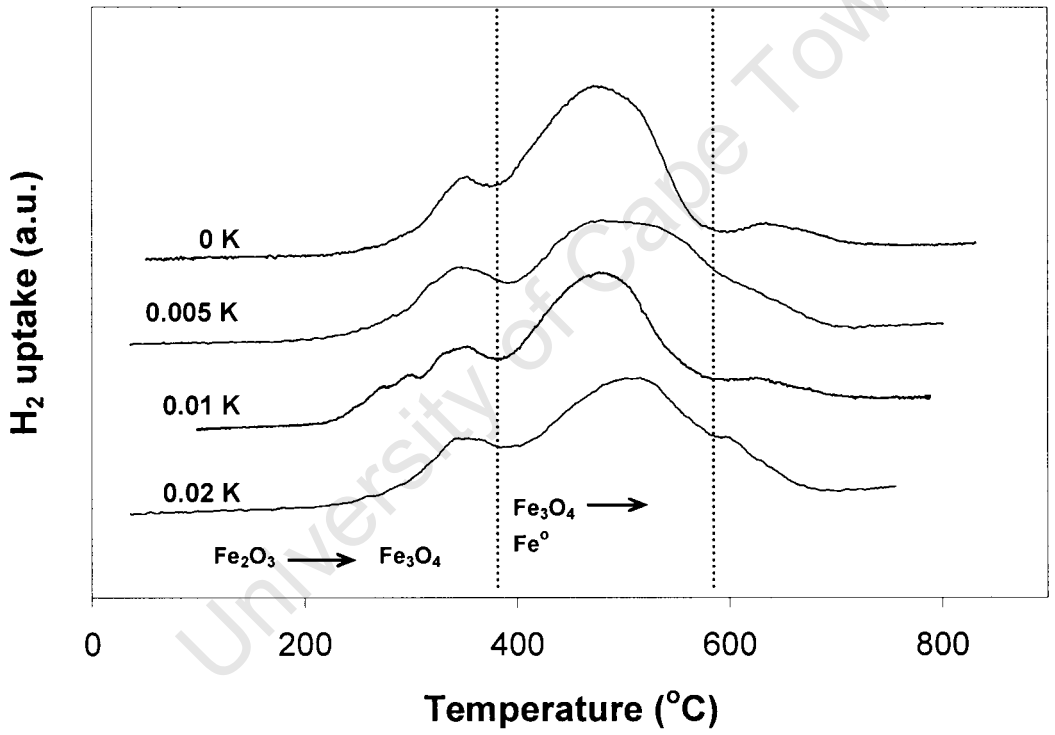

Figure 3.9: Temperature programmed reduction of calcined catalyst supported on silica with varying potassium content (TPR-m=~0.04g, ramping rate 10 ° C/min, H_2-Ar flowrate 50ml/min (NTP).

Theoretically the H_2/Fe mole ratio for the reduction Fe_2O_3 to Fe is 1.5 mol/mol. The TPR results (see Table 3.11) show the H_2/Fe mole ratio to be less than the theoretical ratio. This implies that the catalysts were poorly reduces. The TPR profiles of silica catalysts exhibit two distinct reduction regions in the temperature range of 350 – 580 °C. The first stage of the catalysts is typically attributed to the transformation of $Fe_2O_3 \rightarrow Fe_3O_4$ and the second stage of the catalysts corresponds to the transformation of $Fe_3O_4 \rightarrow$ Fe. The hydrogen consumption of the second stage of the reduction process relative to the hydrogen consumption for the first stage of the reduction process varies between 2.4 and 3.4, which is much lower than anticipated for a sequential reduction of $Fe_2O_3 \rightarrow Fe_3O_4 \rightarrow$ Fe (for which a value of 8 is expected)

Table 3.11: Hydrogen consumption amount during TPR experiments of calcined catalyst supported on base silica with varying potassium content (TPR-m=~0.04g, ramping rate 10 °C/min, H_2-Ar flowrate 50ml/min (NTP).

Catalyst	Reduction peaks	H_2/Fe (mol/mol) [a]	Total H_2/Fe (mol/mol) [a]	Distribution (%)
0 K			1.13	
	1	0.22		20
	2	0.74		65
	3	0.15		13
0.005 K			0.57	
	1	0.13		23
	2	0.43		76
0.01K			1.34	
	1	0.34		25
	2	0.83		62
	3	0.17		12
0.02 K			0.43	
	1	0.10		22
	2	0.26		60
	3	0.05		13

[a] Iron content based on AAS results.

Figure 3.12 shows the TPR-profiles of the iron catalysts supported on APTeS-modified silica. The catalysts with no potassium or little potassium (APTeS MS 0K and APTeS MS 0.005K) show two reduction maxima at ca. 350 °C and 500 °C. The catalysts with a higher potassium loading (APTeS MS 0.01K and APTeS 0.02K) show in addition a high temperature reduction peak at ca. 600 °C.

Iron in the iron catalysts supported on APTeS-modified silica is present as FeOOH. FeOOH can be reduced according to:

$3FeOOH + 1/2\ H_2 \rightarrow Fe_3O_4 + 2H_2O$

$Fe_3O_4 + 4H_2 \rightarrow 3Fe + 4H_2O$

or

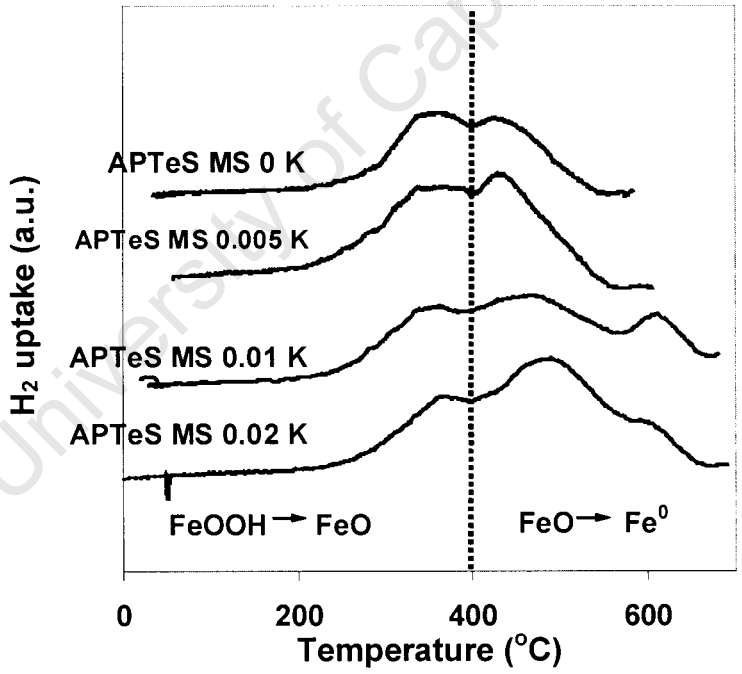

Figure 3.10: Temperature programmed reduction of calcined catalyst supported on APTeS modified silica with varying potassium content (TPR-m=~0.04g, ramping rate 10 ° C/min, H_2-Ar flowrate 50ml/min (NTP).

$FeOOH + 1/2H_2 \rightarrow FeO + H_2O$

$FeO + H_2 \rightarrow Fe + H_2O$

The difference between the two steps is the relative amount of hydrogen consumed in the first two steps. Table 3.12 shows that the ratio of the amount of hydrogen consumed attributable to the second reduction peak relative to amount of hydrogen consumed attributable to the first reduction peak is between 0.7 and 1.8. This indicates that the reduction behaviour might be better represented by FeOOH → FeO → Fe (for which a theoretical ratio of 2 is expected) than by FeOOH → Fe_3O_4 → Fe (for which a theoretical value of 8 is expected).

Table 3.10 shows it was especially difficult to reduce the APTeS MS 0.01 K and APTeS MS 0.02 K catalysts seeing the low amount of hydrogen consumed in the TPR-experiment. The low degree of reduction could be attributed to the different iron oxide structure formation in the catalysts due to the interaction between iron and the APTeS modified silica matrix.

Table 3.12: Hydrogen consumption amount during TPR experiments of calcined iron catalyst supported on APTeS modified silica with varying potassium content (TPR-m=~0.04g, ramping rate 10 °C/min, H_2-Ar flowrate 50ml/min (NTP).

Catalyst	Reduction peaks	H_2/Fe (mol/mol) [a]	Total H_2/Fe (mol/mol) [a]	Distribution (%)
APTeS MS 0 K			0.77	
	1	0.48		63
	2	0.32		41
APTeS MS 0.005 K			0.96	
	1	0.50		52
	2	0.46		34
APTeS MS 0.01K			0.33	
	1	0.10		30
	2	0.18		53
	3	0.06		19
APTeS MS 0.02 K			0.38	
	1	0.12		31
	2	0.22		58
	3	0.03		9

[a] Iron content based on AAS results.

3.2.5 Transmission electron microscopy (TEM)

TEM photographs were taken of the catalyst precursors after drying (120 °C) and calcining (250 °C) in argon to ascertain their morphology. TEM images of all the catalyst precursors are shown in Figure 3.11 and 3.12.

Figure 3.11 shows iron supported on silica catalyst precursors impregnated with potassium. The precursor for the iron supported on silica catalyst is hematite (Fe_2O_3). The iron precursors with 0 K – 0.02 K, display spherical shaped agglomerates of iron oxide. The diameter of the agglomerates for the iron catalysts supported on silica is between 111 -183 nm consisting of smaller crystallites. It can be seen with all the catalyst that the crystallites are mainly found on the support material. Furthermore, the TEM images of the catalyst

showed areas with a high density of iron particles and large areas with no iron present.

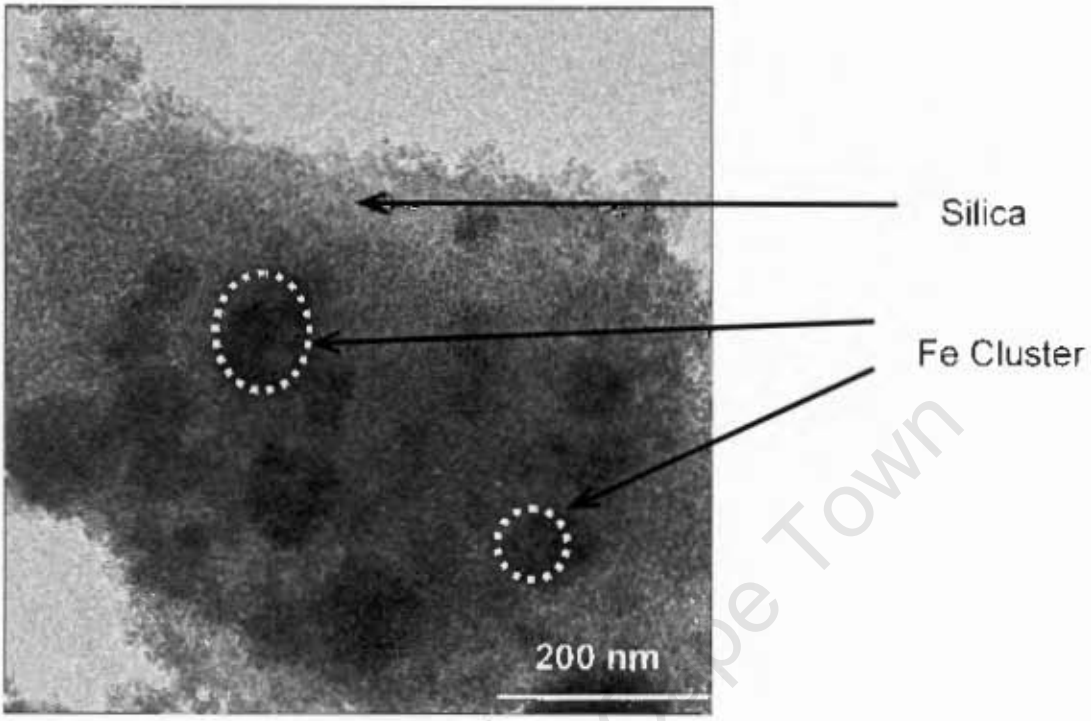

(A)

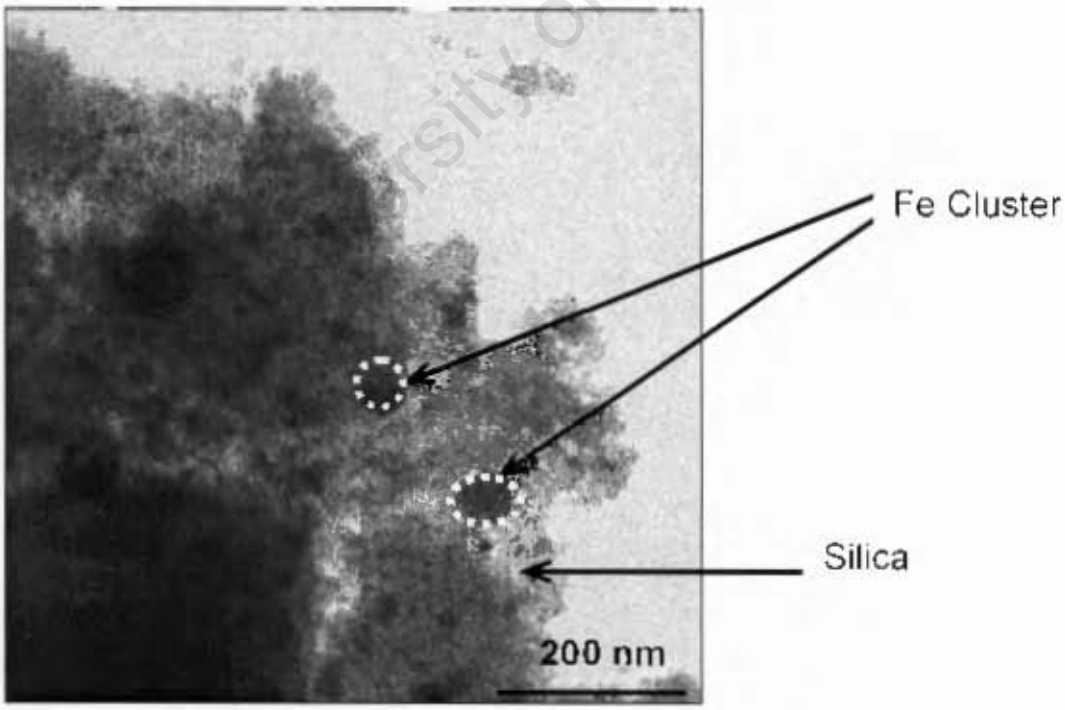

(B)

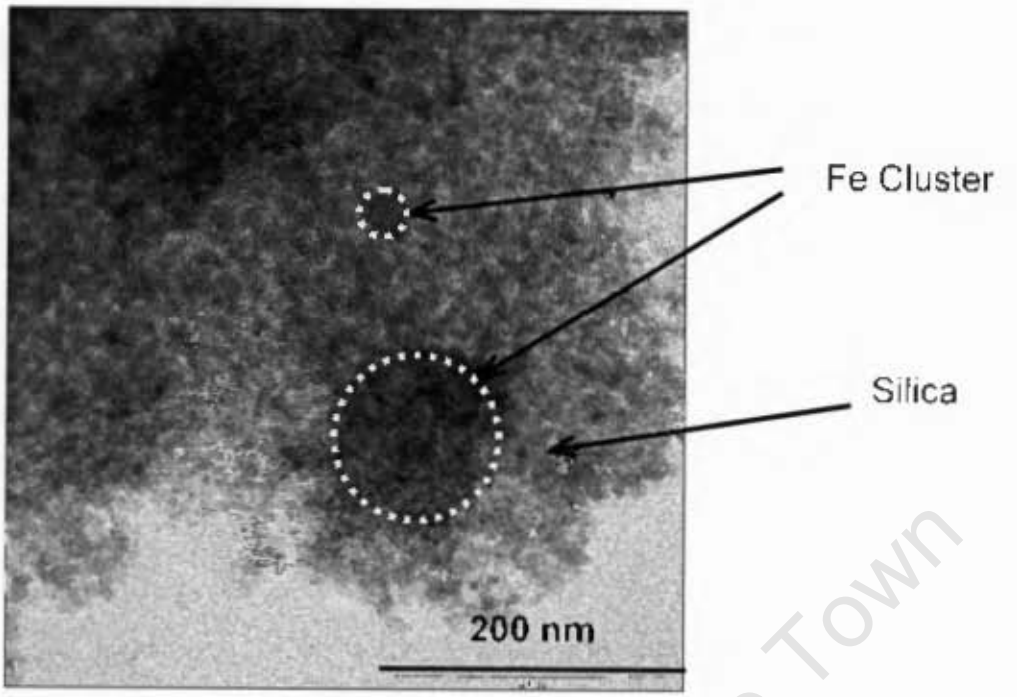

(C)

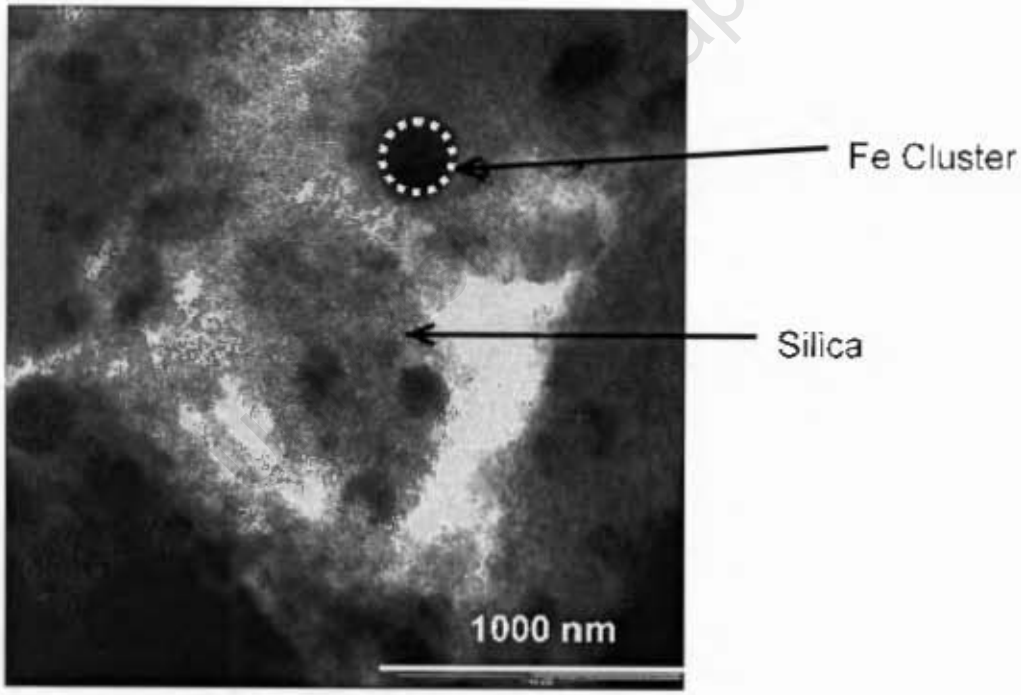

(D)

Figure 3.11: TEM images for iron catalyst precursors supported on silica (A) 0 K, (B) 0.005 K, (C) 0.01 K, (D) 0.02 K.

The iron catalyst supported on silica iron impregnated with potassium formed spherical-shaped iron oxide particles, which are present in agglomerates. The catalysts were prepared by means of incipient wetness. The clusters might be the consequence of the formation of iron nitrate droplets formed after drying the catalyst precursor at 120 °C. The cluster size of the catalyst should then be determined by the size of the iron nitrate droplet during the drying process; similar results were obtained by Feller et al. (1999) for an impregnated Co/SiO_2 catalyst.

Figure 3.12 show the iron supported on APTeS-modified silica impregnated with potassium. All the images show dark islands, which are believed to be iron clusters on the modified silica. The catalysts APTeS MS 0 K, APTeS MS 0.01 K and APTeS MS 0.02 K show irregular shaped agglomerates of smaller particles. The catalyst APTeS MS 0.005 K displays spherical-shaped agglomerates. The diameter of the agglomerates for the iron catalysts supported on APTeS modified silica is between 46 -159 nm. The iron was not evenly spread on the APTeS-modified silica surface as evidenced by the large areas without iron.

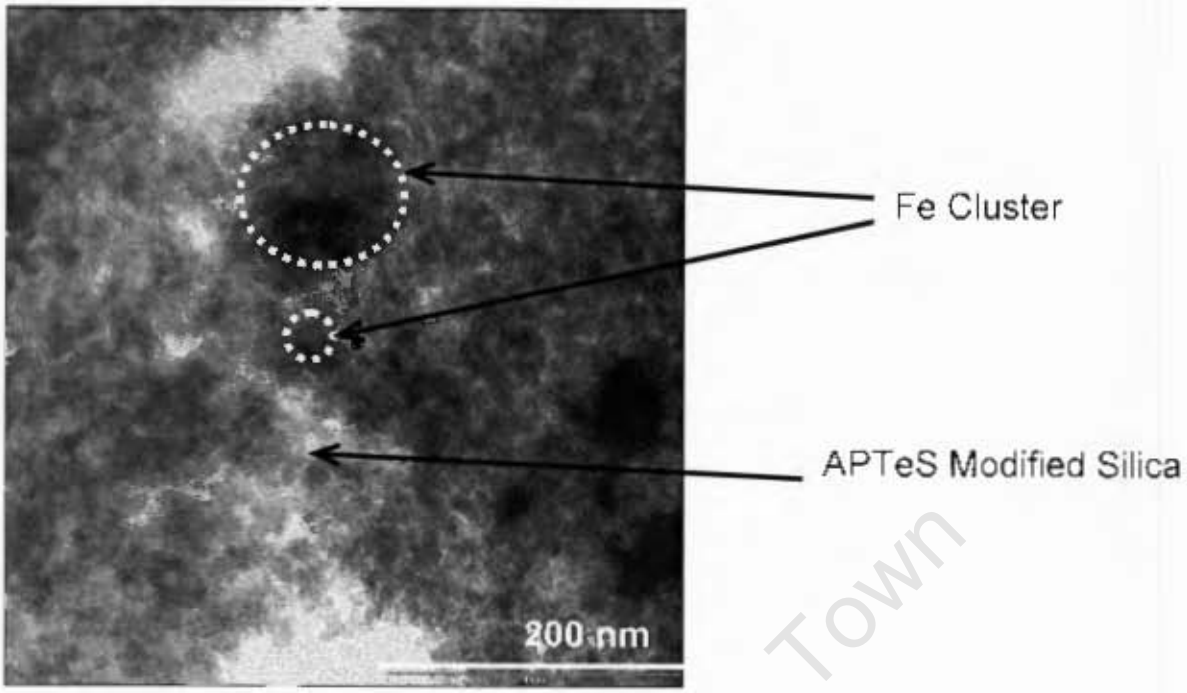

(A)

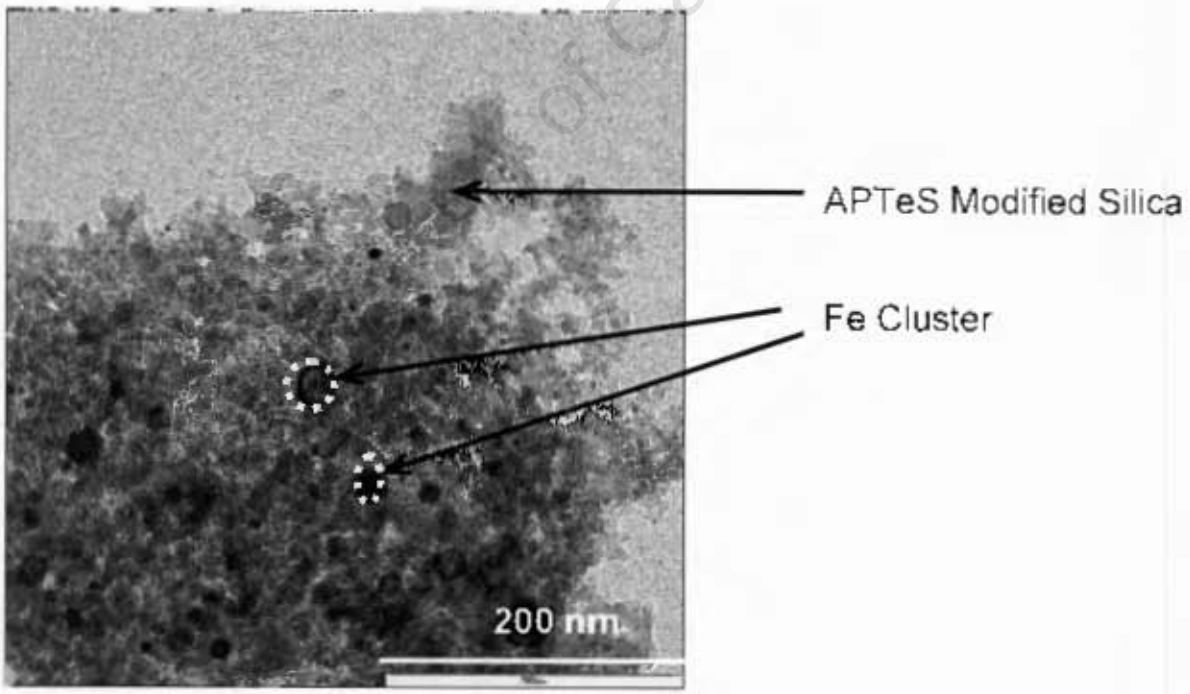

(B)

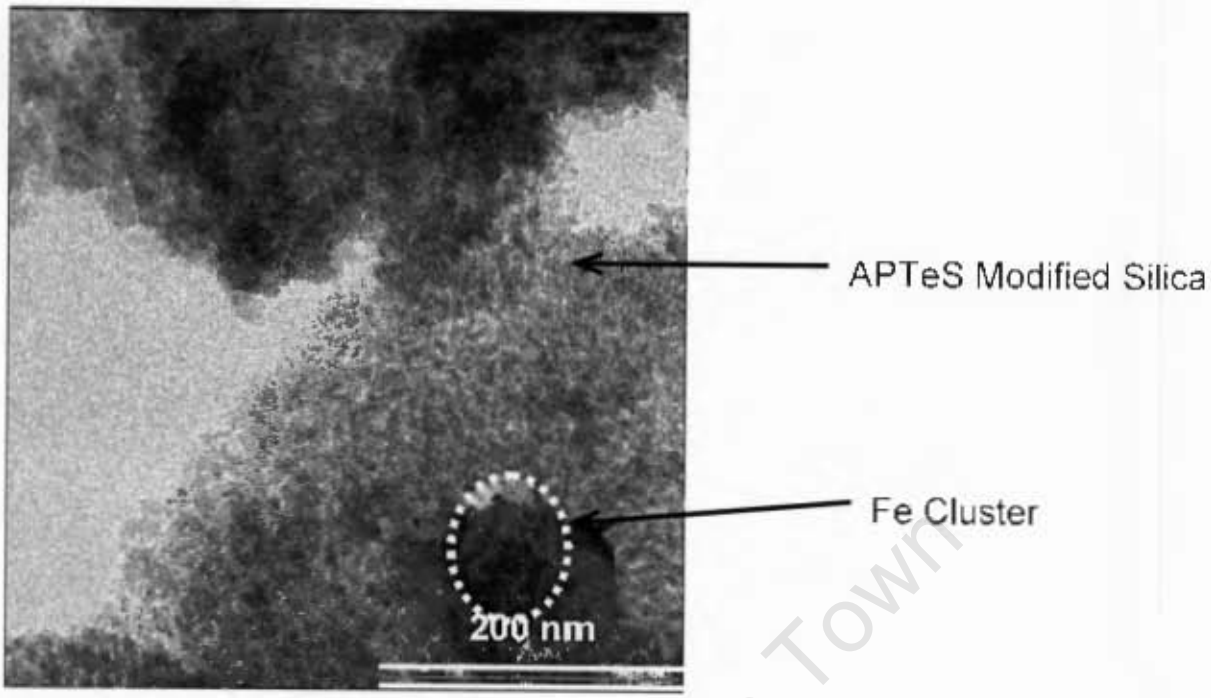

(C)

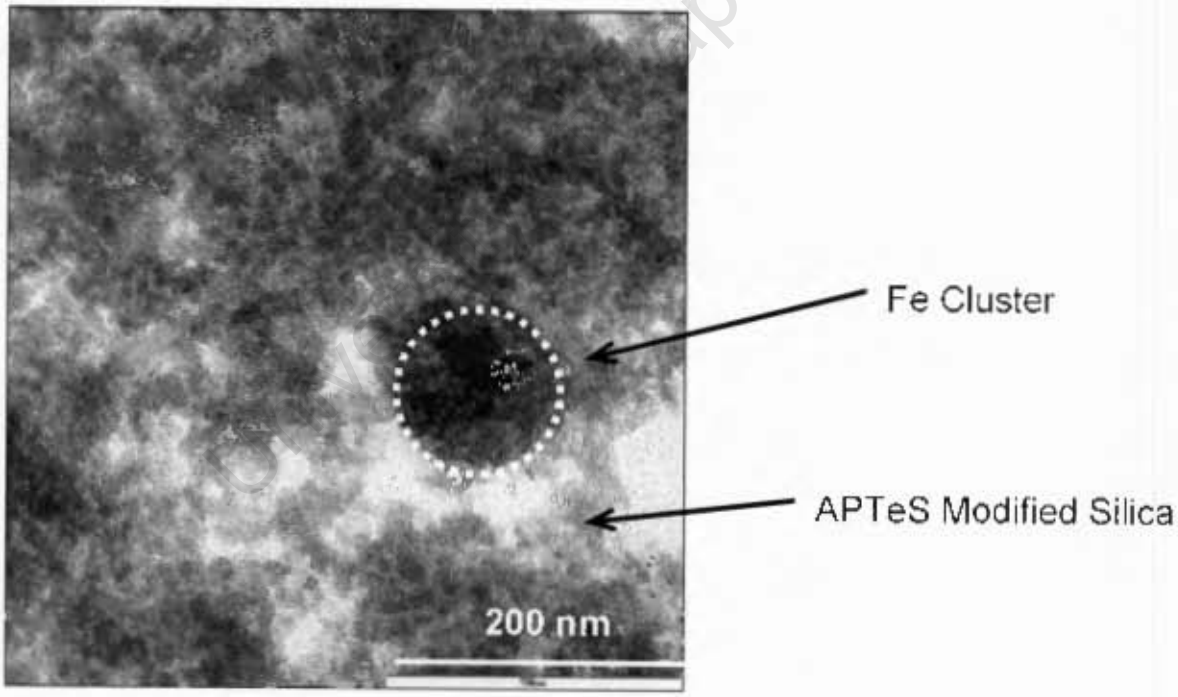

(D)

Figure 3.12: TEM images for iron catalyst precursor supported on APTeS modified silica (A) 0 K, (B) 0.005 K, (C) 0.01 K, (D) 0.02 K.

The crystallite size distribution could not be determined by measuring crystal diameters from TEM pictures of the different catalyst, because the iron crystallites were observed as clusters. The average cluster diameter was determined by measuring on average about 10 clusters manually and randomly from the pictures for each catalyst, shown in Table 3.13.

Table 3.13: Custer diameters for iron catalysts supported on silica and APTeS-modified silica.

Catalysts	Cluster diameter (nm)
0 K	111
0.005 K	183
0.01 K	140
0.02 K	154
APTeS MS 0 K	108
APTeS MS 0.005 K	46
APTeS MS 0.01 K	151
APTeS MS 0.02 K	159

3.3 Fischer-Tropsch synthesis

The effect of potassium promotion on the catalytic performance of an iron catalyst supported on silica and APTeS-modified silica was tested under Fischer-Tropsch conditions in a fixed bed reactor. Prior to the Fischer-Tropsch synthesis the catalysts were activated following identical reduction (H_2 at 350 ^{o}C for 16 hrs; flow rate of 45 ml(NTP)/min). All tests were run for 4 days at 270 ^{o}C at a total pressure of 20 bar and a constant synthesis gas flow rate of 60 ml(NTP)/min. Some of the reported data for specific reaction times is listed in Appendix. Catalyst activity was reflected by the amount of converted CO under the specified test conditions.

3.3.1 CO conversion as a function of time on stream

The CO conversion as a function of time on stream was monitored for each catalyst (see Figure 3.13 and 3.14).

The activity obtained for all catalysts were rather stable, with the exception of the iron catalysts supported on silica with 0 K, 0.06 K and 0.08 K catalysts which decline with time on stream (see Table 3.14).A high CO conversion was obtained with iron catalyst supported on silica with 0.01 K (~46.4 mol %) and 0.02 K catalysts (~40 mol %). In contrast, the iron catalyst supported on silica with 0 K (~17.9 mol %) and with higher potassium loadings (0.06 K:~21.7 mol %, 0.08 K: ~21.6 mol %) show a lower activity after 360 min time on stream. The maximum catalytic activity is obtained at 0.01 K, indicating the optimum potassium loading. The presence of an optimum can be explained in terms of an increase in the activity due to the presence of potassium on the active phase (promotional effect) and the inhibition due to the coverage of the active phase with potassium and thus limiting the promotional effect (Davis et al., 2003).

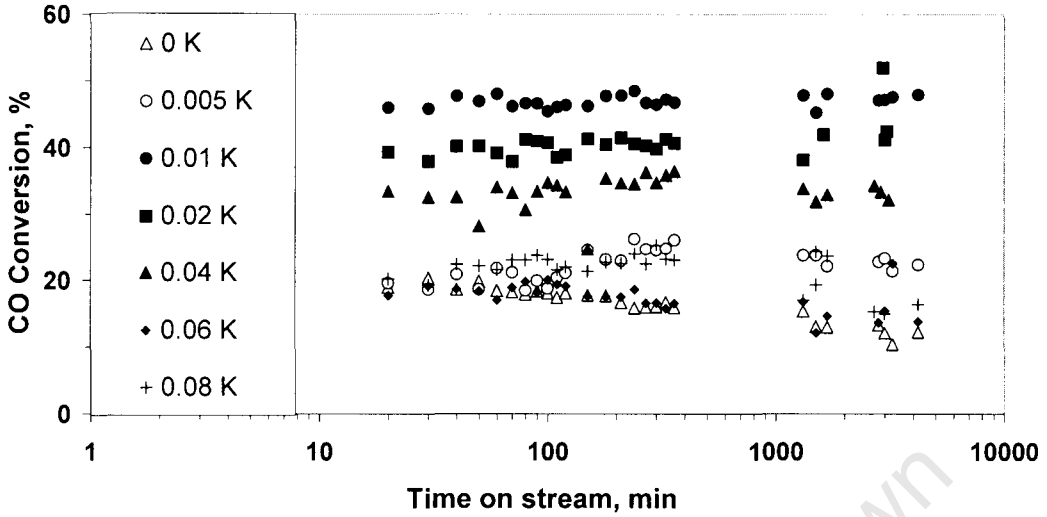

Figure 3.13: Time on stream CO conversion from Fischer-Tropsch synthesis over iron supported on silica(m_{cat} = 1 g, T = 270 °C, P = 20 bar, H_2:CO = 2:1, WHSV = 1800 hr^{-1}).

Table 3.14: Average CO conversion as a function of time on stream during Fischer-Tropsch Synthesis over iron supported on silica (m_{cat} = 1g, T = 270 °C, P = 20 bar, H_2:CO = 2:1, WHSV = 1800 hr^{-1}).

Catalyst Time(min)	X_{CO} (%) 20 - 360	X_{CO} (%) 360 - 3060
0 K	17.9	13.2
0.005 K	22.9	23.2
0.01 K	46.4	47.2
0.02 K	40.0	42.7
0.04 K	35.0	33.6
0.06 K	21.7	20.9
0.08 K	21.6	18.8

Figure 3.14 shows the CO conversion as a function of time on stream for the four iron catalysts supported on APTeS-modified silica promoted with different amounts of potassium. The iron catalysts supported on APTeS-modified silica containing 0.005 K, 0.01 K and 0.02 K show a high CO conversion (~ 35.5 –

40.8 mol %) as a function of time on stream. The APTeS MS 0.02 K catalyst shows a high initial CO conversion of 49 mol % within the first 40 minutes of the reaction, which drops steadily with time on stream to 37.4 – 40.8 mol % until steady state conversion is attained. The maximum catalytic activity is obtained at APTeS MS 0.02 K. Table 3.15 showed that a variation in the potassium loading between 0.005 and 0.02 K has no significant influence in CO conversion with time on stream.

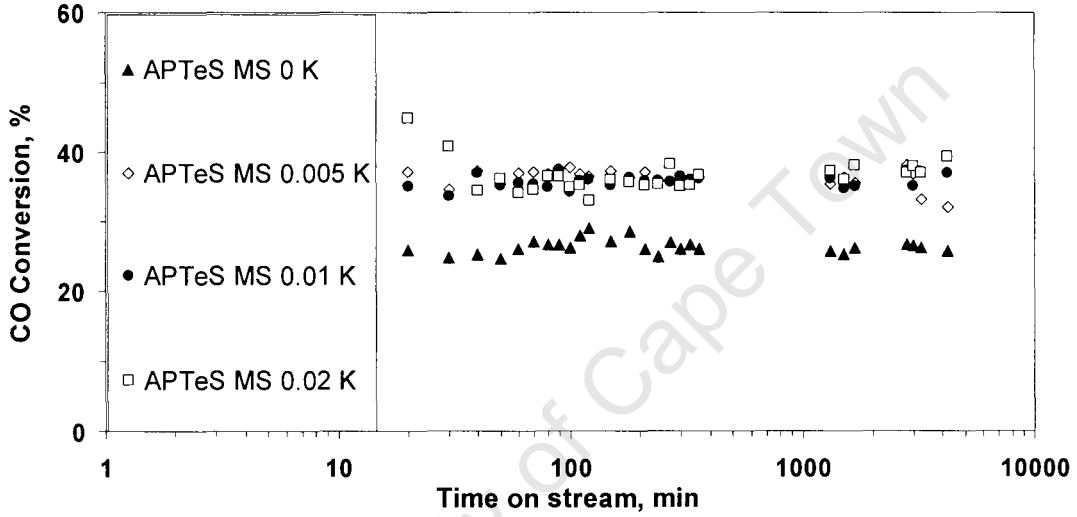

Figure 3.14: Time on stream CO conversion from Fischer-Tropsch synthesis over iron supported on APTeS modified silica (m_{cat} = 1g, T=270 °C, P = 20 bar, H_2:CO = 2:1, WHSV = 1800 hr^{-1}).

Table 3.15: Average CO conversion as a function of time on stream during Fischer -Tropsch Synthesis over iron supported on APTeS-modified silica (m_{cat} = 1 g, T = 270 °C, P = 20 bar, H_2:CO =2:1, WHSV = 1800 hr^{-1}).

Catalyst Time(min)	X_{CO} (%) 20 - 360	X_{CO} (%) 360 - 3060
APTeS MS 0 K	25.9	26.0
APTeS MS 0.005 K	36.7	35.5
APTeS MS 0.01 K	35.7	36.1
APTeS MS 0.02 K	40.8	37.4

3.3.2 CO_2 formation

CO_2 is formed in iron based Fischer-Tropsch synthesis mainly via the water-gas shift reaction. Product water reacts in a reaction with carbon monoxide to form CO_2. Carbon dioxide scatter is observed in Figure 3.15 with time on stream. Due to the small concentration of the CO_2 formed, a low, wide peak was obtained in the GC trace and integration of peaks was inconsistent.

The S_{CO2} for the supported iron catalyst is low in comparison to precipitated iron catalysts (Herranz et al., 2006). The reaction takes place by a redox mechanism. In the supported samples, the WGS reaction occurs by a different mechanism, through formate intermediates, due to the limitations of the Fe cations to change their oxidation state (Rethwisch et al., 1986). This latter mechanism is less effective, so the supported catalysts are less active in the WGS reaction (Herranz et al., 2006).

Figure 3.15 shows the selectivity for CO_2 in the Fischer-Tropsch synthesis over iron catalysts supported on silica with various amounts of potassium as a function of time on stream. The effect of potassium loading on the carbon dioxide selectivity cannot be easily ascertained from a plot like Figure 3.15, since the

different conversions were obtained over the various catalysts. Figure 3.16 shows the carbon dioxide selectivity against CO conversion for the catalysts. The 0 K catalysts show 12 – 31 C-% carbon dioxide selectivity at 18 mol-% CO conversion with time on stream. The 0.05 K catalyst shows a smaller degree of scatter, at 21 mol-% CO conversion, carbon dioxide selectivity of 10 – 15 C-% is obtained. The same amount of scatter of 5 – 12 C-% carbon dioxide selectivity is shown with 0.01 K catalyst (47 mol-% CO conversion); 0.02 K catalyst (40 mol-% CO conversion) and 0.04 K catalyst (33 mol-% CO conversion). The 0.06 K catalyst and 0.08 K catalyst shows a carbon dioxide selectivity of 11 – 28 C-% at 23 mol-% CO conversion. Generally, the carbon dioxide is low for the catalysts with high CO conversions. This is not expected, since with increasing conversion the water-gas shift reaction is expected to get closer to equilibrium. Thus, the more active catalysts seem to be less active for the water gas shift reaction yielding CO_2.

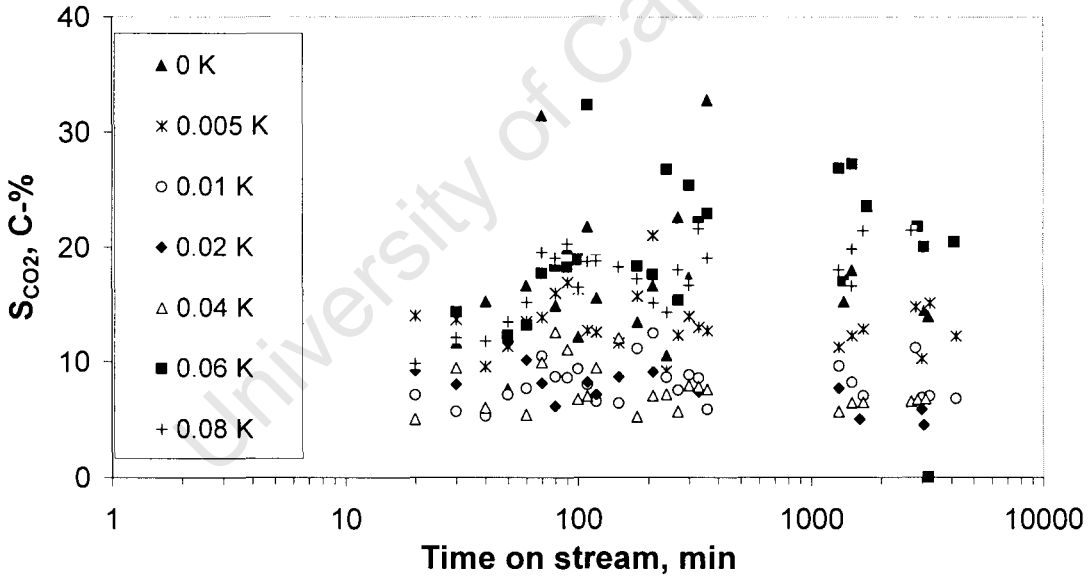

Figure 3.15: Time on stream CO_2 selectivity (S_{CO2}) from Fischer-Tropsch synthesis over iron catalyst supported on silica (m_{cat} = 1 g, T = 270 °C, P = 20 bar, H_2:CO = 2:1, WHSV = 1800 hr^{-1}).

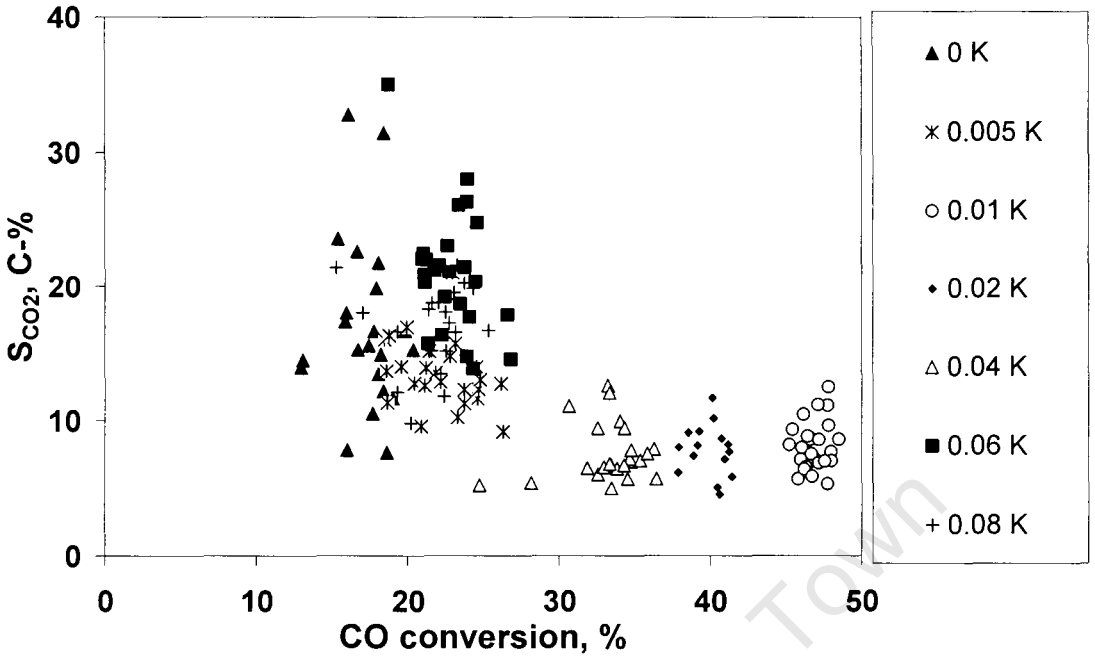

Figure 3.16: Selectivity for CO_2 as a function of the CO conversion in the Fischer-Tropsch synthesis over iron catalyst supported on silica (m_{cat} = 1 g, T = 270 °C, P = 20 bar, H_2:CO = 2:1, WHSV = 1800 hr^{-1})

The catalyst supported on APTeS-modified silica also shows scattered carbon dioxide selectivity with time on stream in Figure 3.17. Most of the modified catalysts shows rather low carbon dioxide selectivities, which seem to increase with increasing time on stream.

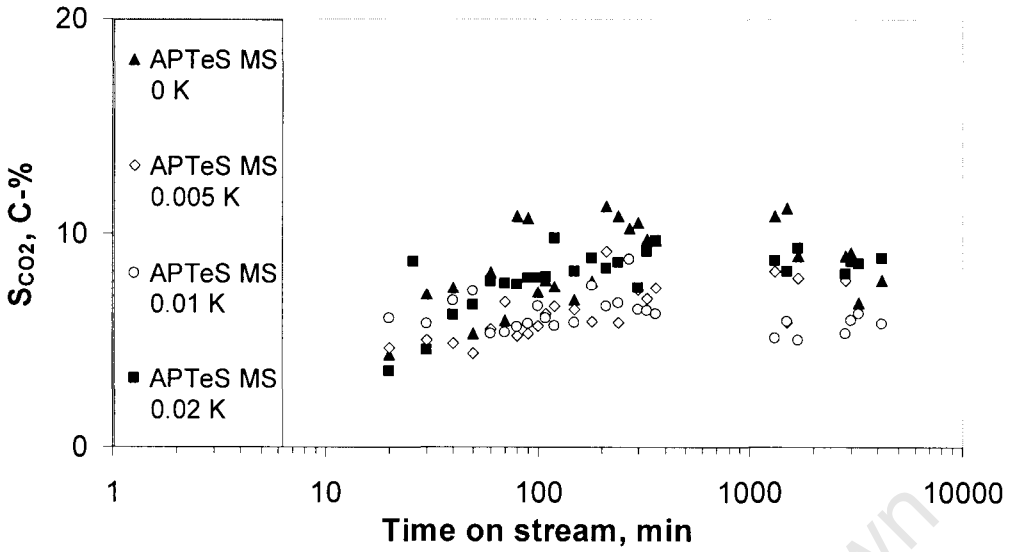

Figure 3.17: CO_2 selectivity (S_{CO2}) in the Fischer-Tropsch synthesis over iron catalyst supported on APTeS-modified silica as a function of time on stream (m_{cat} = 1 g, T = 270 °C, P = 20 bar, H_2:CO = 2:1, WHSV = 1800 hr^{-1}).

The effect of potassium loading on the carbon dioxide selectivity cannot be easily ascertained form Figure 3.17 because of the different conversions exhibited by the four catalysts. Figure 3.18 shows a plot of carbon dioxide selectivity as a function of the CO conversion. The iron catalyst supported on APTeS-modified catalyst without potassium (APTeS MS 0 K) shows a carbon dioxide selectivity of between 4 and 11 C-% at a CO conversion of 25 %. The iron catalysts supported on APTeS-modified with potassium (APTeS MS 0.005 K, APTeS MS 0.01 K and APTeS MS 0.02 K) carbon dioxide selectivity scattered between 2 and 10 C-% at 36 mol -% CO conversion.

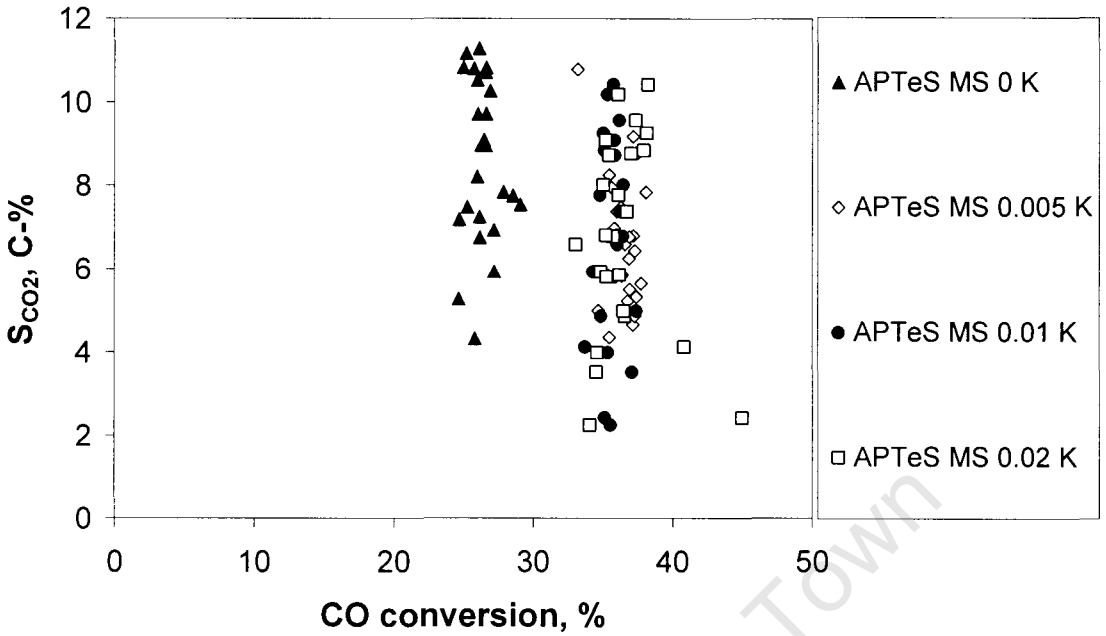

Figure 3.18: Carbon dioxide selectivity (S_{CO2}) as a function of CO-conversion in the Fischer-Tropsch synthesis over iron catalyst supported on APTeS-modified silica (m_{cat} = 1 g, T = 270 °C, P = 20 bar, H_2:CO = 2:1, WHSV = 1800 hr^{-1}).

3.3.3 Methane selectivity

Figure 3.19 shows the variation of the methane selectivity (S_{CH4}) in C-% as a function of time on stream for iron catalyst supported on silica during Fischer-Tropsch synthesis. The methane selectivity obtained with the catalyst containing no potassium (0 K) is initially steady at 18 C-% and after 210 min it increases steadily to 25 C-% after 3060 min. All the potassium promoted catalyst show lower methane selectivity compared to the 0 K catalysts. The methane selectivity of iron catalyst supported on silica containing 0.005 K is around 20 C-% initially and after 150 min it drops steadily to 14 C-% with time on stream. The iron catalysts supported on silica with a higher potassium loading have a lower methane selectivity of ca. 6 -12 C-%. The only exception seems to be the iron catalyst supported on silica with 0.06 K.

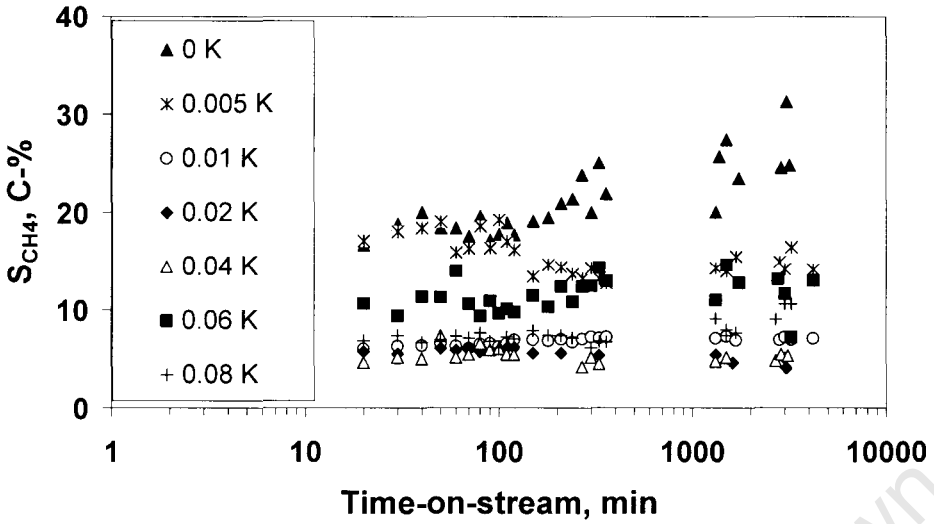

Figure 3.19: Methane selectivity (S_{CH4}) in C-% in the Fischer-Tropsch synthesis over iron catalyst supported on silica as a function of time on stream (m_{cat} = 1 g, T = 270 °C, P =20 bar, H_2:CO = 2:1, WHSV = 1800 hr^{-1}).

The methane selectivity was measured at various levels of CO-conversion. Figure 3.20 shows the methane selectivity as a function of the CO-conversion. The methane selectivity seems to decrease with increasing CO-conversion. The iron catalysts with low potassium loading (0 K and 0.005 K) seem to fall on a single curve. With increasing potassium loading, the curve is shifted towards lower methane selectivity at a given conversion level. Thus, potassium addition lowers the methane selectivity in iron-catalysed Fischer-Tropsch synthesis.

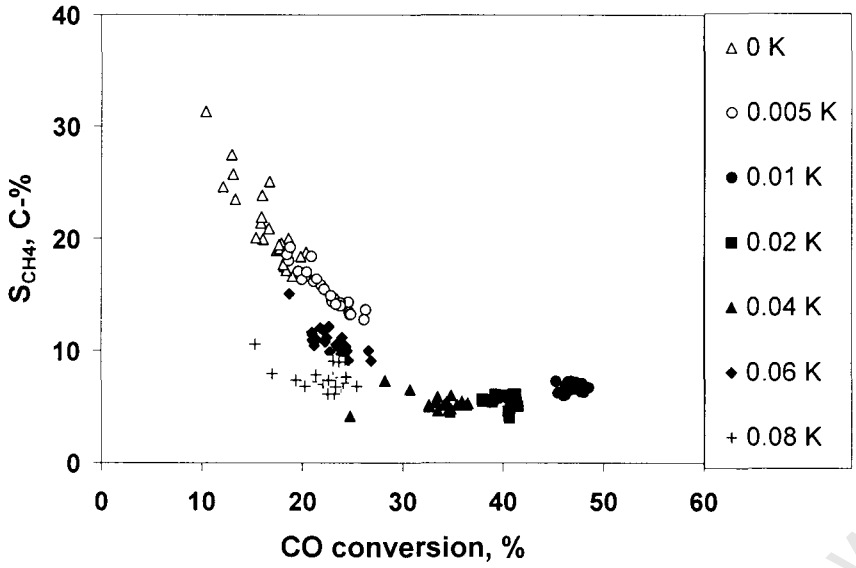

Figure 3.20: Methane selectivity (C-%) in the Fischer-Tropsch synthesis over iron supported on silica as a function of CO-conversion (m_{cat} = 1 g, T = 270 °C, P = 20 bar, H_2:CO = 2:1, WHSV = 1800 hr^{-1}).

Figure 3.21 shows the methane selectivity (S_{CH4}) in C-% obtained over the four supported iron catalysts on APTeS-modified silica in the Fischer-Tropsch synthesis as a function of time on stream. All the potassium promoted catalysts showed lower methane selectivities compared to the iron catalyst supported on APTeS-modified silica without potassium (APTeS MS 0 K), but the methane selectivity increased with time on stream. The initial methane selectivity over APTeS MS 0.005 K increase form 3 C-% to attain steady state at 9 C-%. The initial methane selectivity over the iron catalyst supported on APTeS-modified silica, APTeS MS 0.02 K catalyst is at 7 C-% and increases to ca. 9 C-% with time on stream.

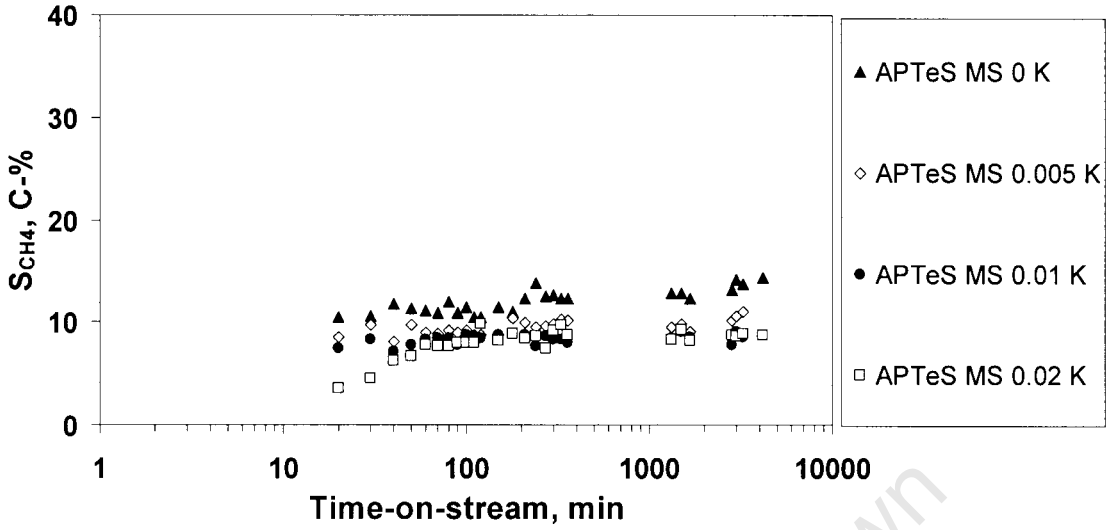

Figure 3.21: Methane selectivity (S_{CH4}) in C-% in the Fischer-Tropsch synthesis over iron supported on APTeS-modified silica as a function of time on stream (m_{cat} = 1 g, T =270 °C, P = 20 bar, H_2:CO = 2:1, WHSV =1800 hr^{-1}).

Figure 3.22 shows the methane selectivity over the iron catalysts supported on APTeS-modified silica as a function of CO-conversion. It seems that the methane selectivity as a function of CO-conversion follows a single curve (with a rather high scatter in the methane selectivity). This implies that either the methane selectivity is not a function of CO-conversion (and thus potassium lowers the methane selectivity) or potassium does not affect methane selectivity. Based on the rather consistent methane readings as a function of time on stream, and the rather high levels of CO-conversion, it is believed that methane selectivity is not a strong function of CO-conversion, thus the potassium addition lowers the methane selectivity during Fischer-Tropsch synthesis.

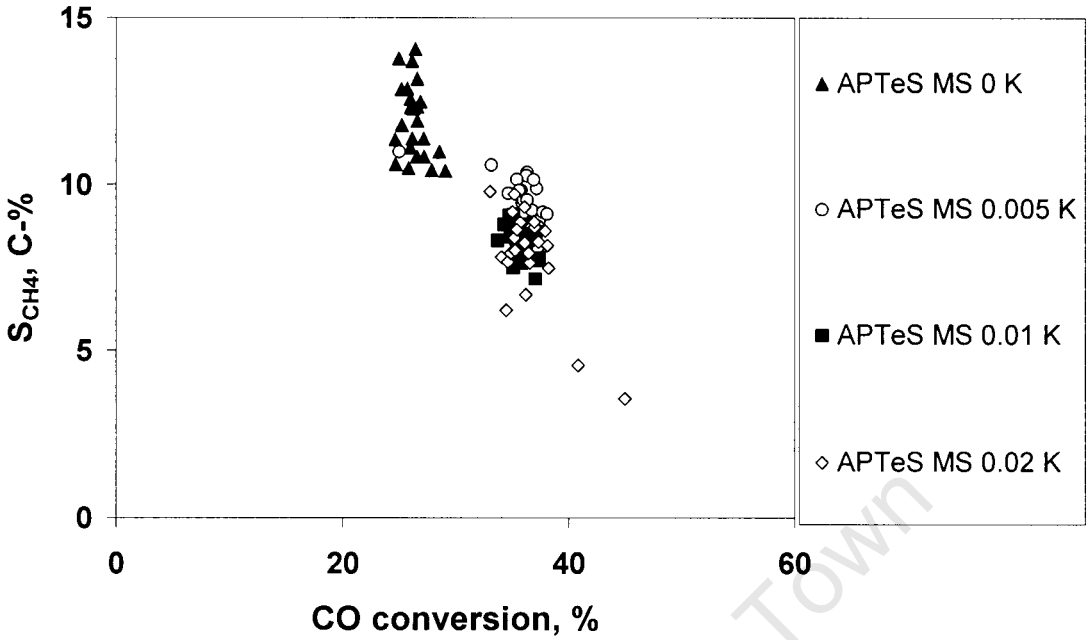

Figure 3.22: Methane selectivity (S_{CH4}) as a function of CO conversion in the Fischer- Tropsch synthesis over iron catalyst supported on APTeS modified silica (m_{cat} = 1 g, T = 270 °C, P = 20 bar, H_2:CO = 2:1, WHSV = 1800 hr^{-1}).

The methane content in the fraction of organic product compounds (S'_{CH4}) was determined as well (see Table 3.15). The methane content can be obtained from the methane selectivity (S_{CH4} – as determined by the analysis of inorganic gases and methane using a TCD) taking into account the amount of CO converted to CO_2 and from the analysis of the organic products formed in the Fischer-Tropsch synthesis using a FID. It can be seen that the methane content was obtained using the FID-analysis was higher than the methane content using the TCD-analysis. The deviation is more severe and CO_2 selectivity. The FID analysis was done for the C_1-C_8-fraction. The omission of the longer chain which attribute to the high methane amount obtained.

The TCD results for the methane content were in non agreement with the results obtained during FID analysis (Table 3.16). The small methane and carbon

dioxide peak formed during TCD analysis for the iron catalyst supported on silica and the iron catalyst supported on APTeS modified silica did not allow for accurate analysis (TCD detection limits). The content of potassium for the catalysts had little effect on the methane selectivity. The iron catalyst supported on silica yielded a methane content of 19.4 – 33.3 C-% and the iron catalyst supported on APTeS modified silica yielded methane selectivity of 29.9 – 35.4 C-% according to the FID analysis. According to the TCD analysis the methane content (5.73 – 28.3 C-%) was much lower than the methane content analyzed by the FID (19.4 - 35.4 C-%) for the iron catalyst supported on silica and the iron catalyst supported on APTeS modified silica. The relative errors are typically ±3 % for TCD analyses and ±1 % for FID analyses.

Table 3.16: Methane content (S'_{CH4}) obtained during FID analysis from Fischer-Tropsch synthesis (m_{cat} = 1 g, T = 270 °C, P = 20 bar, H_2:CO = 2:1, WHSV = 1800 hr^{-1}).

Catalysts	S'_{CH4} (C-%) (FID)[a]	S'_{CH4} (C-%) (TCD)
0 K	28.0	22.7
0.005 K	33.3	23.5
0.01 K	19.4	8.24
0.02 K	26.8	5.73
0.04 K	25.8	6.61
0.06 K	25.4	12.2
0.08 K	19.6	28.3
APTeS MS 0K	32.3	20.3
APTeS MS 0.005 K	35.2	15.0
APTeS MS 0.01 K	35.4	10.6
APTeS MS 0.02 K	29.9	10.8

[a] Methane content measured out of C_1-C_8 carbon content.

3.3.4 Anderson-Schultz-Flory (ASF) product distributions

The growth probability p_g of a growing chain can be derived from slopes from the Anderson-Schultz-Flory distribution:

$$\lg(x_N) = N\lg(p_g) + \lg\left(\frac{1-p_g}{p_g}\right)$$

The logarithmic molar distribution of the linear hydrocarbons versus the carbon number obtained at 3060 min time on stream is shown in Figure 3.23 and Figure 3.24. The curves show the characteristic deviations form ideal distributions, i.e. high values obtained at C_1, lower values at C_2 than expected for ideal polymerisation. Schulz et al., explained in 1995 that the relatively high molar methane content is attributed to additional sites responsible for solely methane production. The lower than expected amount of C_2-product compounds are attributed to secondary reactions (Dry, 1981).

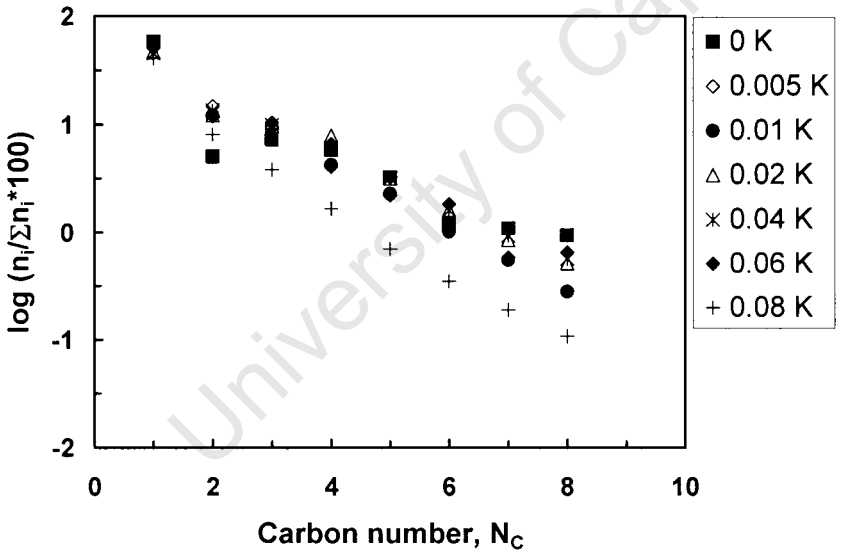

Figure 3.23: Anderson-Schulz-Flory distribution for the iron catalysts supported on silica with varying potassium content at 3060 min time on stream. (m_{cat} ~ 1 g, T = 270 °C, P = 20 bar, H_2:CO = 2:1, WHSV = 1800 hr^{-1}).

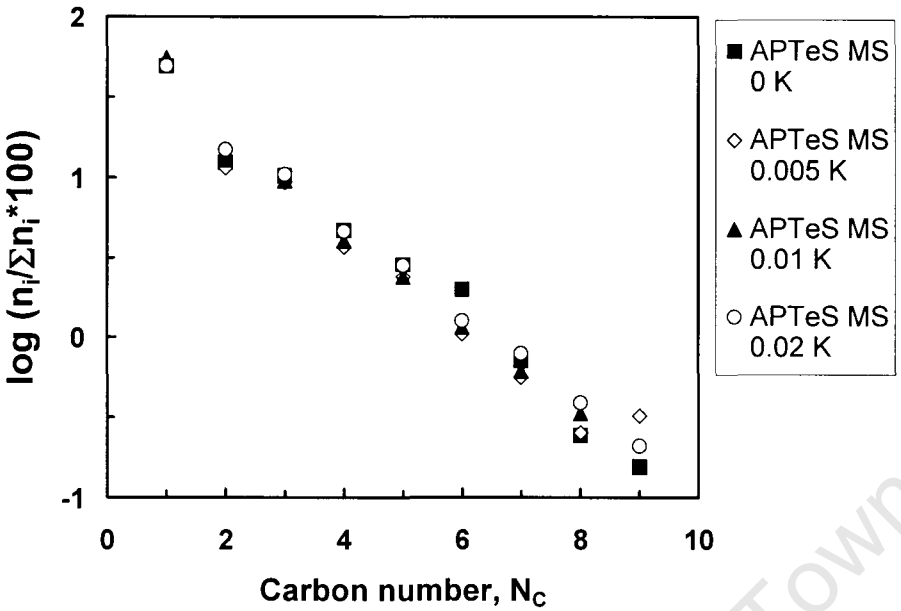

Figure 3.24: Anderson-Schulz-Flory product distribution for the iron catalysts supported on APTeS modified silica with varying potassium content at 3060 min time on stream. (m_{cat} ~ 1 g, T = 270 °C, P = 20 bar, H_2:CO = 2:1, WHSV = 1800 hr^{-1}).

Chain growth probabilities were calculated from slope of the linear hydrocarbon ASF plot between C_3 and C_8 for the iron catalyst supported on silica and between C_3 and C_9 for the iron catalyst supported on APTeS modified silica. It should be noted here that the chain growth probability in this range was assumed to be constant, although deviations from a constant chain growth probability could be detected in this range. Thus, the chain growth probability should only be taken as a rough indication of the actual chain growth probability over a long carbon number range. Table 3.17 and Table 3.18 show values of the chain growth probabilities for each catalyst obtained for 3060 min time on stream. The obtained chain growth probabilities showed a large degree of scatter (attributed to the non-constant slope in the C_3-$C_{8/9}$-range of the Anderson-Schulz-Flory distribution). The iron catalyst supported on silica showed chain growth probabilities between 0.53 and 0.69, whereas the iron catalysts supported on

APTeS-modified silica showed smaller chain growth probabilities between 0.52 and 0.57.

Table 3.17: Chain-growth-probability in the range C_3-C_8 (p_g) for the iron catalysts supported on silica with varying potassium content at 3060 min time on stream (m_{cat} ~ 1 g, T = 270 °C, P = 20 bar, H_2:CO = 2:1, WHSV = 1800 hr^{-1}).

Catalyst	3060 min
	α
0 K	0.68
0.005 K	0.56
0.01 K	0.53
0.02 K	0.69
0.04 K	0.69
0.06 K	0.65
0.08 K	0.68

Table 3.18: Chain-growth-probability in the range C_3-C_9 (p_g) for the iron catalysts supported on APTeS-modified silica with varying potassium content at 3060 min time on stream (m_{cat} ~ 1 g, T = 270 °C, P = 20 bar, H_2:CO = 2:1, WHSV = 1800 hr^{-1}).

Catalyst	3060 min
	α
APTeS MS 0 K	0.57
APTeS MS 0.005 K	0.53
APTeS MS 0.01 K	0.52
APTeS MS 0.02 K	0.55

3.3.5 Olefin formation

Olefins are the main primary organic products of Fischer-Tropsch synthesis (Schulz and Clayes, 1999). They are thought to form via dissociative desorption of growing surface alkyl species. A paraffin can be formed via hydrogen addition

to the alkyl species. Olefin desorption is reversible as olefins can reabsorb and undergo secondary reactions, such as incorporation into growing chains and secondary hydrogenation to the corresponding paraffin. Ethene is the most reactive olefin (Iglesia et al., 1993), which is believed to be readily converted to ethane and incorporated yielding long chain hydrocarbons. A decrease in n-olefin content in the fraction of linear hydrocarbons with increasing in carbon number is attributed to secondary reactions of primary formed olefins. 1-Olefins are believed to act as chain initiators, which in conjunction with hydrogenation of olefins lead to the decrease in olefin content (Claeys et al., 2004).

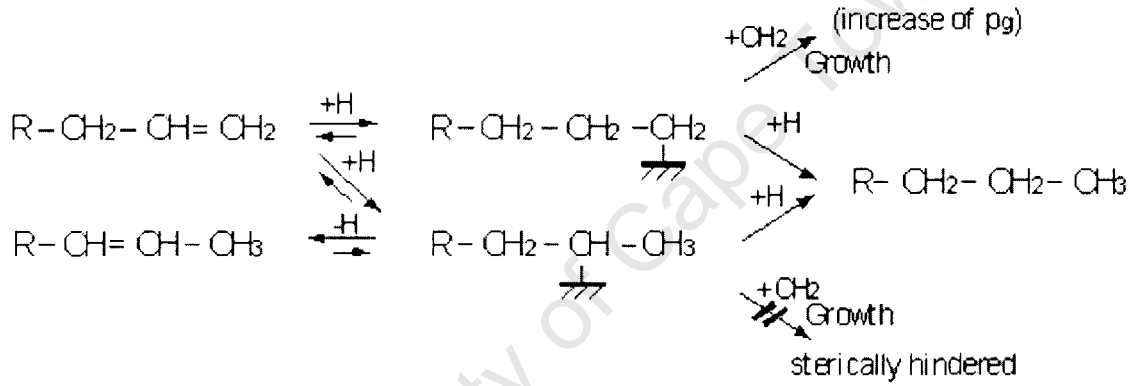

n-Olefin content was calculated on the total linear hydrocarbon product in a carbon number fraction for each catalyst after 3060 minutes on stream (see Figure 3.25 and Figure 3.26). A low n-olefin content for C_2 linear hydrocarbons is observed followed by a high content in C_3-fraction for all the catalysts. The lower C_2 content is indicative of the higher reactivity of ethene in secondary hydrogenation. The n-olefin content decreases gradually with carbon number.

Figure 3.25 shows that n-olefin content in the fraction of linear hydrocarbons increases with increasing potassium loading over all the iron catalyst supported on silica promoted with potassium except for the catalysts 0.005 K and 0.01 K. The lowest n-olefin content was obtained with 0.01 K, which is even lower than 0.005 K catalysts. All the iron catalysts supported on silica promoted with potassium with high CO conversions shows a low olefin content

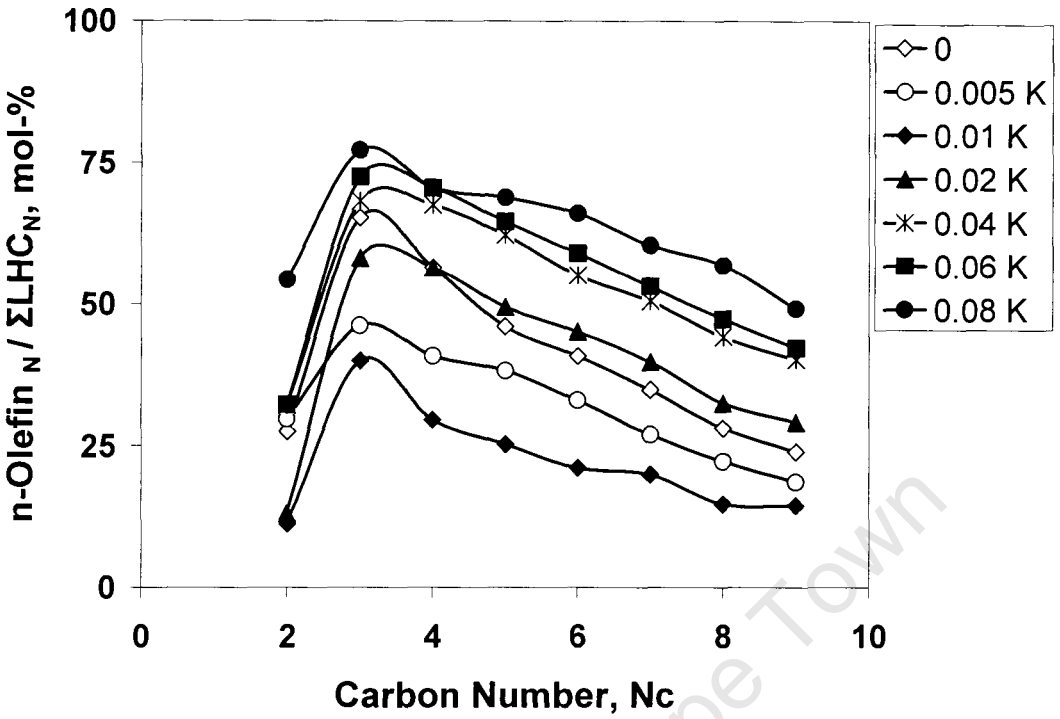

Figure 3.25: Variation in n-olefin content in the fraction of linear hydrocarbons as function of carbon number for iron supported catalyst on silica with varying potassium content after 3060 min time on stream (m_{cat} ~1 g, T = 270 °C, P = 20 bar, H_2:CO = 2:1, WHSV = 1800 hr^{-1}).

The iron catalysts supported on APTeS-modified silica show a similar behaviour (see Figure 3.26), i.e. an increase in the olefin content with increasing potassium loading. The difference in n-olefin content for each catalyst is however small. It is well known that the olefin content of the hydrocarbon product increases with alkali promotion by suppressing the hydrogenation propensity of the iron (Dry et al., 1969).

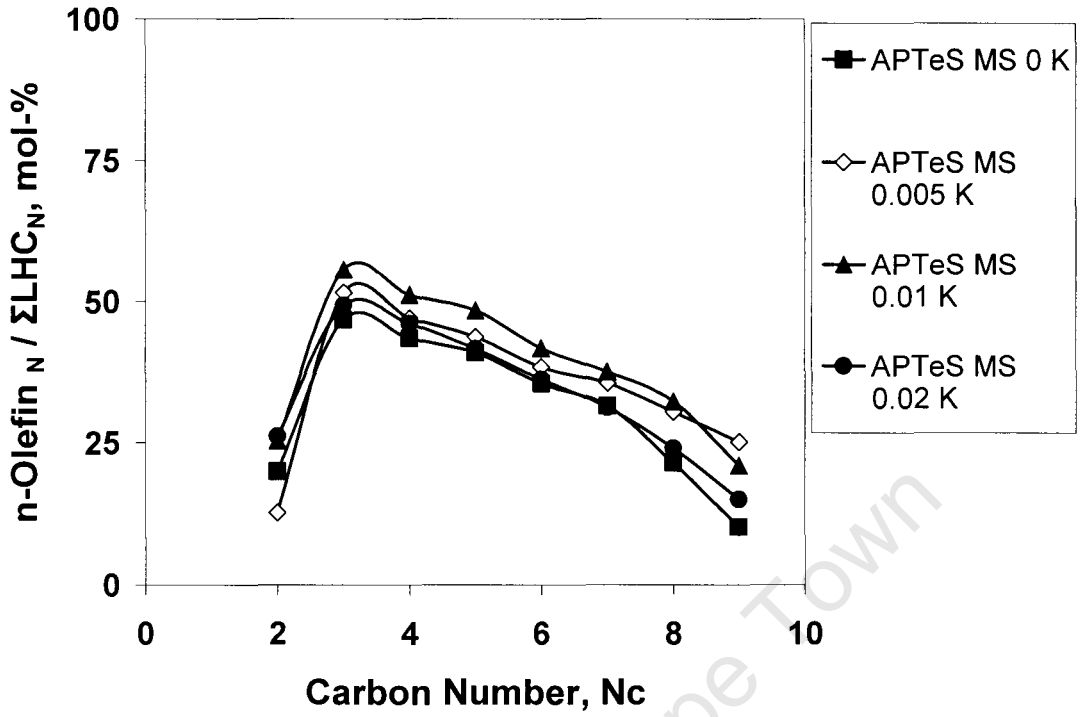

Figure 3.26: Variation in n-olefin content in the fraction of linear hydrocarbons as function of carbon number for iron supported on APTeS-modified silica with varying potassium content at 3060 min time on stream (m_{cat} ~ 1 g, T = 270 °C, P = 20 bar, H_2:CO =2:1, WHSV = 1800 hr^{-1}).

The 1-olefin content in the fraction of linear olefins was calculated as the amount of linear 1-olefin in the total fraction of linear olefin hydrocarbon product. 1-Olefins are formed primarily which can form olefins with internal double bonds after non terminal readsorption to the catalyst surface (Claeys et al., 2004).

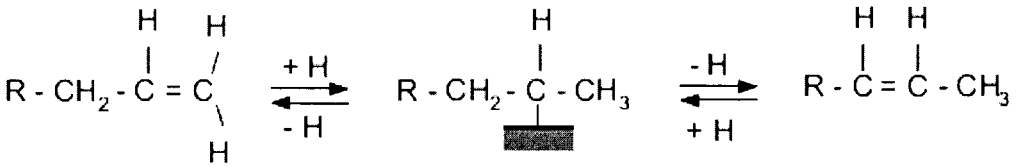

Figure 3.27 and Figure 3.28 shows the variation of 1-olefin content in the fraction of linear olefins as a function of carbon number after 3060 min time on stream. Figure 3.27 show that 1-olefin content in the fraction of linear olefins increases

with increasing potassium loading except for 0.005 K and 0.01 K catalysts which show a low content of 1-olefin, which is consistent with n-olefin content results.

The low 1-olefin content obtained in all the iron catalysts supported on silica (except 0.06 K and 0.08 K catalysts) indicates a large extent of double bond isomerisation, which is characteristic for weakly alkali iron catalysts (Claeys et al. 2004). Increasing potassium content on the catalyst resulted in higher 1-olefin content in the fraction of linear olefins. The observed trend suggest that potassium promotion suppress secondary double bond isomerisation of 1-olefin into internal olefins.

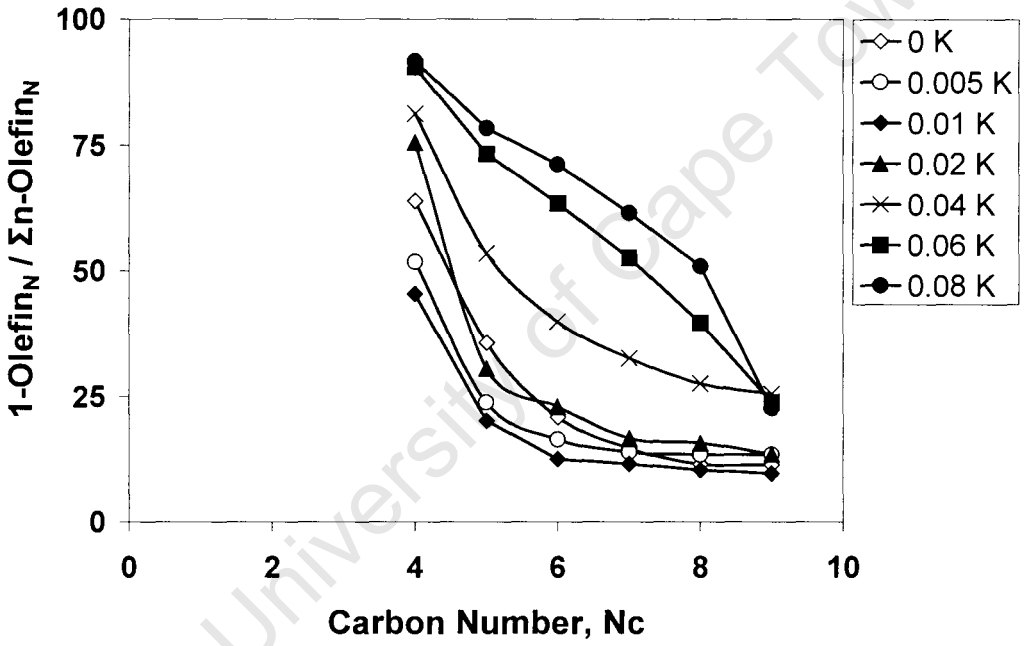

Figure 3.27: Variation in 1-olefin content in the fraction of linear hydrocarbons as function of carbon number for iron supported on silica with varying potassium content at 3060 min time on stream (m_{cat} ~ 1 g, T = 270 °C, P = 20 bar, H_2:CO = 2:1, WHSV = 1800 hr^{-1}).

Figure 3.27 shows the variation of 1-olefin selectivity with an increase in carbon number, the 1-olefin content increase with increase in potassium amount, except for the 0.02 K catalyst. The highest 1-olefin content is obtained with 0.01 K

catalyst. The decrease in olefinicity with increase in carbon number reflects the depletion of 1-olefins via secondary reaction i.e. chain initiation and hydrogenation.

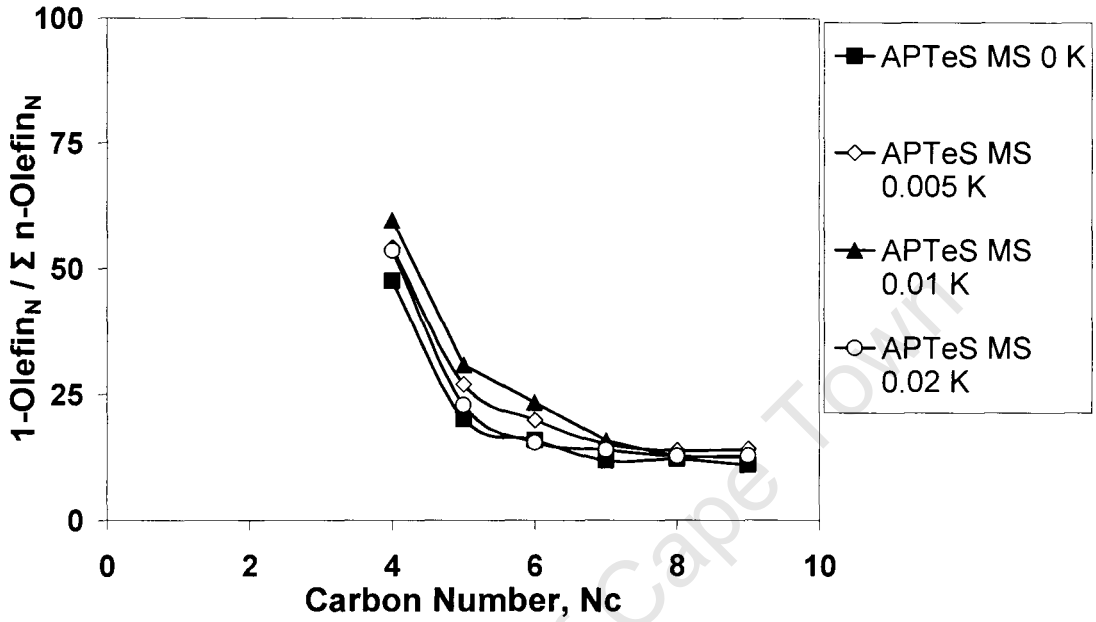

Figure 3.28: Variation in 1-olefin in the fraction of linear hydrocarbons as function of carbon number for iron supported on APTeS modified silica with varying potassium content at 3060 min time on stream(m_{cat} ~ 1 g, T = 270 °C, P = 20 bar, H_2:CO =2:1, WHSV = 1800 hr^{-1}).

3.3.6 Branching

The effect of basicity on product branching was investigated by analysis of the content of branched products in C_5 hydrocarbon fraction. The molar content of iso-C_5 obtained with each catalyst synthesis was plotted against potassium content in the catalyst (see Figure 3.29 and Figure 3.30).

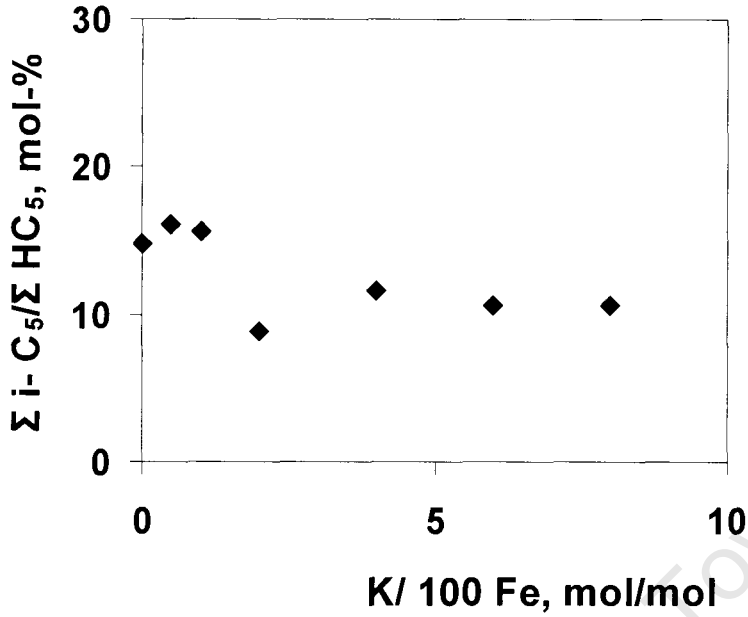

Figure 3.29: Effect of potassium content in iron catalyst supported on silica on the content of iso-C_5 in the C_5 hydrocarbon fraction (m_{cat} ~ 1 g, T = 270 °C, P = 20 bar, H_2:CO = 2:1, WHSV = 1800 hr^{-1}).

The highest iso-C_5 content over the iron catalysts supported on silica was obtained over the catalysts containing 0 K, 0.005 K and 0.01 K with ca. 17 mol-%. A lower constant iso-C_5 content of ca. 11 mol-% was obtained over the iron catalysts supported on silica containing more potassium. The high degree of branching obtained with the 0.005 K catalyst and the 0.01 K catalyst, is characteristic of weak alkali promotion (Clayes, 1997). A decrease of formation of branched compounds has also been associated with alkali promotion effects (Dry, 1981, 2004a), mainly via neutralisation of acid sites, which would catalyze skeletal isomerisation of readsorbed olefins. The opposite trend was obtained with the iron catalysts supported on APTeS-modified silica (see Figure 3.30), for which an increase in the degree of branching with increasing potassium content was observed.

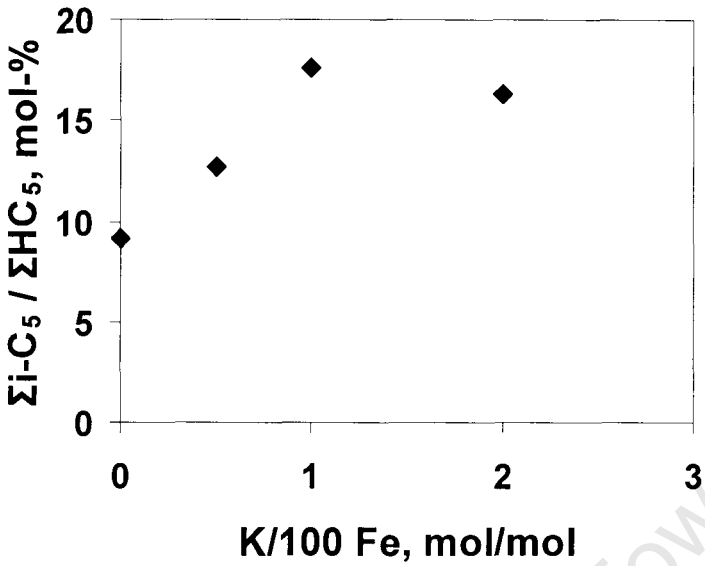

Figure 3.30: Effect of potassium content on iron supported on APTeS-modified silica catalysts on the content of iso-C_5 in the C_5-hydrocarbon fraction(m_{cat} ~ 1 g, T = 270 °C, P = 20 bar, H_2:CO = 2:1, WHSV = 1800 hr^{-1}).

3.3.7 Oxygenate content

Only little is known on the formation of oxygenates. Pichler and Schulz (1970) postulated that oxygen containing surface species can be formed via a CO insertion step. Johnston and Joyner (1993) stated that the same species could be formed by addition of hydroxyl groups to an alkylidene species. Desorption of this species the leads to formation of alcohols or aldehydes respectively.

Generally, reasonable amounts of alcohols plus aldehydes were found in the products over iron supported on silica and on the iron supported on the APTeS-modified silica. The effect of potassium promotion on the oxygenate content of the Fischer-Tropsch product was investigated by evaluating the oxygenate content in the C_2 and C_5 product fraction (see Figure 3.31 and 3.32).

The fraction of oxygenates in the C_2-product fraction increases with increasing potassium content in the iron catalysts support on silica (see Figure 3.31). A similar trend seems to be present for the oxygenates in the C_2 and C_5-product fraction obtained with the iron catalysts supported on APTeS-modified silica (see Figure 3.32). The oxygenate content in the C_5 –fraction increases with increasing potassium loading from 0.7 to 3 mol-%. The oxygenate content in the C_2-fraction is much higher (30 - 35 mol-%). It should be noted that C_2-oxygenates could not be resolved in the product spectra obtained with the catalysts APTeS 0.01 K and APTeS 0.02 K.

Potassium in iron based Fischer-Tropsch synthesis is known to result in higher oxygenate selectivity (Dry, 2004b), most likely due to inhibition of readsorption of primarily formed oxygenates. The much lower oxygenate content in the C_5-fraction compared to the C_2-fraction is attributed to the higher solubility of the C_5-oxygenates in the liquid phase within the pores of the catalysts resulting in a larger extent of secondary conversion of these compounds (it should be noted that the reactivity of oxygenates for secondary reactions in Fischer-Tropsch synthesis is much larger than of corresponding 1-olefins of the same carbon number - Davis, 1993).

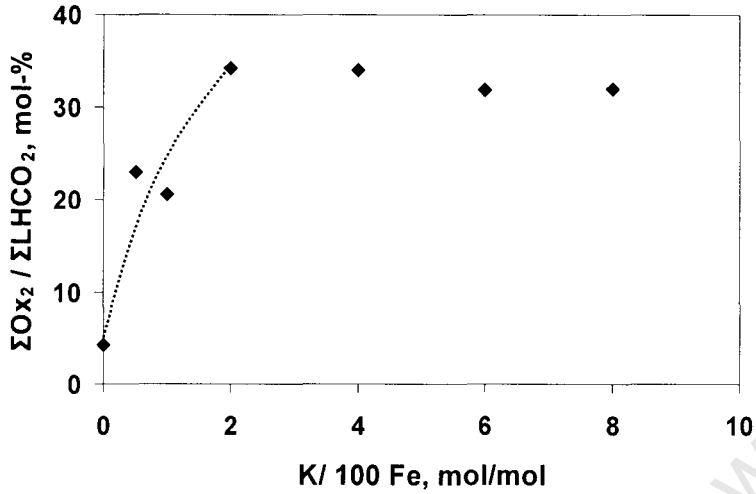

Figure 3.31: Effect of potassium content on iron supported on silica catalysts on the formate of oxygenate product in the C_2 fraction. (m_{cat} ~ 1 g, T = 270 °C, P =20 bar, H_2:CO = 2:1, WHSV = 1800 hr^{-1}).

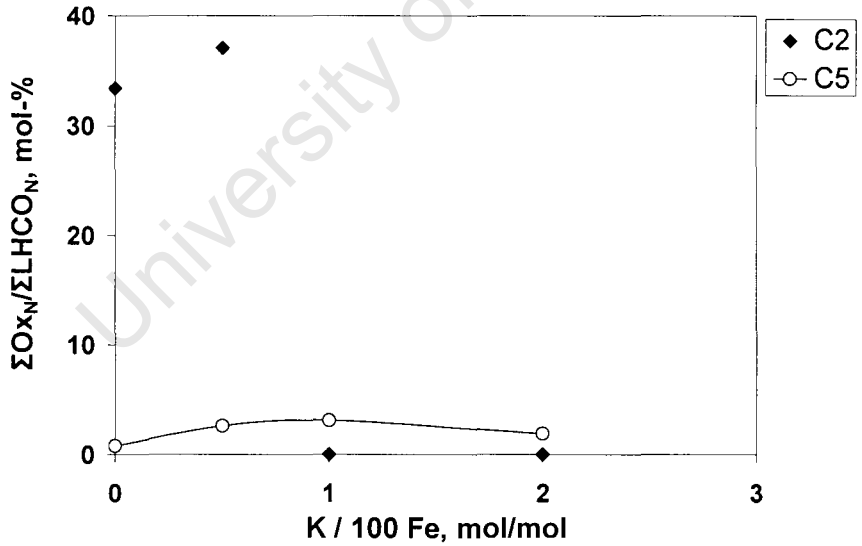

Figure 3.32: Effect of potassium content on iron supported on APTeS modified silica catalysts on the formation of oxygenate product in the C_2 and C_5 fraction. (mcat ~ 1 g, T = 270 °C, P = 20 bar, H_2:CO=2:1,WHSV=1800hr^{-1}).

4. DISCUSSION

A supported iron catalyst has a carrier which functions as a support for the metal. The carrier has to have a high surface area for high dispersion of the metal as well as the right pore size to allow easy diffusion of the feed molecules into the catalyst (Dry, 2004a). The support will increase the mechanical strength and reduce sintering. A large amount of the documented studies on iron-based catalyst has focused on potassium promotion to improve activity and selectivity of the catalyst during Fischer-Tropsch synthesis. Potassium promotion results in an increase in the alkene yield and a decrease in the fraction of methane that is produced. Potassium can also increase the catalytic activity for FTS and WGS reactions. Potassium is a very strong base; the alkali will tend to donate electrons to neighbouring iron atoms.

In this study, a systematic investigation of the effect of the potassium on the modified silica support and the base silica supported iron-base Fischer-Tropsch catalyst was carried out. The effect of the modified support and the potassium promotion was evaluated by relating the physical properties of the catalyst to their catalytic performance under typical industrial Fischer-Tropsch synthesis conditions. The modified support was characterized using BET surface area CHN-analyses, zeta potential measurements, thermo gravimetric analyses (TGA) and infra red spectroscopy (IR). The physico-chemical properties of the modified catalysts and potassium promoted catalysts were characterized using atomic adsorption spectroscopy (AAS), BET surface area measurements, X-ray diffraction (XRD), Temperature Programmed Reduction (TPR), Transmission Electron Microscopy (TEM).

4.1 Characterization of modified supports

The surface modification with APTeS was successful as evidenced with CHN-analysis and IR-spectroscopy. The BET surface area decreased after the

aminopropyltriethoxysilane modification of silica, which is attributed to pore wall coverage, but not pore blockage.

The zeta-potential as a function of pH differed significantly for the APTeS-modified silica from the untreated silica. Zeta potential is a measure of the net surface charge of a solid substance when placed in solution. The equilibrium created by the positive and negative ions on the surface of the solid and the counter ions in solution determines whether the net surface charge is positive or negative. A charge in the pH of the solution affects the equilibrium and hence the net surface charge. An acid site is one that loses an H^+ easily, meaning that its conjugated base has little affinity for the H^+ and is therefore a weak base.

Where as a weak acid is one that loses an H^+ with difficulty and is therefore a strong base. The fact that SiOH is acidic means that SiO^- does not hold the H^+ tightly and RNH_2 is a weak acid, meaning that RNH^- does hold H^+ tightly and is a strong base. The amine-group in the APTeS-modified silica is dominated by the lone pair of electrons on nitrogen. Because of this lone pair, amines are both basic and nucleophilic. The smaller the pK_b value the more favourable the proton-transfer equilibrium and the stronger the base (RNH_2).

The APTeS modified silica shows a change in thermal stability, since a weight loss is observed from 25 – 330 °C, a mass spectrometer would be needed to confirm the exact decomposition of APTeS.

4.2 Characterization of catalysts

The catalysts were prepared by incipient wetness impregnation followed by calcination at 250 °C.

The XRD analysis of the calcined iron catalyst supported on silica indicates hematite as the sole crystalline phase. The XRD analysis for the iron catalyst supported on the APTeS modified silica corresponds to iron oxide hydroxide

(FeOOH). The different crystallite phases might originate from the variation in the local pH in the impregnated or the variation in the crystallite size. In-situ Mössbauer spectroscopy should be done to determine the origin of the change in the phases in each catalyst.

4.3 Effect of potassium loading on Fischer-Tropsch synthesis

Another way of evaluating the effect of potassium promotion is to evaluate the activity per exposed (surface) iron atom (TOF) as a function of the surface potassium loading per surface iron atom.

The resulting average crystallite size of the iron oxide crystallites in the calcined catalysts were estimated using line-broadening analysis in XRD. The reduction of the crystallites will transform the oxides into metallic iron with a reduced crystallite size:

$$d_{Fe} = d_{Fe_2O_3} \cdot \left(\frac{\rho_{Fe_2O_3}}{\rho_{Fe}} \cdot \frac{2 \cdot M_{Fe}}{M_{Fe_2O_3}} \right)^{1/3} = 0.775 \cdot d_{Fe_2O_3}$$

$$d_{Fe} = d_{FeOOH} \cdot \left(\frac{\rho_{FeOOH}}{\rho_{Fe}} \cdot \frac{M_{Fe}}{M_{FeOOH}} \right)^{1/3} = 0.700 \cdot d_{FeOOH}$$

with d: diameter of crystallite (nm)

ρ: density of material (g/cm^3)

M: molar mass of compounds (g/mol)

The surface area of the metallic number of surface Fe-atoms in these crystallites can be estimated knowing the diameter of the metallic iron crystallites:

$$A_{Fe} = \frac{6000}{d_{Fe} \cdot \rho_{Fe}}$$

with A: metal surface area (m^2/g)
d: diameter of crystallite (nm)
ρ: density of material (g/cm^3)

The number of surface iron atoms in metallic iron crystallites can be estimated realising that the most likely exposed metal surface of Fe (Fe(100)) contains 14.6 Fe-atoms per nm^2.

The formation of carbides during the Fischer-Tropsch synthesis might be considered as the dissolution of carbon into the iron (Galuszka et al., 1992) leaving the number of exposed iron crystallites the same (although the size of the crystallites will increase).

It might be assumed that all potassium is associated with the iron crystallites. The molar ratio of the potassium to surface iron can then be estimate knowing the potassium loading. The integral rate per surface iron atom (turn-over frequency) can be estimated from the conversion and the molar flow rate of CO.

$$TOF_{CO} = \frac{X_{CO} \cdot n_{CO,feed}}{14.6 \cdot 10^{18} \cdot A_{Fe}}$$

with X_{CO}: integral CO-conversion
$n_{CO,feed}$: number of molecules of CO fed per s
A: metal surface area (m^2/g)

Figure 4.1 shows the integral rate per surface iron atom as a function of the surface ratio of potassium to iron after 360-3600 minutes on line. A maximum turn-over frequency is observed for surface potassium to surface iron ratio of ca.

0.12. This would mean that 1 K per 8-9 surface Fe-atoms yields the optimum catalyst. It should however be noted that several assumptions made in this analysis may affect this result. The most critical assumptions are that all iron is reduced and all potassium is associated with iron.

It can be further noted that the turn-over frequency of CO over iron crystallites on APTeS-modified seem to be similar (or even slightly less) than the turn-over frequency of CO over iron crystallites supported on silica. Thus, the higher CO-conversion obtained over the iron catalyst supported on APTeS-modified support can be solely attributed to the smaller iron crystallite sizes obtained with this catalyst.

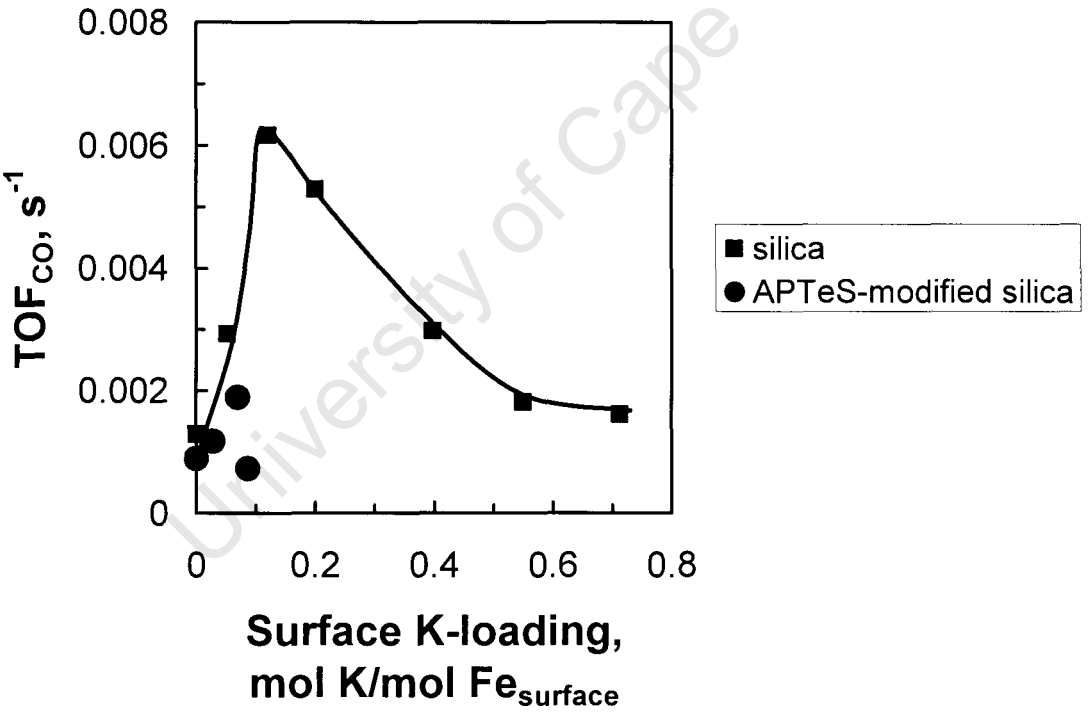

Figure 4.1: Estimated Turn-over frequency for the conversion of CO in the Fischer-Tropsch synthesis over supported iron catalyst as a function of the ratio of potassium to surface iron.

The supported iron catalysts show a low water-gas shift activity. This might be beneficial, since the formation of CO_2 in the Fischer-Tropsch synthesis is not always desired.

n-Olefins are a major product in the Fischer-Tropsch synthesis, which may undergo secondary hydrogenation reactions [Claeys and van Steen, 2004]. Figure 4.2 shows a plot of the CO conversion against the n-olefin content in C_2, C_3 and C_6 for the different catalysts, to evaluate the effect of potassium on the n-olefin content. All the iron catalysts supported on silica promoted with potassium with high CO conversions shows low olefin content and the iron catalysts supported on silica promoted with potassium with low CO conversion show the opposite effect, except for the 0.005 K catalyst. Hence, the change in the olefin content might be ascribed to the variation in the CO-converison.

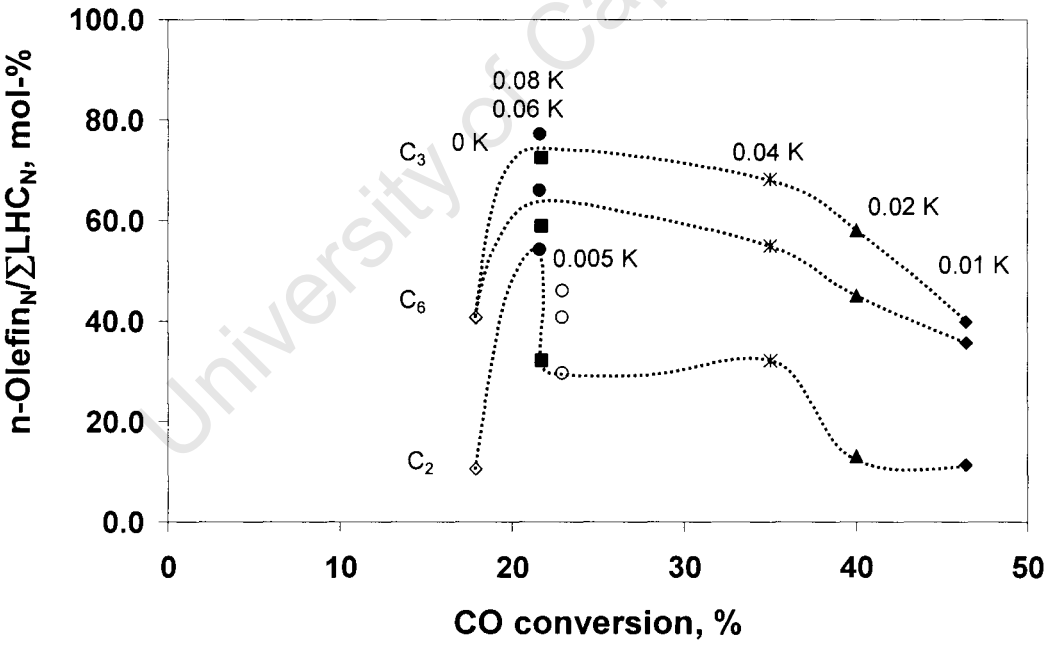

Figure 4.2: CO conversion versus the n-olefin content from Fischer-Tropsch synthesis (m_{cat} ~ 1 g, T = 270 °C, P = 20 bar, H_2:CO = 2:1, WHSV = 1800 hr^{-1}).

Figure 4.3 shows a plot of the CO conversion against the n-olefin content in C_2, C_3 and C_6 for the different iron catalysts supported on APTeS modified silica, to indicate the potassium effect on the n-olefin content. No conclusive trend line could be observed for the catalysts. The highest n-olefin content was obtain with the APTeS MS 0.01 K catalyst (CO conversion of 35.7 mol-%) and the lowest n-olefin content was obtained for the APTeS MS 0 K catalyst (CO conversion of 26 mol-%).

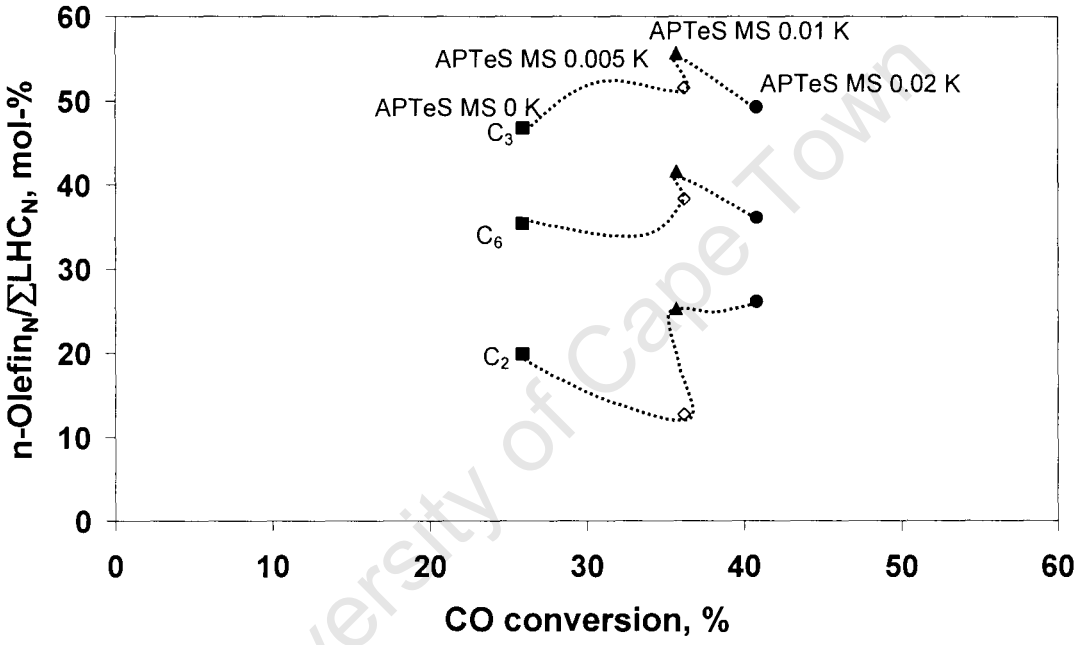

Figure 4.3: CO conversion versus the n-olefin content from Fischer-Tropsch synthesis (m_{cat} ~ 1 g, T = 270 °C, P = 20 bar, H_2:CO = 2:1, WHSV = 1800 hr^{-1}).

1-Olefins are thought to be the primary olefinic product compounds formed in the Fischer-Tropsch synthesis [Claeys and van Steen, 2004}. Figure 4.4 shows a plot of the CO conversion against the 1-olefin content in C_4, C_5 and C_6 for the different iron catalysts supported on silica, to indicate the potassium effect on the 1-olefin content. All iron catalysts supported on silica with high CO conversions promoted with potassium shows low 1-olefin contents and the iron catalysts

supported on silica promoted with potassium with low CO conversion show the opposite effect, except for the 0.005 K catalyst. The low 1-olefin content is associated with the low potassium loading. The catalysts with high potassium loading and low conversion show higher 1-olefin content, i.e. potassium is inhibiting the secondary olefin isomerisation.

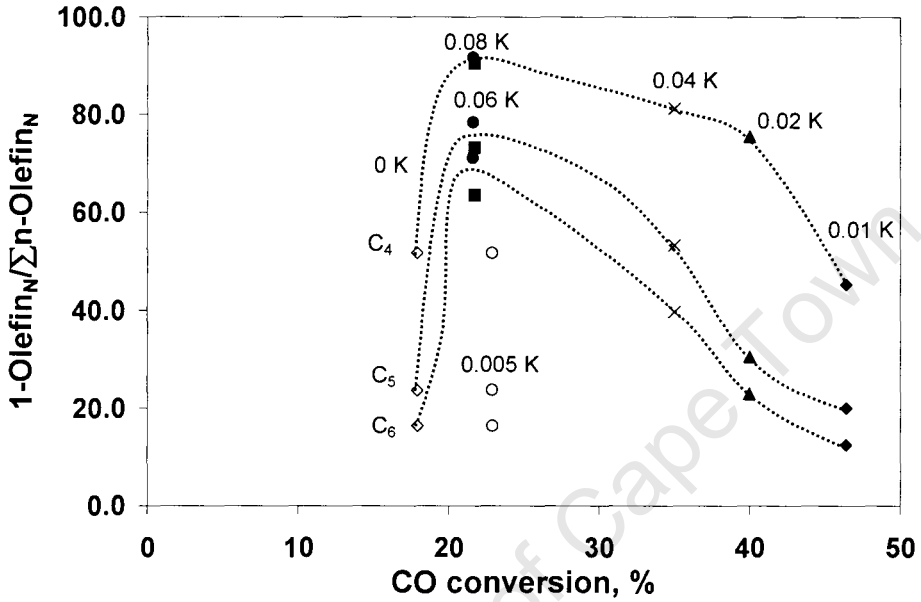

Figure 4.4: CO conversion versus the 1-olefin content from Fischer-Tropsch synthesis (m_{cat} ~ 1 g, T = 270 °C, P = 20 bar, H_2:CO = 2:1, WHSV = 1800 hr^{-1}).

Figure 4.5 shows a plot of the CO conversion against the 1-olefin content in C_4, C_5 and C_6 for the different iron catalysts supported on APTeS modified silica, to indicate the potassium effect on the 1-olefin content. The highest 1-olefin content is observed for the APTeS MS 0.01 K catalyst with a 36.7 mol-% CO conversion and the lowest 1-olefin content was observed for the APTeS MS 0 K catalyst (~26 mol-% CO conversion). The low 1-olefin content of the APTeS MS catalysts are associated with the low potassium loading. The catalysts with high potassium loading and low conversion show higher 1-olefin content, i.e. potassium is inhibiting the secondary olefin isomerisation.

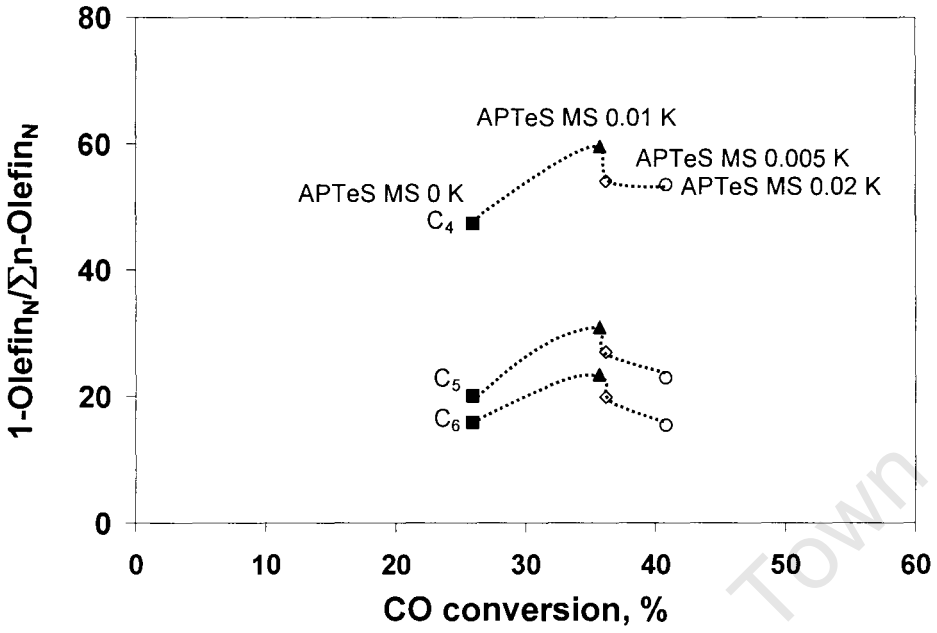

Figure 4.5: CO conversion versus the 1-olefin content from Fischer-Tropsch synthesis (m_{cat} ~ 1 g, T = 270 °C, P = 20 bar, H_2:CO = 2:1, WHSV = 1800 hr^{-1}).

5. Conclusion

Model type iron-based catalysts supported on bare silica and modified silica with varied amount of potassium was synthesized using the incipient wetness impregnation technique. The modified support was characterized with zeta potential measurements, infra red spectroscopy, CHN-analysis and TGA analysis. The APTeS modified support and potassium had some influence on the catalyst performance in the Fischer-Tropsch synthesis. In brief, the overall effect of APTeS modified support and potassium content in the Fischer-Tropsch synthesis can be summarized as follows:

- APTeS modified support and potassium content increase showed higher catalyst activity, the higher CO-conversion obtained over the iron catalyst supported on APTeS-modified support can be solely attributed to the smaller iron crystallite sizes obtained with this catalyst.
- For the APTeS modified catalysts it is believed that methane selectivity is not a strong function of CO-conversion, thus the potassium addition lowers the methane selectivity during Fischer-Tropsch synthesis.
- The increase in basic character on the catalyst imparted by potassium and APTeS modified support, it is expected that less branched products would be obtained, the opposite results where obtained.
- The oxygenate content stabilized with increase in potassium content.

Further investigation is recommended on the model catalysts supported on silica and APTeS modified silica promoted with potassium to obtain the optimum alkali amount.

6. REFERENCES

Anderson, R.B.
In "Catalysis" (P.H. Emmet, Ed.), Vol. IV, Reinhold, New York (1956), Chapters 1-3.

Barbier, A., A. Tuel, I. Arcon, A. Kodre, and G. A. Martin
'Characterisation and catalytic behaviour of Co/SiO_2 catalysts: Influence of dispersion in the Fischer-Tropsch reaction'
J. Catal. **200** (2001), 106.

Blyholder, G.J
'Molecular orbital view of chemisorbed carbon monoxide'
J. Phys. Chem. **68** (1964), 2772.

Bonzel, H.P., Krebs, H.J.
'Surface science approach to heterogeneous catalysis: carbon monoxide hydrogenation on transition metals'
Surf. Sci. **117** (1982), 1-3.

Brady, R.C., Pettit, R.
'On the mechanism of the Fischer-Tropsch reaction. The chain propagation step'
J. Amer. Chem. Soc. **103**, (1981), 1287-1289.

Bukur, D.B., Patel, S.A., Lang, X.
'Fixed bed and slurry bed reactor studies of Fischer-Tropsch synthesis on precipitated iron catalysts'
Appl. Catal. **61** (1990), 329.

Bukur, D.B., Davis, B.H., O'Brien, R.J.
'Mössbauer spectroscopy study of iron-based catalysts used in Fischer-Tropsch synthesis'
Top. Catal. **2** (1995), 71.

Bukur, D.B., Sivaraj, C.
'Supported iron catalysts for slurry phase Fischer-Tropsch synthesis'
Appl. Catal A. **231** (2002), 201-214.

Chen, Z., Hsu, F., Battigelli, D., Chang, H.
'Capture and release of viruses using amino-functionalized silica particles'
Anal. Chimica Acta **569** (2006), 76-82.

Che, M., Clause, O., Marcilly, C.H.
'Supported catalysts'
In "Handbook of Heterogeneous Catalysis" (Ert, G. Knozinger, H., Weitkkamp, J., Eds.), Wiley-VCH: Weinheim, **2** (1997), 120-150.

Claeys, M.: 1997
'Selektivität, Elementarschritte und kinetische Modellierung bei der Fischer-Tropsch-Synthese'
Ph.D. thesis, Universität Fridericiana Karlsruhe.

Claeys, M. and H. Schulz
'Effects of internal mass transfer on activity and selectivity in iron based Fischer-Tropsch syntheses'
Prepr. Pap.-Am. Chem. Soc., Div. Pet. Chem. **2**(2004), 195.

Claeys, M., van Steen, E.
'Fischer-Tropsch technology: Basic studies'
Stud. Surf. Sci. Catal. **152** (2004), 601.

Dancuart, L.P., de Haan, R., de Klerk, A.
'Processing of Primary Fischer-Tropsch Products'
Stud. Surf. Sci. Catal. **152** (2004), 489

Davis, B. H.: 1993
'^{14}C Tracer studies of the Fischer-Tropsch synthesis'
In:*Preprints - Catalysis and catalytic processing*. Cape Town, South Africa, 305.

Dictor, R.A., Bell, A.T.
'A comparison of the activity, selectivity and kinetics of several iron-based Fischer-Tropsch catalysts '
J. Catal. **31** (1986), 126-132.

Donnelly, T.J., Satterfield, C.N.
'Product distribution of the Fischer-Tropsch synthesis on precipitated iron catalysts'
Appl. Catal. **52** (1989), 93-114.

Dry, M.E., Oosthuizen, G.J.
'The correlation between catalyst surface basicity and hydrocarbon selectivity in the Fischer-Tropsch synthesis'
J. Catal. **11** (1968) 18-24.

Dry, M.E., Shingles, T.,Boshoff, L.J., Oosthuizen, G.J.
'Heats of chemisortption on promoted iron surfaces and the role of alkali in Fischer-Tropsch synthesis'
J. Catal. **15** (1969) 190-199.

Dry, M.E.
The Fischer-Tropsch synthesis
In "Catalysis, Science and Technology", Anderson, J.R., Boudart, M. Springer Verlag New York, 1981, 162-169.

Dry, M.E.
'Practical and theoretical aspects of the catalytic Fischer-Tropsch Process'
Appl. Catal. A: General **138** (1996), 319.

Dry, M.E.
'Fischer-Tropsch technology: FT catalysts'
Stud. Surf. Sci. Catal. **152** (2004a), 533-554.

Dry, M.E.
'Fischer-Tropsch technology: Chemical concepts used for engineering purposes'
Stud. Surf. Sci. Catal. **152** (2004b), 211-237.

Espinoza, R.L., Steynberg, A.P., Jager, B., Vosloo, A.C.
'Low temperature Fischer-Tropsch synthesis from a Sasol perspective'
Appl. Catal. A: General **186** (1999), 13.

Feller, A., Claeys, M., van Steen, E.
'Cobalt cluster effects in zirconium promoted Co/SiO_2 Fischer-Tropsch catalysts'
J. Catal. **185** (1999), 120-120.

Galuszk, J., Sano, T., Sawicki, J.A.
'Study of carbonaceous deposits on Fischer-Tropsch oxide-supported iron catalysts'
J. Catal. **136** (1992), 96-109.

Haukka, S., Root, A.,
'The reaction of hexamethyldisilazane and subsequent oxidation of trimethylsilyl groups on silica studied by solid-state NMR and FTIR'
J. Phys. Chem. **98** (1994), 1695-1703.

Herranz, T., Rojas, S., Perez-Alonso, F.J., Ojeda, M., Terreros, P., Fierro, J.L.G.
'Carbon oxide hydrogenation over silica-supported iron-based catalysts: influence of the preparation route'
Appl. Catal. A: General **308** (2006), 19-30.

Hindermann, J.P., Hutchings, G.J., A. Kiennemann, A.
'Mechanistic aspects of the formation of hydrocarbons and alcohols from carbon monoxide hydrogenation'
Catal. Rev.-Sci. Eng. **35** (1993), 1-127.

Iglesia, E., Reyer, S.C., Madon, R.J., Soled, S.L.
'Selectivity control and catalytst design in the Fischer-Tropsch: sites, pellets and reactors'
Adv. Catal. **39** (1993), 221-302.

Iiskola, E.I., Ek S., Niinisto, L.
'Gas-phase deposition of aminopropylalkoxysilane on porous silica'
Langmuir **19** (2003) 3461-3471.

Jal, P.K., Patel, S., Mishra, B.K.
'Chemical modification of silica by immobilization of functional groups for extractive concentration of metal ions'
Talanta **62** (2004), 1005-1028.

Jin, Y., Datye, A.K.
'Phase transformation in iron Fischer-Tropsch catalysts during temperatura-programmed reduction'
J. Catal. **196** (2000), 8-17.

Kaiser, R.: 1969,
'Chromatographie in der Gasphase'
Bibliographisches Institut, Mannheim, band *iii*, **2**. edition.

Kölbel, H., Ralek, M.
'Fischer-Tropsch synthesis in the liquid phase'
Catal. Rev. –Sci. Eng. **21** (1980), 225.

Knacke, O., Kubaschewski, O., Hesselmann, K.
'Thermochemical properties of inorganic substances'
Springer Verlag, Berlin (1991)

Lochmuller, C.H., Wilder, D.R.
J. Chromatogr. Sci. **17** (1979) 574.

Luo, M., O'Brien, R.J., Bao, S, Davis, B.H.
'FTS: Induction and steady-state activity of high-alpha potassium promoted iron catalysts'
Appl. Catal.A: General **239** (2003a), 111-120.

Luo, M., Davis, B.H.
'Fischer-Tropsch synthesis: Group II alkali-earth metal promoted catalysts'
Appl. Catal.A: General **246** (2003b), 171-181.

Milburn, D.R., Cary, K.V.R., Davis, B.H.
'Promoted iron Fischer-Tropsch catalysts: characterization by nitrogen sorption'
Appl. Catal.A: General **144** (1996), 121-132.

Ojeda, M., Rojas, S., Boutonnet, M., Perez-Alonso, F., Garcia-Garcia, F.J. and Fierro, J.L.G.
'Synthesis of Rh nano-particles by the microemulsion technology: Particle size effect on the $CO+H_2$ reaction'
Appl. Catal A: General **274** (2004), 33.

Pakkanen, T.T., Juvaste, H., Iiskola, E.I.
'Aminosilane as a coupling agent for cyclopentadienyl ligands on silica'
J. Organometall. Chem. **587** (1999) 38-45.

Perego, C., Villa, P.
'Catalyst preparation methods'
Catal. Today **34** (1997) 281-305.

Pichler, P., Schulz, H.
'Neuere Erkenntnisse auf dem Gebiet der Synthese von Kohlenwasserstoffen aus CO und H_2'
Chem. Ing. Techn. **42** (1970), 1162-1174.

Rethwisch, D.G., Dumesic, J.A.
'Water-gas shift over supported iron and zinc oxides'
J. Catal. **101** (1986), 35-42.

Röger, H.P.
'Application of the transformation of 1,2,4-trimethylbenzene to monitor the chemical vapour deposition of tetraethoxysilane over ZSM-5'
PhD thesis, University of Cape Town (1998)

Schulz, H.
'Selectivity and mechanism of the Fischer-Tropsch CO-hydrogenation'
C_1 Mol. Chem. **1** (1985), 231-252.

Schulz, H., Beck, K., Erich, E.
'Mechanism of the Fischer-Tropsch process'
Stud. Surf. Sci. Catal. **36** (1988a), 457.

Schulz, H., Beck, K., Erich, E.
'Kinetics of Fischer-Tropsch selectivity'
Fuel Proc. Techn. **38** (1988b), 293.

Schulz, H., Beck, K., Erich, E.
'Fischer-Tropsch CO-hydrogenation, a non-trivial surface polymerization: selectivity of branching'
Proc. 9th Int. Congr. on Catalysis (M. Philips, M. Ternan, Eds.), Vol. 2, p. 829, The Chemical Insitute of Canada (1988c)

Schulz, H., van Steen, E., Claeys, M.
'Selectivity and mechanism of Fischer-Tropsch synthesis with iron and cobalt catalysts'
Stud. Surf. Sci. Catal. **81** (1994), 455.

Schulz, H.
'Short history and present trends of Fischer-Tropsch synthesis'
Appl. Catal. A: General **186** (1999), 3-12.

Scott, R.P.W., Simpson, C.F.
'Silica gel and bonded phases: The silica gel surface'
John Wiley & sons. (1993a) 158.

Steynberg, A.P., Dry, M.E., Davis, B.H., Breman, B.B.
'Fischer-Tropsch reactors'
Stud. Surf. Sci. Catal. **152** (2004), 66-77.

Storch, H.H., Columbic, M.S., Anderson, R.B.
'The Fischer-Tropsch and Related Synthesis'
John Wiley & Sons, (1951).

Van der Laan, G.P., Beenackers, A.A.C.M.
'Kinetics and Selectivity of the Fischer -Tropsch Synthesis: A Literature Review'
Catal.Rev.-Sci.Eng. **41** (1999), 255-318.

Vannice, M.
'The catalytic synthesis of hydrocarbons from H_2/CO-mixtures over the group VIII metals. I The specific activity and product distribution of supported metals'
J. Catal. **37** (1975), 449.

Van Steen, E., Prinsloo, F.F.
'Comparison of preparation methods for carbon nanotubes supported iron Fischer-Tropsh catalysts'
Catal. Today **71** (2002), 327-334.

Vrancken, K.C., van der Voort, P., Possemiers, K., Vansant, E.F.
'Surface and structural properties of silica gel in the modification with γ-Aminopropyltriethoxysilane'
J. Colloid. Interface Sci. **174** (1995), 86-91.

Wan, H-J., Wu, B-S., Tao, Z-C., Li, T-Z., An, X., Xiang, H-W., Li, Y-W.
'Study of an iron-based Fischer-Tropsch synthesis catalyst incorporated with SiO_2'
J. Molec. Catal. A: Chemical **260** (2006), 255-263.

White, L.D., Tripp, C.P.
'Reaction of 3-(aminopropyl)dimethylethoxysilane with amine catalysts on silica surfaces'
J. Colloid Interface Sci. **232** (2000), 400-407.

Yang, Y., Xiang, H-w., Tian, L., Wang, H., Zhang, C-H., Tao, Z-C., Xu, Y-Y., Zhong, B., Li, Y-W.
'Structure and Fischer-Tropsch performance of iron-manganese catalyst incorporated with SiO_2'
Appl. Catal. A: General **284** (2005), 105-122.

Yang, Y., Xiang, H.-W., Xu, Y., Bai, L., Li, Y.
'Effect of potassium promoter on precipitated iron-magnese catalyst for Fischer-Tropsch synthesis'
Appl. Catal. A: General **266** (2004), 181-194.

Xu, G., Zhang, J., Song, G.
'Effect of complexation on the zeta potential of silica powder'
Powder Techn. **134** (2003), 218-222.

Zhang, H.B., Schrader, G.L.
'Charaterization of ammonia/iron catalytic systems by laser Raman spectroscopy'
J. Catal. **99** (1985), 461-471.

Zhang, C-H., Wan, H-J., Yang, Y., Xiang, H-W., Li, Y-W.
'Study on the iron-silica interaction of a co-precipitated Fe/SiO_2 Fischer-Tropsch synthesis catalyst'
Cat. Communications **7** (2006) 733-738.

7. APPENDICES

Appendix: Modification of silica with aminopropyltriethoxysilane

Pre-treatment of silica was performed by calcination at 300 °C. The heat treatment of silica in air at 300 °C leads to a material that contains ca. 6.5 OH groups nm^{-2} (Ek et al., 2003).

Silica surface area = 300 m^2/g

6.5 hydroxyl groups / nm^2 x 300 x 10^{18} nm^2 / g
= 1.95 x 10^{21} hydroxyl groups / g SiO_2

1 Aminopropyltriethoxysilane per hydroxyl group

= 1.95 x 10^{21} mol g silane / 6 x 10^{23} g SiO_2
= 3.25 x 10^{-3} mol of silane/ g SiO_2
M_{silane} = 221.37 g/mol
ρ_{silane} = 0.948 g/cm^3

= 3.25 x 10^{-3} x 221.37 / 0.948
= 0.759 ml of silane / g SiO_2

Appendix: CHN-analysis

Calculated from APTeS

APTeS consist out of: 9 C
23 H
1 N

M_{silane} = 221.37 g/mol

C-wt-%

= (108/221.37)* 100
= 48.79 %

H-wt-%

= (23/221.37)*100
= 10.39 %

N-wt-%

= (14/221.37)*100
= 6.32 %

The conversion at which the phase change form Hägg carbide to magnetite is thermodynamically expected:

C-wt-%
= (4.49/48.79)* 100
= 9.2 %

H-wt-%
= (1.14/10.39)*100
=10.9 %

N-wt-%
= (1.08/6.32)* 100
= 17 %

APTeS modified silica was used to calculate the amount of ethoxy groups which decompose during APTeS attachment to silica and the amount of OH groups which will be present because of moisture adsorption:

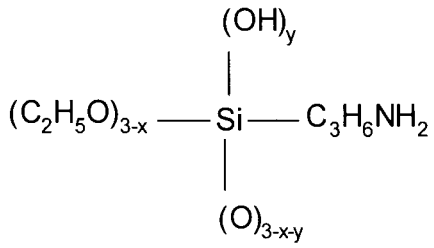

$C = (6 - 2x + 3) \times 12 = 108 - 24x$

$H = (15 - 5x + 8) = 23 - 5x$

$N = (14) \times 1$

Ethoxy groups:

$C : 72 - 24x$

$H : 15 - 5x$

$\frac{C}{H} = 3.94 = \frac{72 - 24x}{15 - 5x}$

$x = \frac{3}{3} = 1$ ethoxy group

OH groups:

$\frac{H}{N} = \frac{C}{N} \div \frac{C}{H}$

$\frac{H}{N} = 1.05 = \frac{23 - 5x + y}{14}$

y = 3.3 OH groups

There are too many OH groups adsorbed onto the APTeS modified silica, which indicate that moisture was absorbed. The low accuracy of CHN analyses,

especially in samples containing small amounts of nitrogen, makes the determination of aminopropyltriethoxysilane on silica difficult. Toluene, methanol and moisture could still be trapped in APTeS modified silica, which will affect the accuracy of the results. APTeS may decompose on exposure to moisture and loose mass due to evaporation after it has been weighed out. The determined carbon/nitrogen ratio gives a rough indication of bonding modes. More detailed information on the surface species of aminopropyltriethoxysilane on the silica could be obtained from the solid sate ^{29} Si and ^{13} C NMR.

Appendix: Urea and Slurry catalysts

Preparation of support to iron catalyst

The catalysts were prepared according to two methods. The first method of preparation was a deposition precipitation with urea. For the preparation of this catalyst 7.23 g $Fe(NO_3)_3.9H_2O$ and urea (1-6 moles urea per mol of iron) were dissolved into 20 cm^3 of deionised water . The mixture was added drop-wise to 10 g of the silica support. The resulting mixture was then left over an oil bath (90 ^{o} C) for 6hrs and dried in a rotavaporator at 90 ^{o}C till dry.

In the second approach, the catalyst was prepared by using a slurry impregnation method. 7.23 g $Fe(NO_3)_3.9H_2O$ was dissolved in 40 cm^3 of deionised water (two times the pore volume). This mixture was added drop-wise to 10 g of silica support. The slurry was dried in a rotovapor at 90 ^{o}C for 20 min. All the catalysts were transferred to a dessicator; a drying agent was present in the dessicator.

Catalyst characterization

Atomic Adsorption Spectroscopy (AAS)

The results for Table AII.1 of these analyses showed iron loading between 6.38 – 8.04 wt.-%.

Table AII.1: Iron (Fe) content determined with AAS for catalyst prepared with slurry method and deposition precipitation with urea.

Catalyst Precursor	Fe (wt.-%)
Urea (1:1)	7.02
Urea (1:2)	8.04
Urea (1:3)	7.09
Urea (1:4)	7.37
Urea (1:5)	7.49
Urea (1:6)	6.38
Slurry	7.52

Table AII.2: Iron (Fe) content determined with titration technique for catalyst prepared with slurry method and deposition precipitation with urea.

Catalyst Precursor	Fe (wt.-%)
Urea (1:1)	7.49
Urea (1:2)	7.98
Urea (1:3)	6.99
Urea (1:4)	7.50
Urea (1:5)	8.00
Urea (1:6)	7.00
Slurry	8.01

Titration technique results in Table AII.2 obtained for the iron weight percent is in agreement with the AAS results (Table AII.1). The hydroscopic character of the samples and the non-homogeneous distribution of the iron on the support (incomplete digestion) contribute to the iron loss.

X-ray diffractometry (XRD)

Figure AIII.1 – Figure AIII.2 shows characteristic main diffraction peaks for Fe_2O_3. The size of the iron oxide crystallites were determined from XRD characterization, the XRD pattern is shown in Figure AIII.1 – AIII.2. Figure AIII.1 shows the crystallite size in the catalysts range form 12.9 – 14.5 nm. Figure AIII.2 shows a crystallite size of 11.1 nm for the catalyst prepared with the slurry method.

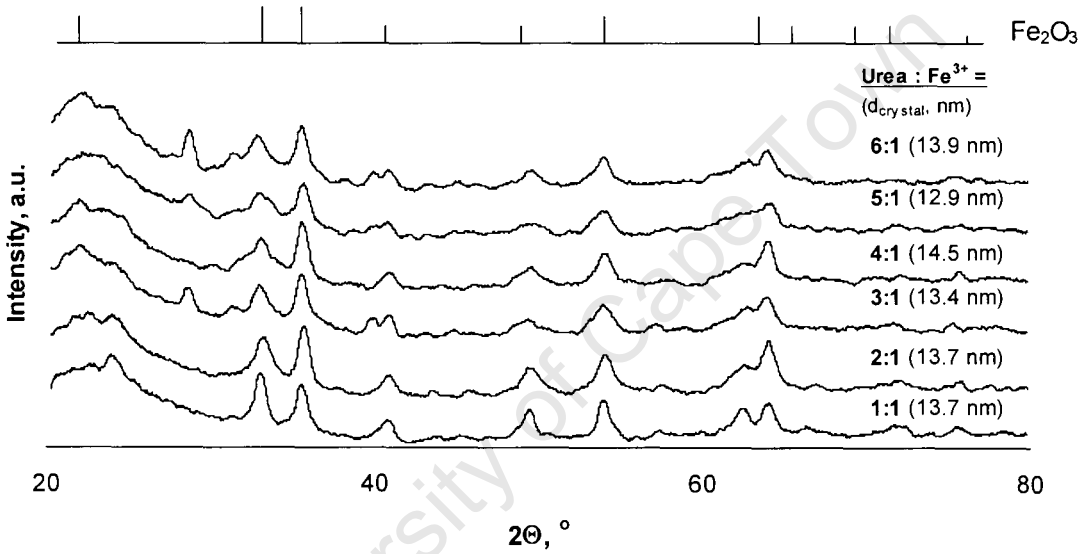

Figure AIII.1: XRD patterns of the catalysts prepared with deposition precipitation with urea.

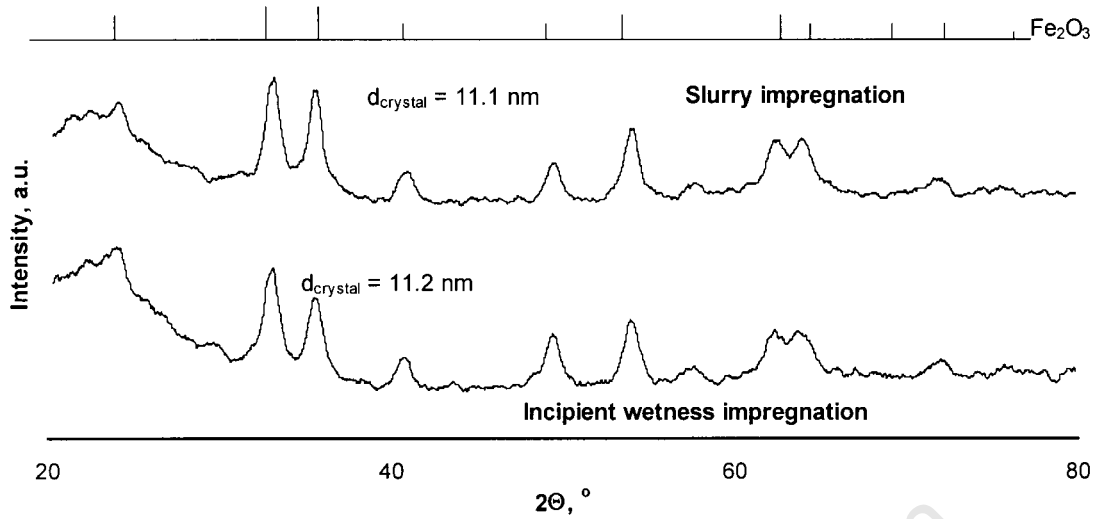

Figure AIII.2: XRD pattern of the catalyst prepared with the slurry method and the incipient wetness impregnation.

Transmission electron microscopy (TEM)

TEM images of the urea and slurry catalyst precursors are shown in Figure AIV.1.

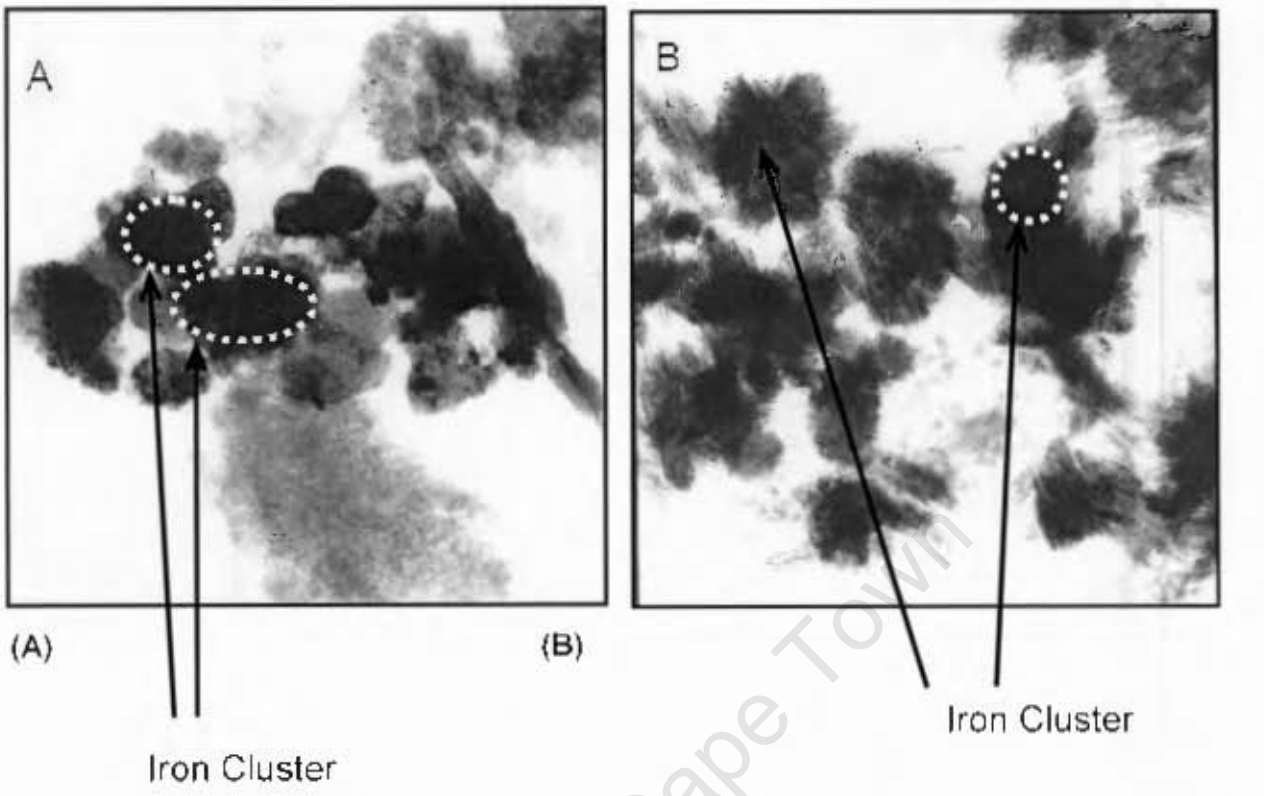

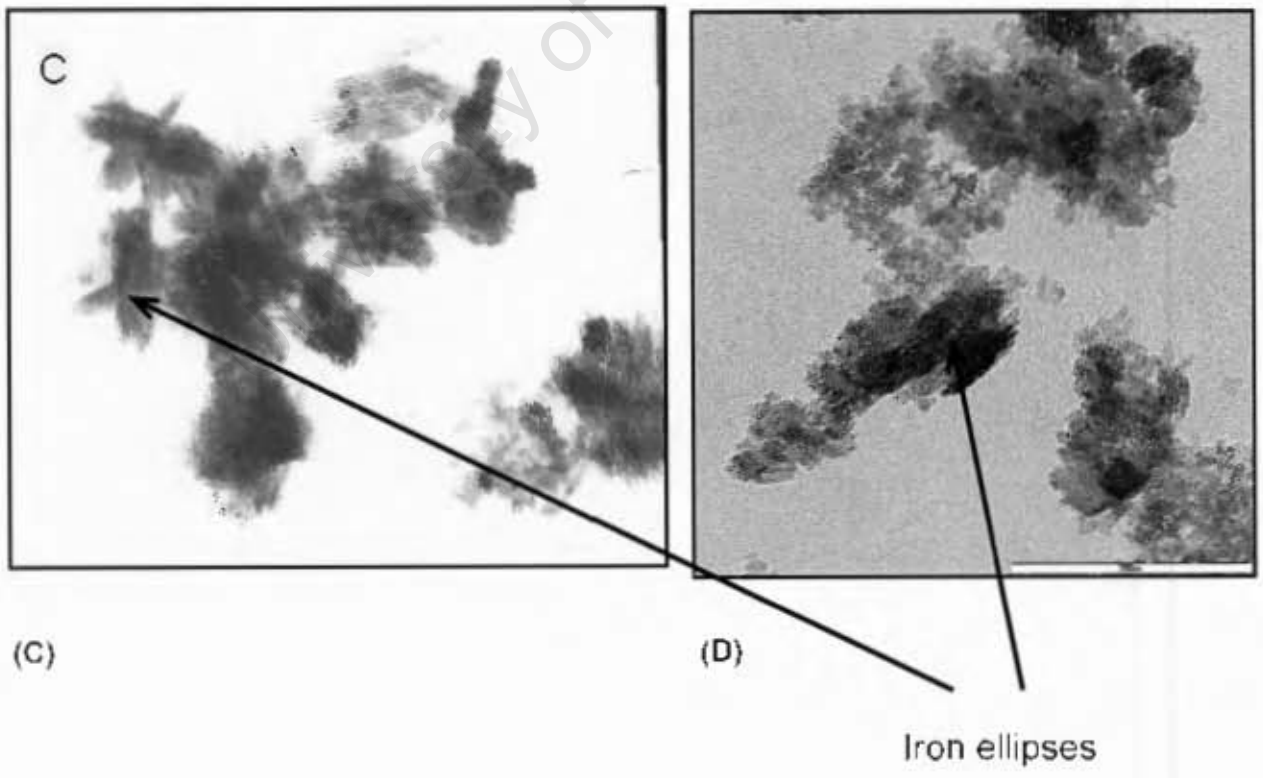

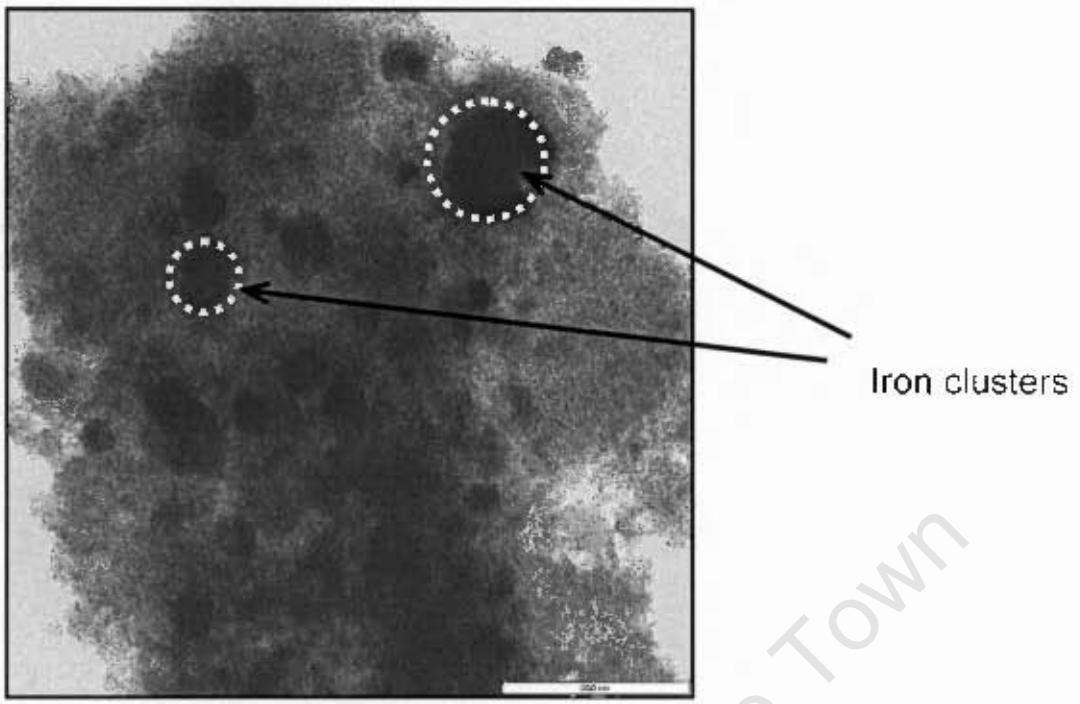

(E)

Figure AIV.1: TEM images for catalyst prepared with deposition precipitation method with urea and slurry method (A) Urea (1:1), (B) Urea (1:2), (C) Urea (1:3), (D) Urea (1:6), (E) Slurry.

The TEM photos in Figure AIV.1, (A) show spherical shaped particles which agglomerated together. It is clearly seen in Figure AIV.1 B-D that these samples display irregular-shaped particles, formed by agglomeration of smaller ones. Some of these small basic units agglomerated to form particles shaped like ellipses, others aggregated together to form clusters, surrounding the large grains. Figure AIV.1 E show the slurry catalyst, with spherical-shaped iron oxides particles agglomerate over some areas of the silica support. The agglomerates diameter was between 54 – 98 nm.

The clusters showed the presence of iron nitrate droplets. The cluster size of the catalyst is determined by the size of the iron nitrate droplet during the drying process; similar results were obtained by Feller et. al, 1999 for a Co/SiO_2

catalyst. The TEM images of the catalyst showed areas with a high density of iron particles and large areas with no iron present.

Appendix: Calibration of mass flow controllers

Mass flow controllers were calibrated by measuring the flow and correcting it with the bubble meter. Figure AV.1 – AV.3 show the calibration curves for H_2, CO and N_2/cyclohexane supply lines.

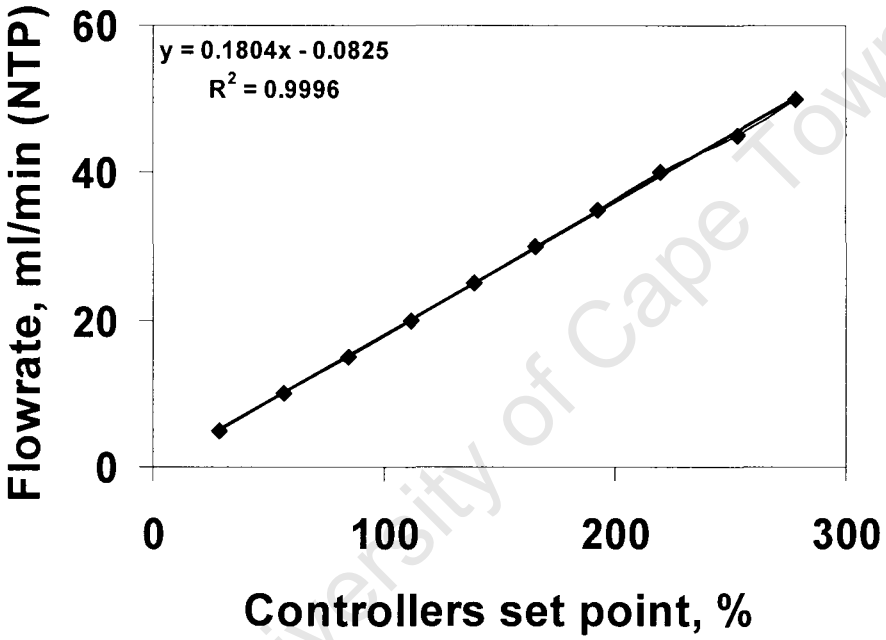

Figure AV.1: Calibration curve for the H_2 mass flow controller.

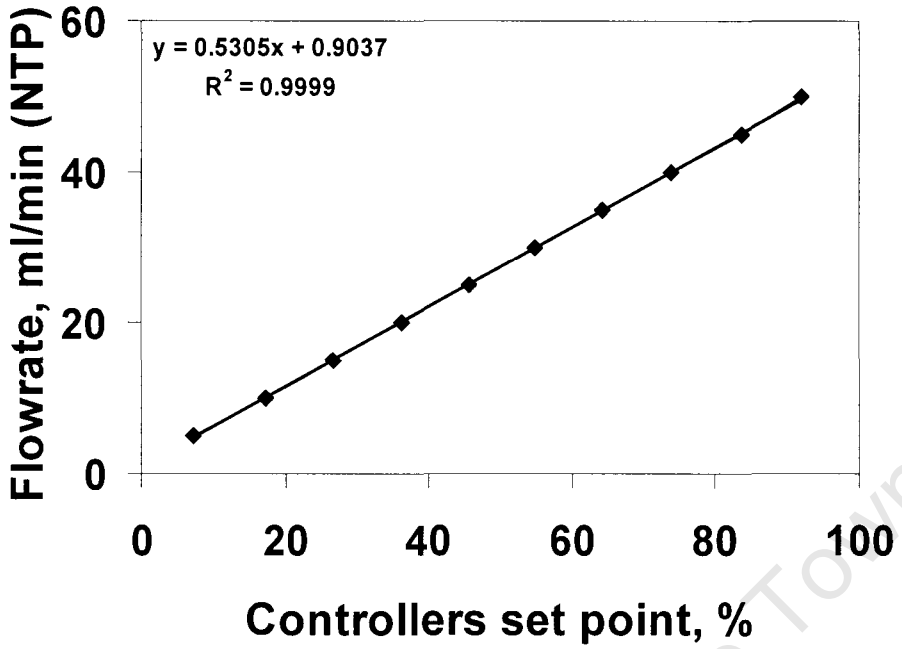

Figure AV.2: Calibration curve for the CO mass flow controller.

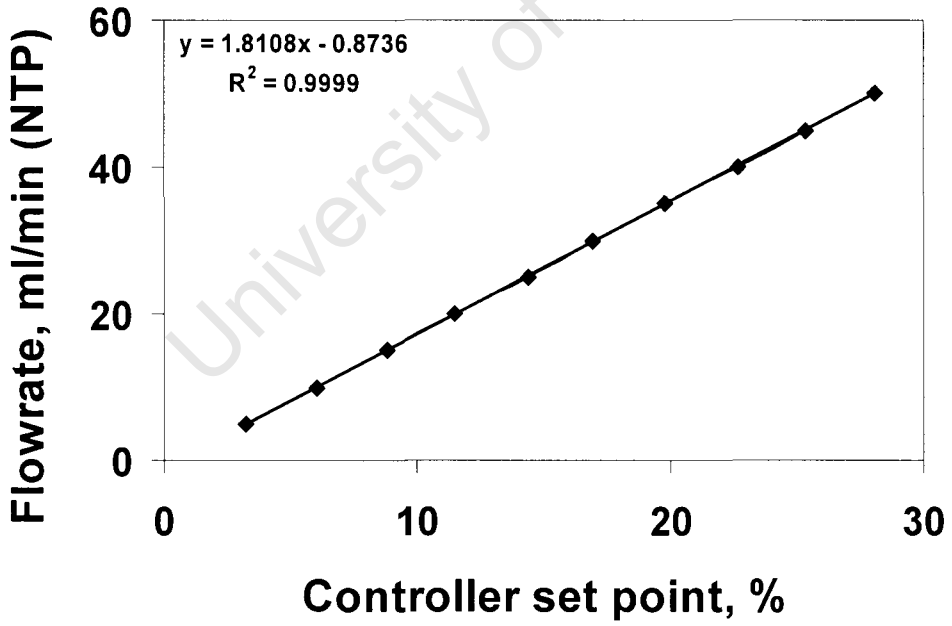

Figure AV.3: Calibration curve for the N_2/cyclohexane mass flow controller.

Appendix: TPR calibration and data analysis

To convert the conductivity signal obtained form the TPR apparatus into H_2 consumed during the reduction program, Ag_2O was used as a standard to calibrate the apparatus. About 0.053 g (0.2287 mmols) was loaded into the TPR quartz tube reactor and was reduced under 5 vol-% H_2-Ar mixture flowing at 50 ml/min (NTP). The reduction was carried out at a ramping rate of 10 °C/min up to 800 °C. The reduction reaction which take place with Ag_2O:

$$Ag_2O + H_2 \rightarrow 2Ag\ (s) + H_2O\ (g)$$

The area under the curve was intergrated. The area under the curve is proportional to the amount of H_2 consumed during Ag_2O reduction since every mole of H removes one oxygen atom when Ag_2O is reduced completely.

The amount of hydrogen consumption by the different catalysts during TPR experiments is given by:

$$C_{H2} = \left(\frac{A_{Cat}}{A_{Ag2O}}\right) \times \left(C_{Ag2O}\right)$$

Where C_{H2} is the hydrogen consumed per experimental run in mmols, A_{H2} and A_{Ag2O} are areas under the curve. C_{Ag2O} (0.2287 mmols) is the number of moles of oxygen atoms consumed in the standard calibration sample.

The amount of H_2 consumed in the reduction of Ag_2O will be:

= (922.26/15049.45)*0.2287
= 0.037 mmols H_2

M_{cat} = 0.0456 g

10% Fe = 0.066*0.0456

= 0.00300 g (0.0538 mmols)

H_2 consumption per mole Fe : (0.00540/0.00538)

= 1.00 mol/mol

Appendix: Time on stream TCD data for Fischer-Tropsch synthesis

0 K catalyst

	Calibration factors
H_2/N_2	0.0803
CO/N_2	1.0901
CH_4/N_2	0.3024
CO_2/N_2	0.9789

H_2	N_2	CO	H_2/CO
7693506	298246	276006	2.07
7679508	297889	276704	2.07
7662710	297641	274046	2.07
7709792	298710	276864	2.07
7575169	296353	269512	2.05

TOS (min)	H_2	N_2	CO	CH_4	CO_2	CO Conversion X_{CO}, C-%	CH_4 Selectivity S_{CH4}, C-%	CO_2 Selectivity S_{CO2}, C-%
10	5791692	305599	191825	27900	8426	31.94	8.60	8.41
20	7059464	311204	232479	32744		19.00	16.66	0.00
30	6901738	304836	223853	38852	7443	20.38	18.81	11.67
40	6968747	307433	230696	38133	8978	18.64	20.02	15.26
50	5760700	256372	189535	31136	3997	19.84	18.41	7.65
60	5829918	255195	191956	28818	8050	18.44	18.42	16.66
70	5864807	257526	194193	27419	15158	18.24	17.56	31.43
80	5745616	253351	191765	29603	6954	17.93	19.60	14.91
90	5774545	253857	191110	26640	9513	18.37	17.18	19.86
100	5764124	253223	191279	27047	5725	18.10	17.75	12.17
110	5763281	250233	190554	27507	9752	17.43	18.97	21.77
120	5712038	252828	190987	26950	7312	18.09	17.72	15.56
150	5222350	238118	180575	26902		17.77	19.12	0.00
180	5151198	234472	178007	26822	5725	17.68	19.46	13.44
210	5207656	236188	181522	27374	6729	16.67	20.92	16.64
240	5194326	234265	181748	26452	4024	15.88	21.39	10.53
270	5189501	234213	181441	29710	8705	16.00	23.84	22.61
300	5200392	232300	179770	24798	6657	16.09	19.96	17.34
330	5315736	239485	183909	33389	3227	16.73	25.06	7.84
360	5174988	231060	179147	26809	12385	15.93	21.90	32.76
1320	4927688	220543	172079	22662		15.40	20.07	0.00
1500	5105506	224016	179568	25075	4591	13.09	25.73	15.25
1680	5085441	226870	182099	26858	5445	12.97	27.46	18.02
2820	5046861	226325	180896	23562	7309	13.34	23.48	23.58
3000	5445218	237339	192372	23510		12.11	24.59	0.00
3240	5139978	230525	190548	24889	3560	10.37	31.30	14.49
4200	5189484	234841	190062	23740	4116	12.25	24.83	13.93

0.005 K catalyst

	Calibration factors
H_2/N_2	0.0803
CO/N_2	1.0901
CH_4/N_2	0.3024
CO_2/N_2	0.9789

H_2	N_2	CO	H_2/CO
7948907	312585	300309	2.04
7861018	310586	297204	2.03
7918726	307032	304274	2.07
7994608	307280	300520	2.09
7968532	313115	306187	2.04

TOS (min)	H_2	N_2	CO	CH_4	CO_2	CO Conversion X_{CO}, C-%	CH_4 Selectivity S_{CH4}, C-%	CO_2 Selectivity S_{CO2}, C-%
10	6E+06	328295	222136	35687	16461	30.45	10.18	15.20
20	7E+06	346129	270744	40683	10293	19.60	17.10	14.00
30	7E+06	342711	271300	40443	9456	18.63	18.06	13.67
40	7E+06	342478	263552	46261	7439	20.90	18.43	9.59
50	7E+06	338916	268260	42195	7756	18.64	19.04	11.33
60	7E+06	339907	258544	41355	10873	21.82	15.90	13.53
70	7E+06	340246	260896	41195	10849	21.19	16.29	13.89
80	7E+06	338742	268676	40807	10842	18.48	18.59	15.99
90	8E+06	348786	271646	39880	12760	19.95	16.34	16.93
100	7E+06	342145	270350	43371	11357	18.78	19.24	16.31
110	7E+06	345668	267620	42195	9718	20.42	17.04	12.71
120	7E+06	346056	265580	41465	9955	21.12	16.18	12.57
150	7E+06	334870	245462	38882	10404	24.66	13.43	11.63
180	7E+06	336778	251810	40050	13252	23.15	14.65	15.69
210	6E+06	336127	251958	38954	17557	22.95	14.40	21.00
240	6E+06	334869	240073	42170	8762	26.31	13.65	9.18
270	6E+06	336682	246556	38576	11101	24.73	13.21	12.31
300	6E+06	334040	245138	41239	12430	24.57	14.33	13.98
330	6E+06	335881	245663	38723	11778	24.82	13.24	13.04
360	6E+06	339083	243614	39743	12227	26.15	12.78	12.73
1320	6E+06	328947	243917	39178	9550	23.78	14.28	11.27
1500	7E+06	332958	246941	38863	10537	23.77	14.00	12.29
1740	6E+06	327407	247957	39362	10112	22.16	15.47	12.87
2760	7E+06	335302	251795	39974	12244	22.81	14.90	14.77
3000	6E+06	319846	238607	37025	8295	23.32	14.15	10.26
3240	6E+06	318775	243681	39328	11187	21.43	16.42	15.12
4200	6E+06	323619	244449	35834	9588	22.36	14.12	12.23

0.01 K catalyst

	Calibration factors
H_2/N_2	0.0803
CO/N_2	1.0901
CH_4/N_2	0.3024
CO_2/N_2	0.9789

H_2	N_2	CO	H_2/CO
7781262	295105	283572	2.12
7962309	304286	292959	2.10
7886792	300352	288994	2.11
7858896	301386	287169	2.09
7837948	299541	285018	2.10

TOS (min)	H_2	N_2	CO	CH_4	CO_2	CO Conversion X_{CO}, C-%	CH_4 Selectivity S_{CH4}, C-%	CO_2 Selectivity S_{CO2}, C-%
20	5E+06	324980	168122	31112	11342	46.00	6.03	7.11
30	5E+06	326642	169547	32626	9078	45.82	6.31	5.69
40	5E+06	323676	162113	34076	8769	47.72	6.39	5.32
50	5E+06	319979	162717	34178	11457	46.92	6.59	7.15
60	5E+06	326949	162850	34299	12902	48.01	6.33	7.70
70	5E+06	329794	170074	31976	17035	46.17	6.08	10.49
80	5E+06	317976	162619	33405	13789	46.62	6.53	8.72
90	5E+06	324967	166213	34523	13927	46.61	6.60	8.62
100	5E+06	323423	169060	31776	14674	45.44	6.26	9.36
110	5E+06	323035	166871	33767	12723	46.08	6.57	8.01
120	5E+06	323967	166495	36042	10527	46.36	6.95	6.57
150	5E+06	309439	159392	34450	9784	46.23	6.97	6.41
180	5E+06	318414	159384	36056	18073	47.75	6.87	11.14
210	5E+06	319018	159553	36992	20350	47.80	7.02	12.51
240	5E+06	313306	154563	35351	14006	48.51	6.74	8.64
270	5E+06	317142	161924	35995	11905	46.71	7.04	7.53
300	5E+06	312258	160196	36498	13701	46.45	7.29	8.85
330	5E+06	311835	157721	36528	13510	47.21	7.19	8.60
360	5E+06	312213	159262	36762	9162	46.76	7.29	5.88
1320	5E+06	311055	155493	36545	15304	47.82	7.11	9.64
1500	5E+06	309365	162316	35369	12264	45.23	7.32	8.21
1740	5E+06	307854	153272	35360	11111	48.03	6.92	7.04
2760	5E+06	302092	153065	34198	17008	47.11	6.96	11.20
3000	5E+06	301143	152338	35441	10404	47.20	7.22	6.86
3240	5E+06	302002	151624	34535	10764	47.60	6.96	7.02
4200	5E+06	305514	152381	35930	10627	47.94	7.10	6.80

0.02 K catalyst

	Calibration factors
H_2/N_2	0.0803
CO/N_2	1.0901
CH_4/N_2	0.3024
CO_2/N_2	0.9789

H_2	N_2	CO	H_2/CO
11365137	469872	413209	1.94
11564601	469569	400754	1.98
11642588	477554	411513	1.96
11593201	475822	410319	1.96
10514208	441194	383874	1.91

TOS (min)	H_2	N_2	CO	CH_4	CO_2	CO Conversion X_{CO}, C-%	CH_4 Selectivity S_{CH4}, C-%	CO_2 Selectivity S_{CO2}, C-%
20	9E+06	541721	284673	38257	18895	39.28	5.76	9.21
30	9E+06	540829	290466	35295	15876	37.94	5.51	8.03
40	9E+06	544274	281908	40339	15116	40.15	5.92	7.18
50	9E+06	532259	275375	40381	24085	40.22	6.05	11.68
60	9E+06	540289	284421	38834	20727	39.17	5.88	10.16
70	9E+06	518224	278512	37459	15436	37.90	6.11	8.16
80	9E+06	531767	270593	38988	13015	41.20	5.70	6.16
90	9E+06	570526	291445	41676	16589	40.97	5.72	7.36
100	9E+06	526899	270172	39734	18132	40.75	5.93	8.76
110	9E+06	550593	292762	40535	16846	38.56	6.12	8.23
120	9E+06	531643	281087	39824	14267	38.91	6.17	7.16
150	8E+06	496761	252450	35747	17180	41.28	5.59	8.69
180	8E+06	500445	257791	34623	17254	40.48	5.48	8.84
210	7E+06	479628	242930	34718	17479	41.47	5.59	9.12
240	8E+06	497800	255787	33306	14188	40.62	5.28	7.28
270	7E+06	481876	248964	32981	13192	40.30	5.44	7.05
300	8E+06	502918	261869	35431	16843	39.83	5.67	8.72
330	8E+06	498343	253241	34804	14649	41.28	5.42	7.39
360	8E+06	513626	263743	35416	13934	40.66	5.44	6.92
1320	8E+06	482858	258463	31228	13650	38.15	5.43	7.69
1620	8E+06	505331	253910	30420	10337	41.94	4.60	5.06
2940	9E+06	705543	293174	36246	11960	51.98	3.17	3.38
3000	8E+06	565031	287711	36686	13130	41.16	5.06	5.86
3060	8E+06	568576	283123	30492	10566	42.46	4.05	4.54
4200	7E+06	511878	263957	29050	12277	40.41	4.50	6.16

0.04 K catalyst

	Calibration factors
H_2/N_2	0.0803
CO/N_2	1.0901
CH_4/N_2	0.3024
CO_2/N_2	0.9789

H_2	N_2	CO	H_2/CO
9477507	458326	343436	2.03
9948820	481856	358993	2.04
9865179	471987	360347	2.02
10229867	498860	375946	2.00
9772578	470281	356302	2.02

TOS (min)	H_2	N_2	CO	CH_4	CO_2	CO Conversion X_{CO}, C-%	CH_4 Selectivity S_{CH4}, C-%	CO_2 Selectivity S_{CO2}, C-%
20	9E+06	565960	283904	23882	7961	33.45	4.64	5.01
30	8E+06	556887	283056	25417	14386	32.57	5.16	9.45
40	8E+06	551847	280414	24515	9096	32.59	5.02	6.02
50	9E+06	531077	287477	29909	0	28.19	7.35	0.00
60	7E+06	512816	254874	24476	7939	34.07	5.16	5.41
70	8E+06	539259	271399	26437	14955	33.24	5.43	9.94
80	9E+06	543720	284147	29673	17645	30.67	6.55	12.60
90	8E+06	545219	273521	29281	16974	33.45	5.91	11.09
100	8E+06	540395	265665	30804	10643	34.78	6.03	6.75
110	8E+06	534779	264684	27221	10764	34.34	5.45	6.98
120	8E+06	546731	274711	26942	14466	33.34	5.44	9.45
150	9E+06	537352	304953	32558	13454	24.71	9.02	12.07
180	8E+06	549500	267611	24701	8548	35.39	4.67	5.24
210	8E+06	542310	266974	26127	11157	34.69	5.11	7.06
240	8E+06	535916	264373	24562	11176	34.56	4.88	7.19
270	8E+06	549396	263763	22628	9515	36.31	4.17	5.68
300	7E+06	524085	257610	25702	12143	34.79	5.19	7.93
330	8E+06	545642	263817	24183	12877	35.86	4.55	7.84
360	8E+06	546175	261598	24097	12701	36.46	4.45	7.60
1320	7E+06	533600	266067	23410	8639	33.85	4.77	5.70
1500	7E+06	521170	267569	23236	9011	31.89	5.14	6.46
1680	8E+06	538842	272238	23276	9694	32.98	4.82	6.50
2700	8E+06	590929	292544	26450	11186	34.33	4.80	6.57
2880	8E+06	576386	289515	28661	10813	33.37	5.48	6.70
3120	8E+06	543739	277999	25249	9964	32.18	5.31	6.78
4200	8E+06	545855	288996	27134	13791	29.77	6.15	10.11

0.06 K catalyst

	Calibration factors
H_2/N_2	0.0803
CO/N_2	1.0901
CH_4/N_2	0.3024
CO_2/N_2	0.9789

H_2	N_2	CO	H_2/CO
9587794	391828	353946	1.96
9421218	373890	356438	2.02
9222849	376392	332675	1.97
9205939	373196	338780	1.98
9277844	371534	338073	2.01

TOS (min)	H_2	N_2	CO	CH_4	CO_2	CO Conversion X_{CO}, C-%	CH_4 Selectivity S_{CH4}, C-%	CO_2 Selectivity S_{CO2}, C-%
10	6561335	320161	190334	10620	11822	36.64	2.68	9.64
20	8161996	332624	256902	21179	8818	17.69	10.64	14.35
30	7938056	332632	252248	20265	8460	19.18	9.39	12.69
40	7815022	327186	249568	23550	7872	18.71	11.38	12.31
50	7853550	327335	250648	22962	8308	18.39	11.28	13.21
60	7916844	326276	254022	26317	10303	17.03	14.01	17.75
70	7925107	328089	249634	22284	11879	18.91	10.62	18.32
80	7984998	327675	246517	20555	12363	19.82	9.36	18.22
90	7966132	327030	251096	21925	11747	18.17	10.91	18.92
100	7995024	326979	245226	21366	22167	20.07	9.63	32.33
110	7935296	331740	250908	21971	12656	19.39	10.10	18.83
120	7949716	324477	246318	20483	13768	19.10	9.77	21.27
150	7276015	311353	240691	21331	10509	17.61	11.50	18.34
180	7404449	319080	247036	19471	10261	17.49	10.32	17.60
210	7490634	324655	251255	23885	15899	17.52	12.42	26.75
240	7582433	334514	255418	22825	10007	18.62	10.83	15.37
270	7248386	313229	245111	21828	13805	16.60	12.41	25.41
300	7421014	317477	248325	22316	12247	16.64	12.49	22.19
330	7476221	323283	255466	24851	12227	15.78	14.40	22.94
360	7449228	322853	252787	23543	14997	16.55	13.02	26.86
1320	7541506	319003	249119	19936	9546	16.77	11.02	17.08
1500	7404358	311227	256648	18653	10733	12.11	14.63	27.24
1740	7588725	311855	249753	19754	11278	14.65	12.79	23.63
2760	7598688	312550	253134	19066	9728	13.68	13.18	21.77
3000	7599602	308439	244796	18703	9951	15.42	11.63	20.03
3240	8370527	323749	235296	17798	9940	22.54	7.21	13.03
4200	7603499	325777	263388	19825	9630	13.83	13.00	20.45

0.08 K catalyst

	Calibration factors
H_2/N_2	0.0803
CO/N_2	1.0901
CH_4/N_2	0.3024
CO_2/N_2	0.9789

H_2	N_2	CO	H_2/CO
7287134	287542	265711	2.04
7351226	284980	257622	2.07
7261240	285989	254492	2.04
7346462	288024	260934	2.05
7306912	287523	260601	2.04
7314610	286598	258316	2.05

TOS (min)	H_2	N_2	CO	CH_4	CO_2	CO Conversion X_{CO}, C-%	CH_4 Selectivity S_{CH4}, C-%	CO_2 Selectivity S_{CO2}, C-%
10	6038382	288408	198623	7053	8856	23.99	3.12	12.69
20	7107096	311267	225049	14104	6230	20.20	6.87	9.82
30	7147389	315914	230995	14729	7438	19.30	7.40	12.09
40	7122396	318011	223583	15597	8472	22.40	6.70	11.79
50	7046500	312528	220401	15740	9423	22.17	6.96	13.48
60	6685040	307201	218281	15886	10157	21.58	7.34	15.19
70	7062268	315507	219909	16903	14342	23.07	7.11	19.53
80	7055870	314593	219320	18092	13899	23.06	7.64	18.99
90	7023778	311399	215122	16400	15102	23.75	6.79	20.23
100	7089952	315505	219693	14642	12193	23.15	6.14	16.55
110	6808157	306279	217550	15646	11719	21.60	7.24	17.55
120	7132312	314048	221854	15871	13067	22.03	7.02	18.72
150	6482364	297576	211963	16357	12062	21.38	7.87	18.79
180	6570877	303190	212236	16663	12701	22.74	7.40	18.26
210	6556039	299344	210050	16305	11751	22.55	7.39	17.25
240	6515006	303502	208936	17022	11148	24.02	7.15	15.16
270	6516450	298529	209651	15726	14622	22.49	7.17	21.58
300	6563756	315956	213680	16136	11577	25.36	6.17	14.32
330	6536669	305109	212142	15864	12928	23.26	6.84	18.05
360	6568050	307090	213978	15727	11948	23.10	6.79	16.70
1320	6973284	302934	227752	15338	11240	17.02	9.11	21.60
1500	6980439	312664	228508	15725	11625	19.34	7.96	19.06
1500	7855484	400596	274658	23511	17714	24.33	7.39	18.01
1680	7862192	413209	285752	24513	16400	23.67	7.67	16.62
2700	7188504	309568	237538	13967	9480	15.31	9.02	19.82
3000	7228240	302580	233055	15684	9805	14.99	10.59	21.42
3240	7227432	302819	233579	14939	9718	14.99	10.59	21.42
4200	7144146	313887	237768	13749	10539	16.40	8.18	20.30

APTeS modified silica catalyst 0 K

	Calibration factors
H_2/N_2	0.0803
CO/N_2	1.0901
CH_4/N_2	0.3024
CO_2/N_2	0.9789

H_2	N_2	CO	H_2/CO
9396363	369045	346550	2.00
9357398	362526	348950	1.98
9461446	367223	340328	2.05
9487529	353887	342689	2.04
9479553	365753	351708	1.99

TOS (min)	H_2	N_2	CO	CH_4	CO_2	CO Conversion X_{CO}, C-%	CH_4 Selectivity S_{CH4}, C-%	CO_2 Selectivity S_{CO2}, C-%
20	7926254	383236	270505	35648	4541	25.83	10.50	4.33
30	7424200	354707	254203	31887	6673	24.69	10.61	7.19
40	7387464	357135	254048	36481	7150	25.25	11.79	7.48
50	7406392	353240	253285	33928	4878	24.65	11.36	5.29
60	7408758	352064	248003	34860	7962	25.98	11.11	8.21
70	7384608	353410	244832	35781	6054	27.20	10.85	5.94
80	7337460	351226	245270	38250	10736	26.62	11.93	10.83
90	7390798	352762	246444	34882	10661	26.59	10.84	10.72
100	7482108	355822	250076	36354	7151	26.15	11.39	7.25
110	7353782	353449	242632	35254	8193	27.87	10.43	7.85
120	7197463	350854	236828	36420	8151	29.07	10.41	7.54
150	6644602	329479	228408	34960	6569	27.15	11.39	6.93
180	6645200	330664	224832	35574	7765	28.55	10.98	7.76
210	6740884	336661	236737	37112	10518	26.11	12.31	11.29
240	6625946	329508	235265	38936	9450	24.97	13.79	10.84
270	6522370	323503	225004	37315	9483	26.91	12.49	10.28
300	6552509	325275	229127	36468	9437	25.98	12.58	10.54
330	6612322	327537	228725	36890	8991	26.62	12.33	9.73
360	6711310	336288	236739	36997	9012	26.03	12.32	9.72
1320	6579740	327047	231144	37182	9642	25.73	12.88	10.81
1500	6329300	321162	228635	35706	9579	25.19	12.86	11.17
1740	6555014	316856	222423	35040	7901	26.24	12.29	8.97
2760	6446548	315314	220258	37928	7960	26.60	13.18	8.96
3000	6540183	319220	223413	40773	8145	26.46	14.07	9.10
3240	6530462	309391	217396	38074	5797	26.17	13.71	6.76
4200	6393909	311211	220157	39199	6612	25.66	14.31	7.81

APTeS modified silica catalyst 0.005 K

	Calibration factors
H_2/N_2	0.0803
CO/N_2	1.0901
CH_4/N_2	0.3024
CO_2/N_2	0.9789

H_2	N_2	CO	H_2/CO
9814183	383235	303357	2.06
9919984	383353	323630	2.08
9906298	389646	326443	2.04
10037759	379904	322486	2.12
9934122	384590	320283	2.07

TOS (min)	H_2	N_2	CO	CH_4	CO_2	CO Conversion X_{CO}, C-%	CH_4 Selectivity S_{CH4}, C-%	CO_2 Selectivity S_{CO2}, C-%
20	7E+06	401143	209528	38005	6431	37.15	8.51	4.66
30	7E+06	392223	212957	39645	6284	34.67	9.73	4.99
40	7E+06	398019	207459	36042	6681	37.28	8.11	4.87
50	7E+06	392470	210471	40481	5612	35.47	9.71	4.36
60	7E+06	418322	219343	41562	7857	36.91	8.99	5.50
70	7E+06	425043	221896	41751	9943	37.18	8.82	6.80
80	7E+06	423787	222713	43022	7534	36.76	9.22	5.23
90	8E+06	432186	224887	43199	7969	37.39	8.92	5.33
100	7E+06	425670	220281	44091	8394	37.73	9.16	5.65
110	7E+06	413300	216885	39751	8804	36.85	8.71	6.25
120	7E+06	411367	216794	39589	9179	36.58	8.78	6.59
150	7E+06	416055	216818	40594	9239	37.29	8.73	6.43
180	7E+06	396362	209733	44720	7819	36.33	10.37	5.87
210	7E+06	399785	208772	43980	12615	37.16	9.88	9.18
240	7E+06	390387	207965	39614	7526	35.90	9.44	5.80
270	7E+06	385422	205007	39682	9472	36.00	9.55	7.38
300	6E+06	384933	205361	40559	8901	35.80	9.82	6.98
330	7E+06	401344	212554	44761	10066	36.27	10.26	7.47
360	7E+06	402556	216021	43407	10891	35.43	10.16	8.25
1320	7E+06	389522	206093	40430	7639	36.33	9.54	5.83
1500	7E+06	388326	207848	40675	10178	35.59	9.82	7.96
1740	7E+06	405693	208740	42153	11204	38.09	9.11	7.84
2760	7E+06	395982	207653	44390	9156	36.90	10.14	6.77
3000	6E+06	392609	218088	41310	13007	33.16	10.59	10.80
3240	6E+06	391981	221108	41435	12762	32.12	10.98	10.95
4200	6E+06	388309	210419	43088	14888	34.79	10.65	11.91

APTeS modified silica catalyst 0.01 K

	Calibration factors
H_2/N_2	0.0803
CO/N_2	1.0901
CH_4/N_2	0.3024
CO_2/N_2	0.9789

H_2	N_2	CO	H_2/CO
10057866	394185	361404	2.05
10155959	407620	382108	1.96
9941629	403136	375417	1.95
9804337	393882	375056	1.93
10105959	397631	385904	1.93

TOS (min)	H_2	N_2	CO	CH_4	CO_2	CO Conversion X_{CO}, C-%	CH_4 Selectivity S_{CH4}, C-%	CO_2 Selectivity S_{CO2}, C-%
20	7708970	419297	256269	37353	9337	35.09	7.48	6.05
30	8532444	462992	288998	44058	9468	33.71	8.32	5.78
40	8255122	465232	275810	41807	12343	37.04	7.15	6.83
50	8169510	456678	278622	42275	12309	35.21	7.75	7.30
60	8208118	455390	276452	45379	9001	35.53	8.26	5.31
70	8219754	451959	275087	45340	8979	35.36	8.36	5.36
80	8146474	450315	276197	44914	9209	34.86	8.43	5.59
90	8064074	461732	272151	45640	10412	37.41	7.78	5.75
100	8116046	444233	274971	45393	10502	34.27	8.79	6.58
110	8198274	454494	274734	47370	10288	35.81	8.58	6.03
120	8188200	458942	276528	46941	9848	36.01	8.37	5.68
150	7539418	439160	267502	46197	9451	35.31	8.78	5.81
180	7554460	438209	262344	47621	12655	36.42	8.79	7.56
210	7574182	443426	268048	47259	11006	35.80	8.77	6.61
240	7629834	443927	268176	41222	11302	35.85	7.63	6.77
270	7604030	441482	267211	46380	14610	35.72	8.66	8.83
300	7862037	460062	275356	47372	11340	36.44	8.32	6.45
330	7525805	438728	264450	44584	10617	35.99	8.32	6.41
360	7577648	450470	270496	44353	10647	36.23	8.01	6.22
1320	7635667	452808	272209	46849	8741	36.16	8.43	5.09
1500	7593056	443847	272612	47497	9496	34.77	9.07	5.87
1740	7631642	442150	270585	44822	8133	35.01	8.53	5.01
2760	7801968	480496	283476	47046	9958	37.35	7.72	5.29
3000	7754620	451640	276011	48894	9889	35.10	9.09	5.95
3240	7789800	454718	269354	49073	11000	37.09	8.57	6.22
4200	7639959	457628	271501	49628	10292	37.00	8.64	5.80

APTeS modified silica catalyst 0.02 K

	Calibration factors
H_2/N_2	0.0803
CO/N_2	1.0901
CH_4/N_2	0.3024
CO_2/N_2	0.9789

H_2	N_2	CO	H_2/CO
9249455	385381	330568	1.93
9137903	379737	348477	1.93
8894937	374107	334588	1.91
8821412	372545	327667	1.90
8767137	363569	335948	1.94

TOS (min)	H_2	N_2	CO	CH_4	CO_2	CO Conversion X_{CO}, C-%	CH_4 Selectivity S_{CH4}, C-%	CO_2 Selectivity S_{CO2}, C-%
20	7274754	512035	252148	26450	5548	44.96	3.56	2.42
30	8043941	546776	289400	32843	9179	40.84	4.56	4.13
40	7043549	441318	258706	30448	5336	34.48	6.20	3.52
50	6762910	420356	240010	32718	8883	36.18	6.67	5.86
60	6557385	400914	236558	34377	3052	34.05	7.81	2.24
70	6507274	403352	235989	34504	5550	34.61	7.66	3.99
80	6425667	399133	226522	35910	7076	36.57	7.63	4.87
90	6500031	402647	228904	37546	7299	36.46	7.93	4.99
100	6486092	399741	233028	35612	8227	34.84	7.93	5.93
110	6464456	402858	233333	36687	8231	35.26	8.01	5.82
120	7994190	458730	274848	47835	9949	33.03	9.79	6.59
150	6057616	395811	226335	37942	14496	36.09	8.24	10.19
180	5899882	377217	217025	38457	9093	35.69	8.86	6.78
210	6031508	379277	219975	36084	12079	35.17	8.39	9.09
240	6063190	379847	219514	37457	11695	35.41	8.64	8.73
270	5829190	379425	209765	34981		38.21	7.48	0.00
300	5834887	378332	219968	39189	13765	35.01	9.17	10.43
330	5843122	372054	215714	40989	10456	35.20	9.71	8.01
360	6139014	396667	224537	41115	9886	36.73	8.75	6.81
1320	5934010	375182	210295	37374	10293	37.35	8.27	7.37
1500	6034880	372661	213053	40452	12825	36.10	9.32	9.57
1740	5826328	376648	208512	37763	11111	38.12	8.15	7.77
2760	5833006	377241	212669	39223	12866	36.99	8.72	9.25
3000	6006680	392609	218088	41310	13007	37.91	8.61	8.77
3240	6136646	391981	221108	41435	12762	36.95	8.87	8.84
4200	6126710	388309	210419	43088	14888	39.43	8.73	9.76

Appendix: Time on stream FID data for Fischer-Tropsch synthesis

Iron catalyst supported on silica with different ratios of potassium

0 K TOS 3060 min Carbon number NC	A_{Tot}	Paraffin	1-Olefin	n-Olefin	Ald+Alc	$\log(A_i / A_{Tot})$	$X_{n\text{-}Olef}$	$X_{1\text{-}Olef}$	$X_{Oxyg.}$	X_{Branch}
1	601325	566695			34630	1.69			10.00	
2	266843	232015	27351		7477	1.05	10.55		6.074	
3	370629	204366	139929		26334	1.00	40.64		14.87	
4	307667	115336	82683	100685	8963	0.71	55.01	63.93	6.074	3.245
5	145047	65834	16476	57835	4902	0.38	49.06	25.99	2.857	15.84
6	73664	42163	6042	25459		0.01	40.78	20.81		27.19
7	45403	29092	3751	12560		-0.16	35.92	23.00		16.05
8	37731	22837	2664	12230		-0.32	34.20	22.45		19.56
9	83848	58276	4903	20669		0.14	30.50	19.17		4.574

0.005 K TOS 3060 min Carbon number NC	A_{Tot}	Paraffin	1-Olefin	n-Olefin	Ald+Alc	$\log(A_i / A_{Tot})$	$X_{n\text{-}Olef}$	$X_{1\text{-}Olef}$	$X_{Oxyg.}$	X_{Branch}
1	59.72	54.53			5.19	1.71			8.698	
2	18.28	10.22	4.31		3.76	1.14	29.65		22.95	
3	10.12	4.94	4.23		0.95	0.94	46.13		9.400	
4	2.67	0.70	0.97	0.90	0.10	0.58	40.80	51.74	13.08	16.14
5	2.44	1.65	0.24	0.50	0.06	0.31	38.20	23.76	0.629	16.14
6	1.08	0.79	0.06	0.21	0.01	0.00	33.01	16.45	0.919	7.179
7	0.66	0.55	0.03	0.08		-0.26	26.92	13.95		12.65
8	0.26	0.22	0.01	0.04		-0.58	22.23	13.39		4.574
9	0.14	0.13		0.01		-0.83	18.60	13.41		37.80

0.01 K TOS 3060 min Carbon number NC	A_{Tot}	Paraffin	1-Olefin	n-Olefin	Ald+Alc	$\log(A_i / A_{Tot})$	$X_{n\text{-}Olef}$	$X_{1\text{-}Olef}$	$X_{Oxyg.}$	X_{Branch}
1	41.18	37.45			3.73	1.56			9.06	
2	17.35	7.60	0.96		8.79	0.92	11.39		20.58	
3	9.20	4.09	2.72		2.39	0.82	39.93		25.97	
4	1.66	0.00	0.57	0.69	0.41	0.79	42.50	45.34	64.96	1.130
5	7.58	6.08	0.41	1.09		0.66	43.90	20.11	2.104	16.00
6	3.41	2.78	0.09	0.41	0.12	0.31	35.68	12.53	2.622	22.71
7	1.95	1.72	0.05	0.18		0.04	36.78	11.54		10.49
8	1.08	1.02	0.02	0.04		-0.25	31.84	10.30		22.88
9	2.33	2.00	0.03	0.31		0.19	21.54	9.63		

0.02 K TOS 3060 min Carbon number NC	A_{Tot}	Paraffin	1-Olefin	n-Olefin	Ald+Alc	$\log(A_i / A_{Tot})$	$X_{n\text{-}Olef}$	$X_{1\text{-}Olef}$	$X_{Oxyg.}$	X_{Branch}
1	1231500	1135416			96084	1.67			13.33	
2	821840	517511	77925		226404	1.08	13.09		34.17	
3	850843	320132	444244		86467	1.02	58.12		14.60	
4	781475	340350	325895	105475	9755	0.89	56.35	75.55	7.975	1.428
5	431647	197008	58875	154252	21512	0.50	49.42	30.59	4.592	8.879
6	256975	130222	24562	96332	5859	0.21	45.06	23.00	2.349	18.01
7	103362	3026	48413	48413	3510	-0.07	39.74	16.65	2.384	2.04
8	104424	68499	5175	30750		-0.29	32.52	15.68		12.99
9	112711	79891	4433	28387		-0.29	29.12	13.51		3.402

Iron catalyst supported on APTeS modified silica promoted with different ratios of potassium

0 K TOS 3060 min

Carbon number NC	A_{Tot}	Paraffin	1-Olefin	n-Olefin	Ald+Alc	$\log(A_i / A_{Tot})$	$X_{n\text{-}Olef}$	$X_{1\text{-}Olef}$	$X_{Oxyg.}$	X_{Branch}
1	265.24	248.54			16.70	1.69			18.30	
2	154.51	100.53	25.00		28.98	1.09	19.92		33.41	
3	166.66	82.82	72.82		11.01	1.01	46.79		7.68	
4	99.14	53.59	19.58	21.63	4.34	0.67	43.47	47.50	7.07	2.07
5	71.85	38.93	5.96	26.97		0.46	40.87	20.08	0.77	9.12
6	17.99	8.03	0.90	9.06		0.30	35.42	15.88		35.91
7	24.91	17.22	0.73	6.96		-0.15	31.44	11.84		7.24
8	12.62	10.76		1.86		-0.61	21.41	12.14		3.21
9						-0.80	10.21	10.97		4.42

0.005 K TOS 3060 min

Carbon number NC	A_{Tot}	Paraffin	1-Olefin	n-Olefin	Ald+Alc	$\log(A_i / A_{Tot})$	$X_{n\text{-}Olef}$	$X_{1\text{-}Olef}$	$X_{Oxyg.}$	X_{Branch}
1	324.24	307.19			17.05	1.72			15.61	
2	173.01	118.85	17.28		36.88	1.06	12.70		37.06	
3	179.70	80.02	85.21		14.46	0.97	51.57		9.34	
4	105.26	49.28	22.24	18.85	14.89	0.57	47.03	54.1	20.46	1.20
5	76.58	35.75	8.31	31.00	1.52	0.38	43.66	27.0	2.61	12.73
6	38.13	22.82	3.82	10.99	0.51	0.02	38.34	19.8	1.67	9.59
7	25.82	14.97	1.25	9.60		-0.25	35.48	15.2		11.29
8	14.48	9.35	0.61	4.53		-0.60	30.42	13.9	6.25	12.55
9	17.38	11.84	0.61	4.93		-0.49	25.15	14.2		

0.01 K TOS 3060 min

Carbon number NC	A_{Tot}	Paraffin	1-Olefin	n-Olefin	Ald+Alc	$\log(A_i / A_{Tot})$	$X_{n\text{-}Olef}$	$X_{1\text{-}Olef}$	$X_{Oxyg.}$	X_{Branch}
1	249.54	236.37			13.17	1.74			15.66	
2	110.57	82.56	28.01			1.11	25.33			
3	134.11	54.48	68.43		11.20	0.98	55.68		9.68	
4	86.64	36.74	21.10	14.28	14.52	0.61	51.19	59.63	24.30	1.43
5	49.15	26.30	7.63	13.84	1.38	0.38	48.40	30.91	3.12	17.60
6	32.88	17.24	2.89	12.76		0.06	41.71	23.41	1.52	12.45
7	18.43	11.47	1.09	5.87		-0.21	37.53	15.85		12.53
8	12.58	7.74		4.85		-0.48	32.22	12.69	5.11	23.18
9	6.83	4.71		2.12		-0.81	21.02	12.56		2.78

0.02 K TOS 3060 min

Carbon number NC	A_{Tot}	Paraffin	1-Olefin	n-Olefin	Ald+Alc	$\log(A_i / A_{Tot})$	$X_{n\text{-}Olef}$	$X_{1\text{-}Olef}$	$X_{Oxyg.}$	X_{Branch}
1	276.67	259.47			17.21	1.69			18.1	
2	156.94	115.94	41.00			1.17	26.12			
3	178.91	83.74	81.46		13.71	1.02	49.31		8.89	
4	133.30	52.58	24.04	34.55	22.14	0.67	46.04	53.58	23.31	11.75
5	74.84	37.62	7.11	28.92	1.20	0.45	41.61	22.89	1.89	16.35
6	44.45	25.51	4.23	14.71		0.10	36.15	15.43	1.38	18.71
7	28.12	18.07	1.27	8.77		-0.10	31.21	13.99		10.37
8	17.68	12.42	0.59	4.66		-0.41	23.99	12.70	4.248	22.70
9	11.12	8.45		2.67		-0.68	15.05	12.77		4.54